Journal of Medicinal Chemistry

pubs.acs.org/jmc

Article

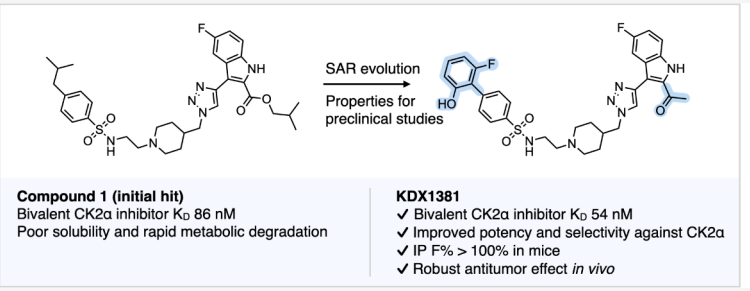
Discovery of KDX1381, a Bivalent CK2α Inhibitor for the Treatment of Solid Tumors as a Single Agent or in Combination

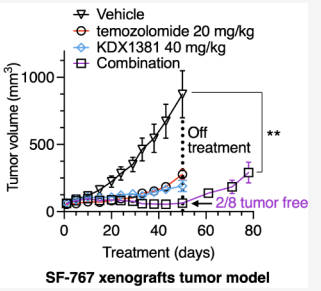
Léna Marlhoux,[#] Alexandre Arnaud,[#] Céline Hervieu, Gabriela Makulyte, Charlotte Martinasso, Angélique Mularoni, Jean-Guy Delcros, Isabelle Krimm, Hector Hernandez-Vargas, Gabriel Ichim, Olivier Meurette, David Neves,* and Alexandre Bancet*

Cite This: https://doi.org/10.1021/acs.jmedchem.5c00695

Read Online

ACCESS | Metrics & More | Article Recommendations | Supporting Information





ABSTRACT: Casein kinase 2 (CK2) has emerged as a promising therapeutic target across a broad spectrum of malignancies, including pediatric and orphan cancers. The identification of a ligandable allosteric αD pocket on the CK2α subunit has enabled the development of bivalent inhibitors, which bind simultaneously to both the adenosine triphosphate (ATP) site and the allosteric pocket. Here, we report the discovery and pharmacological characterization of **KDX1381**, a structure-guided bivalent CK2α inhibitor with low-nanomolar potency and high selectivity, confirmed by cocrystal structures. In mice, **KDX1381** suppressed CK2-driven tumor growth as a monotherapy and enhanced therapeutic efficacy when combined with vascular endothelial growth factor receptor (VEGFR) inhibitors or DNA-damaging agents in hepatocellular carcinoma and glioma models. These findings support bivalent CK2α inhibition as a differentiated therapeutic strategy with broad applicability in CK2-dependent cancers.

Downloaded via Alexandre Bancet on June 10, 2025 at 21:31:17 (UTC).
See https://pubs.acs.org/sharingguidelines for options on how to legitimately share published articles.

INTRODUCTION

Casein kinase 2 (CK2) is a ubiquitous serine/threonine kinase that predominantly functions as a tetrameric complex composed of two catalytic (CK2α or CK2α') and two regulatory (CK2β) subunits. The latter modulate substrate specificity and contribute to enzyme stability.[1] Notably, imbalanced expression of CK2α or CK2α' in the absence of compensatory CK2β expression has been shown to promote cellular transformation, initially observed in *Ha-ras*-transfected fibroblasts.[2] These findings suggest that the monomeric form of CK2 may be more closely linked to oncogenic phenotypes than the fully assembled tetrameric form, a hypothesis later supported by subsequent studies. Supporting this view, downregulation of CK2β has also been linked to epithelial-mesenchymal transition (EMT), a key driver of metastatic progression.[3,4] Although CK2 dysregulation confers pro-oncogenic properties, recurrent activating mutations have not been identified in human cancers. Instead, cancer-associated alterations reflect context-specific shifts in activity and substrate engagement distinct from normal tissue.[5,6] Unlike most kinases which propagate signaling through vertical cascades, CK2 functions laterally, modulating diverse oncogenic and nononcogenic pathways — including phosphatidylinositol 3-kinase (PI3K)/AKT, Wnt/β-catenin, cell cycle regulation, and angiogenesis.[7,8] Elevated expression of CK2α and/or CK2α' has been documented across a wide range of solid and hematologic malignancies.[9−13] Functional studies have consistently shown that CK2 activity is critical for cancer cell proliferation, migration, and invasion. In contrast, nontransformed cells exhibit greater tolerance to CK2 inhibition. This differential sensitivity is further supported by evidence that residual CK2 activity, maintained through expression of a truncated CK2α' isoform, can sustain viability in nonmalignant clones.[14] Although documented in a limited number of models, these complementary findings collectively suggest a therapeutic window that could be selectively exploited through CK2-targeted strategies. CK2 has also been implicated in tumor immune evasion,[15,16] metabolic

Received: March 9, 2025
Revised: May 11, 2025
Accepted: May 29, 2025

© XXXX American Chemical Society

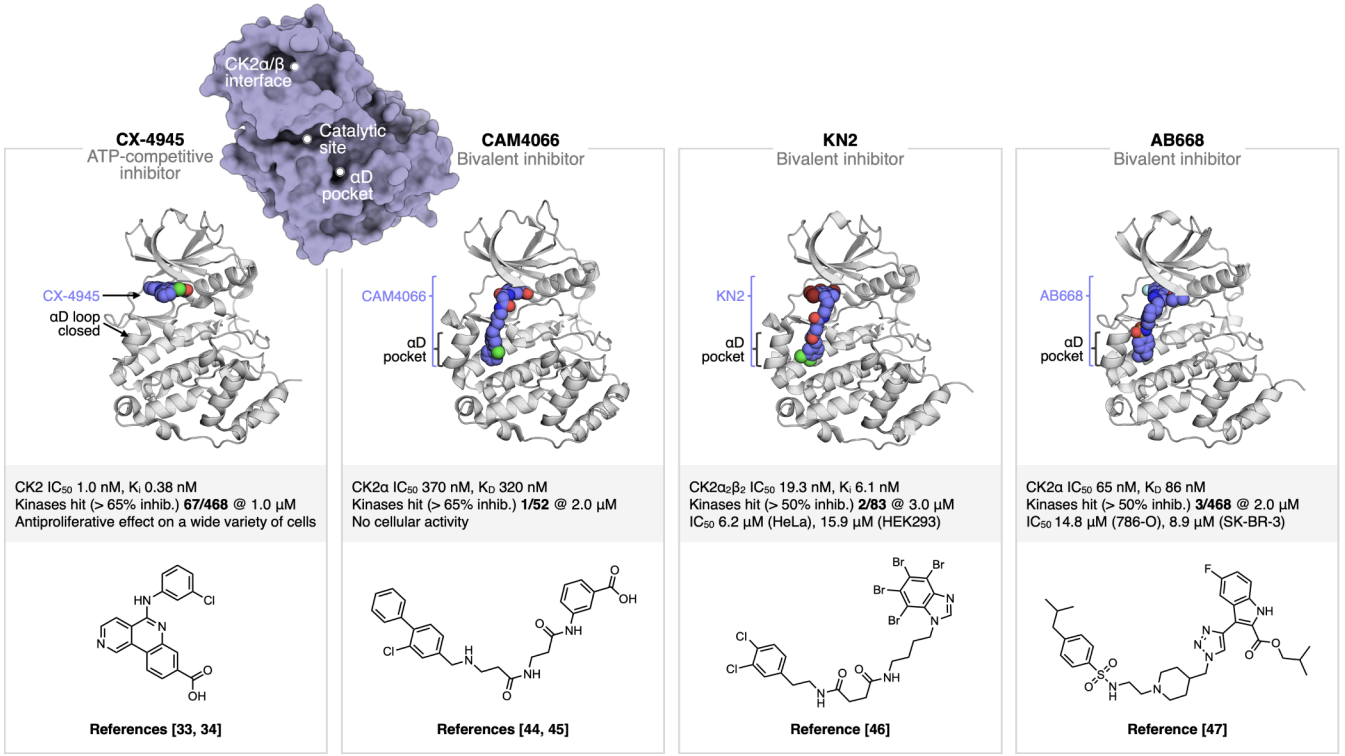


Figure 1. Surface representation of the human CK2α catalytic subunit, highlighting critical binding sites targeted by small molecules. Co-crystal structures, key features and chemical structures of representative CK2 inhibitors, such as CX-4945 (PDB 3PE1), a clinical-stage ATP competitive inhibitor, and prototype bivalent CK2 inhibitors, CAM4066 (PDB 5MO8), KN2 (PDB 7AT5) and AB668 (PDB 8C5Q). Inhib., inhibition; PDB, Protein Data Bank.

adaptation,[17] and resistance to therapy.[18] Consequently, substantial academic and industrial efforts have focused on developing small-molecule and peptide inhibitors targeting CK2.[19−32] Among them, **CX-4945** (silmitasertib, Figure 1), an adenosine triphosphate (ATP)-competitive CK2 inhibitor, has progressed to clinical evaluation in both pediatric and adult cancers.[33,34] However, like other compounds targeting the conserved catalytic site,[35] **CX-4945** faces several limitations.[36−38]

1.Cancer persistence. ATP-competitive inhibitors primarily disrupt catalytic activity, but tumor cells may rapidly adapt to preserve essential signaling, limiting durable therapeutic responses.[39]

2.Off-target toxicities. ATP-competitive inhibitors are predisposed to off-target interactions given the presence of ATP-binding domains in nearly 1,400 human proteins, raising concerns about selectivity and adverse effects.[40,41]

3.Limited impact on CK2's broader biological functions. Emerging evidence suggests that CK2, independent of its catalytic function, may contribute to tumorigenic signaling through protein−protein interactions.[42,43]

In 2016, Brear and coworkers introduced a novel strategy to address these limitations, by employing a bivalent inhibitor designed to specifically target the CK2α protein.[44,45] In their study, the authors identified a cryptic allosteric pocket adjacent to the ATP-binding site − the αD pocket − which is conserved within CK2 but differs significantly across the broader kinome, enabling selective ligand engagement (Figure 1). Subsequent bivalent inhibitors targeting both the ATP site and αD pocket, demonstrated remarkable selectivity and mechanism of action distinct from that of conventional CK2 ATP-competitive inhibitors (Figure 1).[46,47] This dual targeting mechanism could provide a more nuanced disruption of CK2's multiple biological roles, potentially leading to more effective inhibition of its pro-tumorigenic functions. However, this strategy necessitates further investigation to assess *in vivo* antitumor efficacy and toxicity. Indeed, the early bivalent inhibitors reported thus far in the literature exhibit physicochemical properties that limit their cellular potency, indicating that additional refinements are essential to develop a viable *in vivo* chemical probe for CK2α inhibition. In this context, we describe the hit-optimization campaign to identify a potent and selective bivalent CK2α inhibitor, **KDX1381**, which possesses suitable properties to achieve proof-of-concept in tumor-bearing mice, both as a single agent and in combination with other targeted therapies.

RESULTS AND DISCUSSION

Hit-Optimization Campaign. Starting from the initial CK2α/CK2β interface binder **CCH503**,[30] early optimization efforts focused on the indole, linker, and phenyl sulfonamide moieties, leading to a new chemical series that transitioned from interface binding to dual engagement of the ATP pocket and adjacent αD site of CK2α (Figure 2a). This work led to the identification of compound **1** (**AB668**), whose binding mode was confirmed by cocrystallization with CK2α at 2.5 Å resolution (PDB 8C5Q), supporting its selection as a scaffold for bivalent inhibitor development.[47] The indole core of ligand **1** anchors to the ATP site, while the substituted phenyl sulfonamide is deeply embedded in the hydrophobic αD pocket. A flexible linker bridges the two motifs, occupying a shallow groove and stabilized by a network of hydrogen bonds (Figure 2b). Although compound **1** displayed nanomolar potency in biochemical assays, its poor permeability restricted

https://doi.org/10.1021/acs.jmedchem.5c00695
J. Med. Chem. XXXX, XXX, XXX−XXX

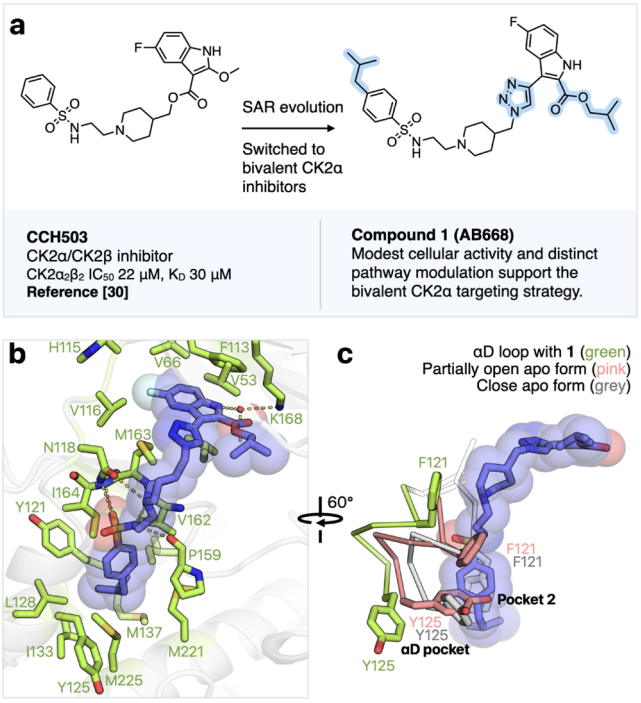
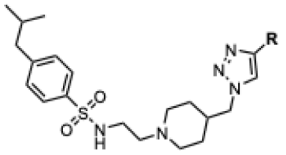
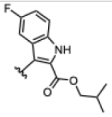
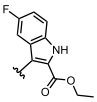
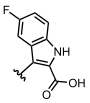
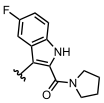
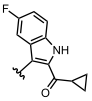
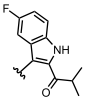
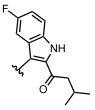
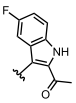


Figure 2. (a) Chemical structures of CCH503 and compound 1, highlighting in blue the modification distinguishing 1 from the initial CK2α/CK2β interface inhibitor. (b) Co-crystal structure of CK2α in complex with compound 1 (PDB 8C5Q). The inset shows key interactions, with water molecules represented as red spheres and hydrogen bonds in yellow dashed lines. *Adapted from Bancet et al., iScience 2024, 27, 108903. Licensed under CC BY 4.0.* (c) Comparative analysis of the binding mode of 1 and the conformational states of the αD loop, in both its partially open (pink, PDB 3WAR), and closed (gray, PDB 3WFQ) forms. In the closed state, residue Y125 obstructs the entrance of a water channel (Pocket 2), suggesting that strategic modifications to the phenyl sulfonamide moiety could displace bound water molecules while preserving favorable binding energetics. PDB, Protein Data Bank; SAR, structure−activity relationship.

its ability to modulate CK2 signaling in cellular contexts. This profile was reflected in half-maximal inhibitory concentration (IC_{50}) values of 14.8 μM and 8.9 μM in the renal carcinoma 786-O and breast SK-BR-3 models, respectively − both characterized by elevated CK2α expression. Absorption, distribution, metabolism, and excretion (ADME) profiling further revealed poor solubility (<0.5 μg/mL) and rapid metabolic degradation in primary mouse hepatocytes (PMHs), with less than 10% of parent compound remaining after 30 min of incubation. Consequently, compound **1** was deemed unsuitable for *in vivo* antitumor studies. We postulated that its high lipophilicity contributed to rapid metabolic turnover, while the ester group could represent a primary site for metabolic degradation. Accordingly, the hit-optimization campaign was focused on improving cellular permeability, metabolic stability, and solubility − properties critical for achieving single-agent efficacy in preclinical models − while preserving biochemical potency. A panel of derivatives was synthesized through iterative structure−activity relationship (SAR), with structures and associated data presented in Tables 1 and 2, and synthetic routes detailed in Schemes 1−3. CK2α inhibition was measured using an enzymatic assay based on the phosphorylation of a synthetic peptide substrate by recombinant full-length human CK2α at the ATP Michaelis−Menten

Table 1. Initial SAR of the ATP-Binding Site[ab]



	Substituent **R**	IC_{50} (μM)	K_D (μM)	Solubility (μg/mL)[a]	Stability PMHs (%)[b]	786-O IC_{50} (μM)
1		0.07	0.09	< 0.5	< 10	> 10
2		0.37	0.69	1.5	25	6.8
3		0.74	1.16	2.7	18	5.9
4		0.11	0.19	< 0.5	< 10	> 10
5		> 3	> 3	-	-	-
6		> 3	> 3	-	-	-
7		0.46	1.87	< 0.5	-	> 10
8		0.61	> 3	0.9	15	> 10
9		> 3	> 3	-	-	-
10		0.06	0.09	10.4	53	3.2

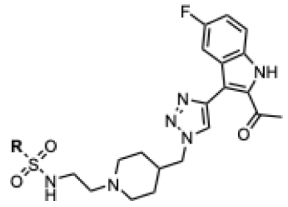
[a]Solubility was assessed in phosphate-buffered saline (PBS, pH 7.4). [b]Metabolic stability in primary mouse hepatocytes (PMHs) was evaluated after 30 min of incubation. All incubations were performed in duplicate.

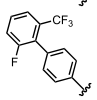
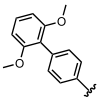
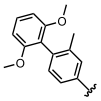
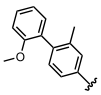
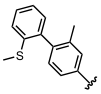
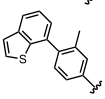
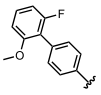
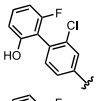
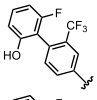
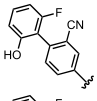
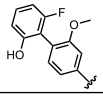
constant (Km 10 μM). In parallel, target engagement was assessed via the KINOMEscan platform, a competitive binding assay that quantifies ATP-independent thermodynamic interactions at the catalytic site. Dissociation constants (K_D) were incorporated into our SAR strategy to capture the full binding contribution of each compound, including interaction within the αD-pocket engagement, which may not be reflected in enzymatic IC_{50} values. Selected analogues were further profiled for aqueous solubility and metabolic stability in PMHs. Cell viability was evaluated in the 786-O cell line, a validated model for probing sensitivity to bivalent CK2α inhibition.[47]

SAR exploration began with modifications at the C2 and C5 substitutions of the indole ring in compound **1** (Table 1).

https://doi.org/10.1021/acs.jmedchem.5c00695
J. Med. Chem. XXXX, XXX, XXX−XXX

Table 2. SAR of the αD Pocket[ab]



	Substituent R	IC_{50} (μM)	K_D (μM)	Solubility (μg/mL)[a]	Stability PMHs (%)[b]	786-O IC_{50} (μM)
11		0.025	0.057	< 0.5	-	3.9
12		0.048	0.084	< 0.5	-	> 10
13		0.042	0.071	8.0	67	> 10
14		< 0.003	0.005	1.9	44	1.7
15		0.013	0.023	-	-	2.9
16		< 0.003	0.009	< 0.5	26	> 10
17		0.117	0.140	-	-	> 10
18		0.081	0.098	18.5	46	0.9
19		0.017	0.054	10.7	42	0.8
20		0.024	0.050	< 0.5	-	3.3
21		0.120	0.267	5.4	48	> 10
22		0.008	0.019	3.4	27	6.6
23		0.013	0.022	< 0.5	-	> 10
24		0.018	0.024	1.1	< 10	3.6
25		> 3	> 3	25.5	-	-
26		0.049	0.077	3.2	39	> 10

[a]Solubility was assessed in phosphate-buffered saline (PBS, pH 7.4). [b]Metabolic stability in primary mouse hepatocytes (PMHs) was evaluated after 30 min of incubation. All incubations were performed in duplicate.

Removal of either the isobutyl ester (**2**) or the fluorine atom (**3**) led to a pronounced 6−12-fold decrease in biochemical potency, indicating a functional of both substituents. To further probe steric and electronic effects within the ATP-binding pocket while maintaining the 5-fluoroindole core, we prioritized optimization at the C2 position (compounds **4**−**10**, Table 1). Structural insights from the X-ray complex of compound **1** revealed that the isobutyl ester was solvent-exposed, while the indole engages K68 indirectly via a hydrogen bond network mediated by a conserved water molecule (Figure 2b). Although the carbonyl group may stabilize the indole core, we questioned whether the appended aliphatic chain was essential for inhibitory activity. A truncated analogue (**4**), incorporating an ethyl 5-fluoroindole-2-carboxylate, retained CK2α binding activity (K_D 193 ± 14 nM) but exhibited poor metabolic stability (<10% parent compound remaining after 30 min in PMHs). In contrast, the carboxylic acid derivative **5** was inactive under identical conditions. Similarly, bulkier replacements such as a cyclic amide (**6**), cyclopropylethanone (**7**), 3-methylbutan-2-one (**8**), or 4-methylpentan-2-one (**9**) − led to complete loss of activity across all assays. To reduce lipophilicity while maintaining steric fit, we designed the acetyl analogue **10**, which preserved the activity of compound **1** and exhibited improved metabolic stability (53% remaining after 30 min), enhanced solubility (10.4 μg/mL), and acceptable cellular potency (786-O IC_{50} 3.2 μM). These results marked an initial milestone in the optimization campaign, combining target engagement with improved physicochemical properties.

Building on the established C2 substitution, we next focused on optimizing interactions within the hydrophobic αD pocket, as summarized in Table 2. The cocrystal structure of CK2α with compound **1**, alongside the closed *apo* structure (PDB 3WFQ), revealed a distinct side channel extending from the main pocket. This channel, characterized by structured water molecules,[48] was hypothesized to offer additional binding opportunities. In the closed conformation of the αD loop, residue Y125 occupies this channel (Figure 2b), suggesting that appropriately positioned groups could engage or displace these waters to enhance affinity. To test this, we synthesized a series of biphenyl derivatives with *ortho*-substituents (compounds **11**−**13**) on the phenyl ring directed toward the base of the αD pocket. Introduction of larger functional groups, such as *o*-trifluorotolyl (**11** and **12**) and *o*-dimethoxyphenyl (**13**) resulted in modest improvements (∼1.5-fold) in CK2α inhibitory potency relative to compound **10**. Further modification by incorporating a *para*-methyl group on the distal phenyl ring (**14**) led to a substantial increase in affinity (K_D 5.8 ± 0.4 nM), representing a 15-fold improvement over the derivative **10**. In contrast, reduced affinity observed for analogue **15** (K_D 23 ± 4 nM) may reflect subtle variations in biphenyl orientation, although this remains to be confirmed structurally. Replacement of the *o*-methoxy group with an *o*-methylthio substituent (**16**) further increased affinity, suggesting that the channel tolerates bulkier substituents. Conversely, introduction of a benzothiophene core (**17**) proved detrimental (K_D 140 ± 50 nM). Although compounds **11**−**16** displayed substantial improvements in biochemical potency

https://doi.org/10.1021/acs.jmedchem.5c00695
J. Med. Chem. XXXX, XXX, XXX−XXX

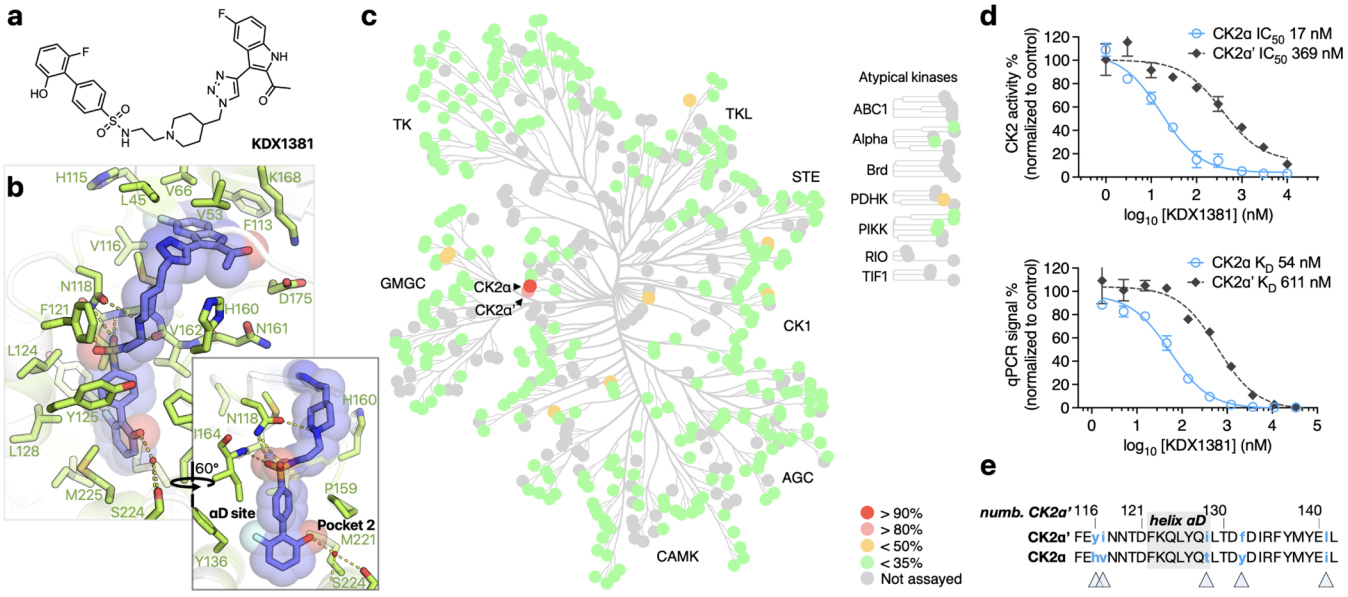


Figure 3. (a) Chemical structure of KDX1381. (b) Co-crystal structure of CK2α in complex with KDX1381 (PDB 9HPH). The inset highlights the inhibitor's occupancy within the αD pocket. Water molecules are depicted as red spheres, and hydrogen bonds are indicated by yellow dashed lines, emphasizing critical interactions stabilizing the inhibitor. (c) Kinase selectivity profile of KDX1381 at 5.0 μM, screened against 413 kinases using the Eurofins KinaseProfiler platform. ATP concentrations were individually adjusted to the Michaelis−Menten (Km) value of each kinase. Only CK2α and its isoform CK2α' exhibited >50% inhibition (red). Kinases inhibited by <35% are shown in green, those with 35−50% inhibition in orange, and kinases not included in the panel are denoted in gray. Data represent the mean of two independent experiments, visualized using CORAL.[49] Detailed percent inhibition values for each kinase are listed in Table S2. (d) Potency and affinity of KDX1381 for CK2α and CK2α' were assessed by enzymatic assays and KINOMEscan binding profiling. IC_{50} values were determined using human full-length CK2α or CK2α' and a synthetic peptide substrate at 10 μM ATP; K_D values were obtained via competitive binding assays. Results represent the mean of three independent experiments and are normalized to vehicle controls. (e) Aligned sequences of human CK2α' and CK2α covering the KDX1381 binding region, including the interdomain hinge and αD helix. Numbering (numb.) refers to CK2α' and CK2α residues are offset by −1. Identical residues are shown in capital letters; differences are indicated in lowercase blue with blue triangles. PDB, Protein Data Bank; qPCR, quantitative polymerase chain reaction.

and hepatocyte stability, gains in cellular activity were limited, likely due to increased hydrophobicity and poor solubility (Table 2). To address these limitations, we introduced a polar hydroxyl group (**18**), which combined potent CK2α inhibition (K_D 98 ± 15 nM) with submicromolar activity in 786-O cells (IC_{50} 0.91 μM) and improved aqueous solubility (18.5 μg/mL). Structural analysis (PDB 5OSL) revealed that the *o*-hydroxyphenyl moiety forms a hydrogen bond with a conserved water molecule within the side channel (Figure 2c, Pocket 2), potentially stabilizing ligand binding. Addition of fluorine (**19**) or chlorine (**20**) at the second *ortho*-position led to a ∼ 1.5−3-fold improvement in both biochemical and cellular potency compared to compound **10**. While derivative **19** retained favorable solubility (10.7 μg/mL), compound **20** showed a marked decrease (<0.5 μg/mL). Importantly, the *o*-hydroxyphenyl scaffold showed no evidence of phenol-driven metabolic instability; compound **19** exhibited hepatocyte stability comparable to ligand **10**. Likewise, replacement of the hydroxyl group by a *o*-methoxy moiety (**21**) had no significant impact on stability, suggesting that the hydroxyl was not the primary site of degradation (Table 2). To further explore αD pocket interactions, we modified the *para*-position of the distal phenyl ring. Substituents such as methyl (**22**), chloro (**23**), or trifluorotolyl (**24**) resulted in a ∼ 2-fold increases in CK2α binding affinity compared to compound **19**. However, despite these biochemical gains, analogues **22**−**24** failed to translate improvements into enhanced cellular activity. Attempts to introduce a polar group − nitrile (**25**) or methoxy (**26**) − were similarly unsuccessful, providing no clear benefit in potency or physicochemical properties. Modifications to the central linker region were not prioritized in this phase. Prior work had shown that altering the linker − by introducing a 1,2,3-triazole motif or modifying the piperidine core − could shift the binding mode between the CK2α/CK2β interface and the CK2α active site. However, such dual-targeting behavior was not aligned with our objectives of achieving selective CK2α inhibition via αD pocket engagement. As a result, compound **19** − renamed **KDX1381** (Figure 3a) following its selection for internal preclinical development − emerged as the first validated hit from our optimization campaign targeting the αD site-binding region. Inhibition of the CK2 holoenzyme ($\alpha_2\beta_2$) at 10 μM ATP yielded an IC_{50} of 60 ± 4.2 nM and an estimated inhibition constant (K_i) of 45.6 ± 3.8 nM, indicating slightly reduced potency compared to monomeric CK2α. Notably, **KDX1381** retained a binding affinity comparable to that of compound **1** (IC_{50} 67 ± 9 nM; K_i 51.8 ± 8.1 nM under identical conditions), supporting the classification of this scaffold series as high-affinity CK2α ligands. In contrast, **KDX1381** displayed improved solubility, enhanced metabolic stability, and superior antiproliferative activity in cell-based assays, supporting its advancement for further pharmacological development.

Characterization of KDX1381 as a Bivalent CK2α Inhibitor. The cocrystal structure of **KDX1381** bound to CK2α subunit was solved at 2.16 Å resolution by molecular replacement. Structural comparisons with compound **1** revealed a remarkably conserved binding mode (Figure 3b). The optimized biphenyl substituent of **KDX1381** effectively

https://doi.org/10.1021/acs.jmedchem.5c00695
J. Med. Chem. XXXX, XXX, XXX−XXX

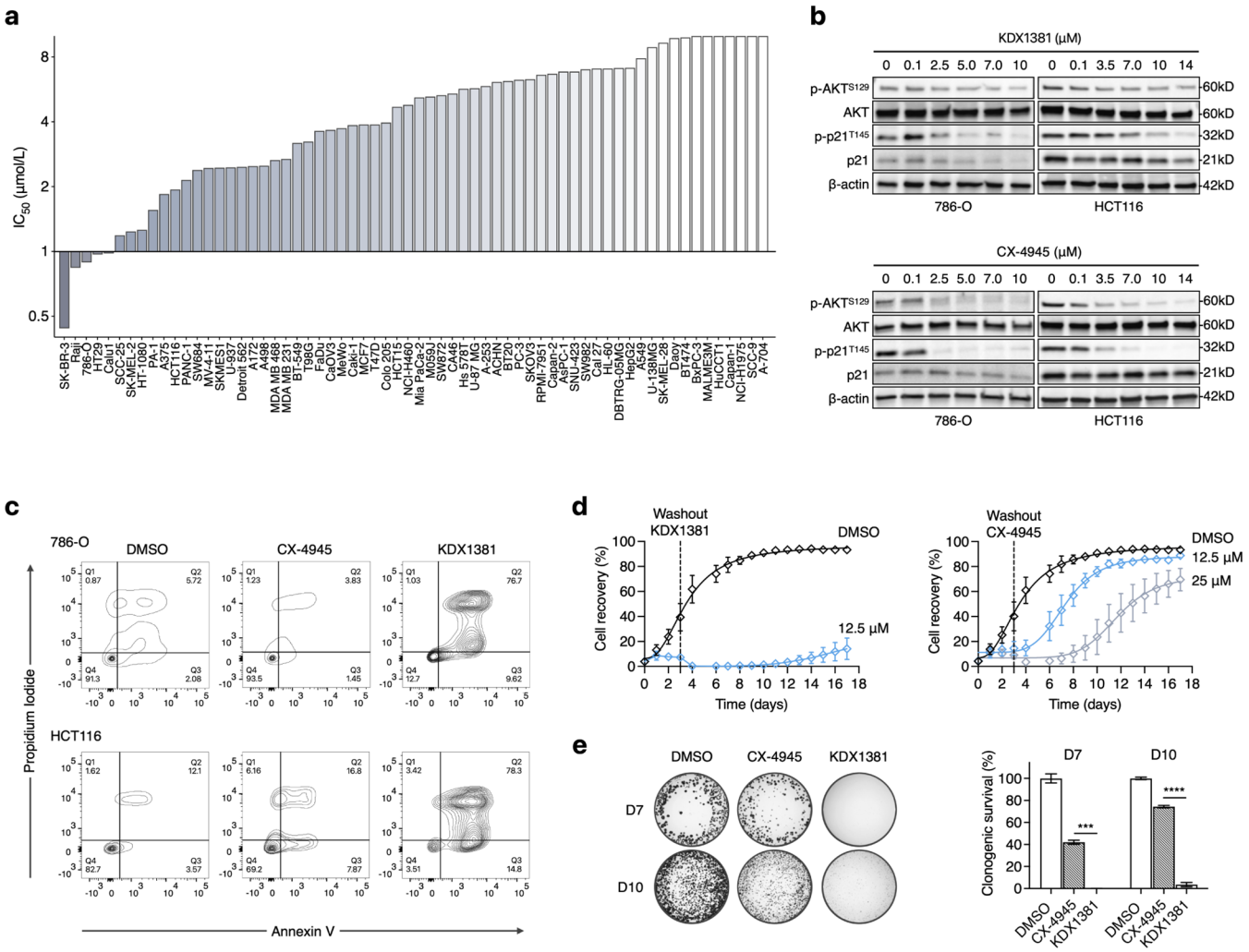


Figure 4. (a) Waterfall plot of IC_{50} values for KDX1381 across a panel of 64 cell lines from the OncoPanel collection. Each bar represents an individual cell line, color-coded based on the relative drug sensitivity observed after a 3-day treatment period. (b) Western blot analysis of CK2 pathway targets in 786-O (VHL mutant renal cancer) and HCT116 (PIK3CA mutant colorectal cancer) cells treated with KDX1381 or the reference CK2 inhibitor CX-4945 over a five-point dose range. Treatments were performed for 3 h, with results showing representative data from three independent experiments. (c) Flow cytometric analysis of cell death in 786-O and HCT116 cells treated with CK2 inhibitors (10 μM) for 3 days. Cells were stained with Annexin V and propidium iodide (PI), and representative dot plots illustrate the distribution of necrotic (Q1, Annexin V−/PI+), late apoptotic/necrotic (Q2, Annexin V+/PI+), early apoptotic (Q3, Annexin V^+/PI−), and viable (Q4, Annexin V−/PI−) populations. Classification is based on fluorescence intensity. (d) Long-term proliferation assays in HCT116 cells comparing the effects of KDX1381 and CX-4945. Cells were treated initially with each compound, and live-cell imaging was performed to monitor proliferation over time. Data are mean ± s.d. (n = 3). (e) Clonogenic survival assay in HCT116 cells. Cells were seeded at 1,000 or 5,000 cells/well for a 7- or 10-day regrowth period, respectively, and treated with CK2 inhibitors (KDX1381 or CX-4945) at their respective HCT116 IC_{50}, for 3 days. Following treatment, cells were replated in drug-free media, and colony formation was quantified after the respective regrowth periods. Survival fractions were normalized to dimethyl sulfoxide (DMSO)-treated controls. Data are mean ± s.d. (n = 2). Statistical significance was determined using one-way ANOVA followed by Dunnett's multiple comparisons test (***p < 0.001, ****p < 0.0001). D, day; s.d., standard deviation.

occupies the hydrophobic αD pocket, driving enhanced potency and selectivity for CK2α. As expected, the o-hydroxyphenyl moiety forms a hydrogen bond with the side chains of S224 and M221, mediated by a structured water molecule. On the opposite end of the bivalent inhibitor, the indole core anchors within the conserved ATP-binding site, with its 5-substituted phenyl group directed toward H115 and V116 in the hinge region. The C2 acetyl group is oriented toward a solvent-accessible region. Key linker interactions include engagement of the sulfonamide group with the backbone amides of V162 and I164, while the nitrogen atom of the piperidine ring forms a critical hydrogen bond with the side chain of N118. Binding of **KDX1381** induces a conformational shift in the αD-helix, altering the positions of F121 and Y125, as evidenced by elevated B-factor values for residues N118 to T127. These structural adaptations mirror those observed in the CK2α−compound **1** complex (Figure 2c). Kinome profiling across a panel of over 400 protein and lipid kinases confirmed the high selectivity of **KDX1381** for CK2α (Figure 3c). At a concentration ∼ 250-fold higher than its enzymatic CK2α IC_{50} (5.0 μM), substantial inhibition was observed only for the CK2α′ isoform (82%), with a few additional kinases showing residual activity close to 50% (Table S2). Although these values fall below standard thresholds for target engagement, their potential contribution under conditions of prolonged or elevated compound exposure

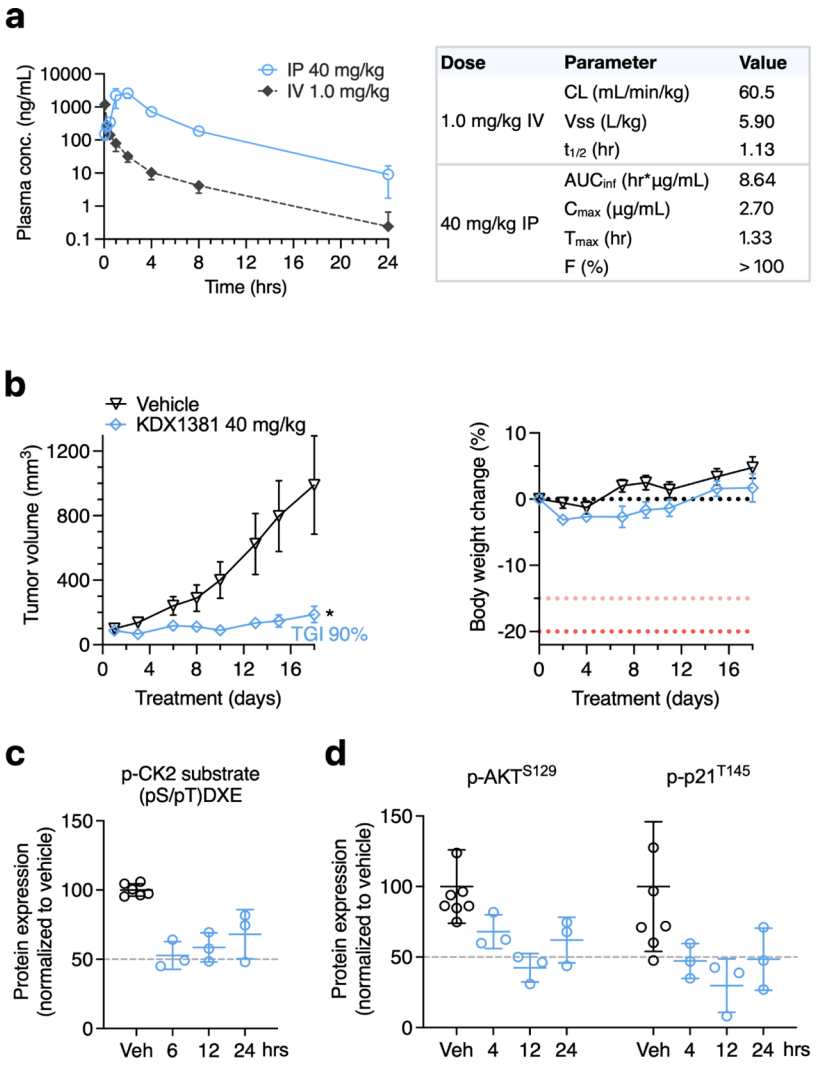
https://doi.org/10.1021/acs.jmedchem.5c00695
J. Med. Chem. XXXX, XXX, XXX−XXX

– such as *in cellulo* or *in vivo* – cannot be definitively excluded. In parallel, titration assays confirmed that **KDX1381** is ∼ 10-fold more potent toward CK2α than CK2α', with IC_{50} and K_D values exceeding 0.35 μM for the latter (Figure 3d). This reduced affinity likely reflects isoform-specific sequence differences that affect ligand recognition (Figure 3e). As previously noted, the indole moiety of **KDX1381** projects toward H115 and V116 in the CK2α hinge, which are substituted by Y116 and I117 in CK2α'. Although not directly involved in ligand binding, these residues may modulate local dynamics through side-chain variations. Additionally, I140 in CK2α – located near the αD pocket – is replaced by L141 in CK2α', potentially altering the binding environment further. Collectively, these subtle differences are through to contribute to the lower affinity observed for CK2α'.

Comprehensive genomic profiling of CK2α across diverse human cancers, based on RNA sequencing (RNa-seq) data sets from The Cancer Genome Atlas (TCGA), reveals widespread dysregulation of CK2α-associated genes in oncogenic contexts (Figure S1), consistent with several prior reports.,[6,8,11] In light of this observation, **KDX1381** was further evaluated in cell viability assays using an extensive panel of human cancer cell lines from the OncoPanel collection (Eurofins), representing a spectrum of oncogenic signaling landscapes. Cancer cell lines were exposed to **KDX1381** across a ten-point dilution series starting at 10 μM, and cell viability was assessed to calculate IC_{50} values. Among the 64 cell lines tested, 66% demonstrated intermediate sensitivity with IC_{50} values ranging from 2.0 to 8.0 μM, 17% exhibited high sensitivity with IC_{50} values below 2.0 μM, and the remaining 17% were classified as insensitive, with IC_{50} values exceeding 8.0 μM (Figure 4a). These findings establish **KDX1381** as a member of a novel class of antitumor agents, with a spectrum of activity across diverse cancer cell lines. However, no definitive correlation has been established between CK2α protein levels and antiproliferative efficacy in this preliminary screening. Among solid tumors, the over-expression of CK2α is associated with various related processes in colorectal carcinoma (CRC), hepatocellular carcinoma (HCC), and renal cell carcinoma (RCC). In CRC, CK2α supports tumor proliferation and invasion by stabilizing β-catenin, thereby amplifying the Wnt/β-catenin signaling cascade – a hallmark of CRC driven by APC or CTNNB1 mutations.[50,51] In HCC, CK2α stabilizes AKT and promotes its activity. This dual effect enhances cell survival and suppresses pro-apoptotic signaling, contributing to both tumor progression and chemotherapeutic resistance.[52] In RCC, CK2α significantly augments vascular endothelial growth factor receptor (VEGFR)-driven angiogenesis, particularly in the context of von Hippel-Lindau tumor suppressor (VHL) mutations that disrupt hypoxia-inducible factor (HIF) regulation. By amplifying HIF-dependent signaling, CK2α facilitates tumor vascularization and growth.[53,54] Notably, **KDX1381** demonstrated comparable or superior effects on cell viability relative to standard kinase inhibitors commonly used in colon, liver, and renal cancer models, reinforcing its potential as a targeted therapeutic agent for tumors driven by CK2α dysregulation (Table S3). Given CK2's critical role in the regulation of the PI3K/AKT signaling pathway,[55] evidence supporting the efficacy of **KDX1381** as a CK2α inhibitor was demonstrated in 786-O renal cancer cells, characterized by VHL loss-of-function mutations, and HCT116 colorectal cancer cells harboring an activating phosphatidylinositol-4,5-bisphosphate 3-kinase catalytic subunit alpha (PIK3CA) mutation. Specifically, after a 3-h treatment with **KDX1381**, a concentration-dependent inhibition of CK2 signaling was observed, as evidenced by reduced phosphorylation levels of p-AKT^{S129} and its downstream effector p-$p21^{T145}$. These profiles mirror those reported for the clinical candidate **CX-4945**, although the ATP-competitive inhibitor produced a more pronounced decrease in AKT and p21 phosphorylation (Figure 4b). This outcome likely reflects the broader kinase engagement of **CX-4945** and its similar potency toward both CK2α isoforms, which together could contribute to more extensive suppression of CK2 enzymatic activity. However, this response appears to be phenotype-dependent, as **KDX1381** elicited greater inhibition of CK2-relevant phosphorylation events than **CX-4945** in the Hep3B model (Figure S2). Building on prior evidence that bivalent CK2α inhibition impacts cancer cell survival,[47] we investigated whether treatment with **KDX1381** could promote cell death. Human cancer cell lines 786-O and HCT116 were treated with either **KDX1381** or **CX-4945** at equivalent concentrations, and cell death was assessed using Annexin V and propidium iodide (PI) staining, followed by flow cytometric analysis. Notably, **KDX1381** triggered marked cancer cell death – a response not observed with **CX-4945** under the same conditions (Figure 4c). Importantly, **KDX1381** may modulate specific CK2-regulated pathways implicated in tumorigenesis through its bivalent binding mode, thereby contributing to the observed cytotoxic effects – consistent with prior findings for its precursor, compound **1**. Comparative analyses support a mechanistic association between bivalent CK2α inhibition and cancer cell death induction (Figure S2). Nonetheless, while bivalent inhibitors demonstrate a clear cytotoxic potential, it remains to be determined whether the antitumor activity of **KDX1381** at the tested concentrations results exclusively from CK2α inhibition or also involves additional molecular interactions. To further investigate the contribution of CK2α inhibition to cancer cell persistence, we next assessed the sustained proliferative capacity of treated cells. In long-term proliferation assays monitored via live-cell imaging, **KDX1381** exhibited sustained inhibition of cell recovery for over 15 days following compound washout, a striking contrast to the modest delay in cell proliferation induced by **CX-4945** even at concentrations exceeding 20 μM (Figure 4d). Long-term clonogenic survival assays were conducted to assess the effects of **KDX1381** and **CX-4945** on colony formation in various cancer models. Remarkably in the HCT116 cells, treatment with **KDX1381** abrogated colony formation, regardless of initial cell density (Figure 4e). Similar results were obtained in both the renal 786-O and murine RENCA models (Data not shown), further supporting the robust antitumor activity of **KDX1381** in various contexts.

Several cancer models exhibit strong dependence on CK2 activity to sustain proliferation and survival. Conversely, residual activity from a truncated CK2α' isoform was found to support viability in nontransformed clones.[14] This observation suggests that a minimal threshold of CK2 function may suffice to maintain basal cellular processes in normal tissues. To investigate this selectivity, we assessed the effects of **KDX1381** in the 786-O renal carcinoma cell line and in nonmalignant renal proximal tubule epithelial cells (RPTECs). While **KDX1381** markedly impaired cancer cell viability, no cytotoxicity was observed in RPTECs, even at the highest concentration tested (20 μM). Likewise, primary human hepatocytes showed no evidence of toxicity in response to

https://doi.org/10.1021/acs.jmedchem.5c00695
J. Med. Chem. XXXX, XXX, XXX–XXX



Dose	Parameter	Value
1.0 mg/kg IV	CL (mL/min/kg)	60.5
	Vss (L/kg)	5.90
	$t_{1/2}$ (hr)	1.13
40 mg/kg IP	AUC_{inf} (hr*μg/mL)	8.64
	C_{max} (μg/mL)	2.70
	T_{max} (hr)	1.33
	F (%)	>100

Figure 5. (a) Plasma concentration profiles of KDX1381 were assessed in CD-1 mice following intravenous (IV) administration at 1.0 mg/kg and intraperitoneal (IP) administration at 40 mg/kg. Plasma samples were collected at predefined intervals (0.083, 0.25, 0.5, 1, 2, 4, 8, 12, and 24 h postdosing), and concentrations were quantified, with values expressed as mean ± s.d. (n = 3/time point). (b) Antitumor efficacy of KDX1381 was assessed in 786-O xenografts. Body weight changes across all groups remained below the 10% threshold throughout the study, confirming tolerability. Data are shown as mean ± s.e.m. and were analyzed using two-tailed Student's t test (*p = 0.0146; n = 8 mice/group). (c, d) Pharmacodynamic evaluation in 786-O tumor-bearing mice treated with a single IP dose of KDX1381 (40 mg/kg) showed time-dependent inhibition of CK2α pathway activity. Immunoblot analyses of phosphorylated targets in tumor lysates (n = 6 or 8 mice for vehicle control; n = 3 mice for treated groups) were quantified by densitometry, normalized to vehicle controls. Data are reported as mean ± s.d. AUCinf, area under the curve; CL, clearance; Cmax, maximum plasma concentration; F, bioavailability; hrs, hours; s.d., standard deviation; s.e.m., standard error of the mean; $t_{1/2}$, terminal half-life; TGI, tumor growth inhibition; Veh, vehicle; Vss, steady-state volume of distribution.

KDX1381 exposure (Figure S3). Although on-target effects in nontransformed cells cannot be ruled out, these findings indicate that **KDX1381** exerts antiproliferative effects in a tumor-selective manner that are not attributable to nonspecific cytotoxicity.

Bivalent CK2α Inhibitor Displays Antitumor Activity in Mice. **KDX1381** exhibits a pH-dependent solubility profile, characterized by moderate solubility under simulated gastric conditions (28.2 μg/mL at pH 1.0), substantially enhanced dissolution in an intestinal-like environment (>100 μg/mL at pH 6.5), and a pronounced decrease at physiological pH (10.7 μg/mL, in phosphate-buffered saline (PBS), pH 7.4) (Table S4). Stability assessments confirmed the compound's robust integrity, with no degradation observed following 24 h of incubation in PBS at 37 °C. Conversely, minimal degradation occurred upon exposure to 0.1 N hydrochloric acid (HCl) at pH 1.0, where 98% of the compound remained intact after 24 h. The anhydrous crystalline form of **KDX1381** exhibits a melting point between 237 and 240 °C, alongside a high crystal lattice energy of −96 J/g, indicative of a well-ordered crystalline structure (Figure S4). Formulation screening revealed that **KDX1381** demonstrates moderate solubility (~25 mg/mL) in high hydrophilic−lipophilic balance (HLB) surfactants, such as Cremophor EL, polysorbate 20, and 80, as well as the hydrophilic solvent polyethylene glycol. Conversely, its solubility in lipid-based media and low-HLB surfactants was poor (<1.0 mg/mL) (Table S5). These findings guided the selection of micellar formulation prototypes as the most appropriate strategy for subsequent *in vivo* studies. To assess the suitability of **KDX1381** as a candidate for antitumor efficacy studies, its ADME and pharmacokinetic (PK) properties were evaluated (Figure 5a). In the MDR1-

https://doi.org/10.1021/acs.jmedchem.5c00695
J. Med. Chem. XXXX, XXX, XXX−XXX

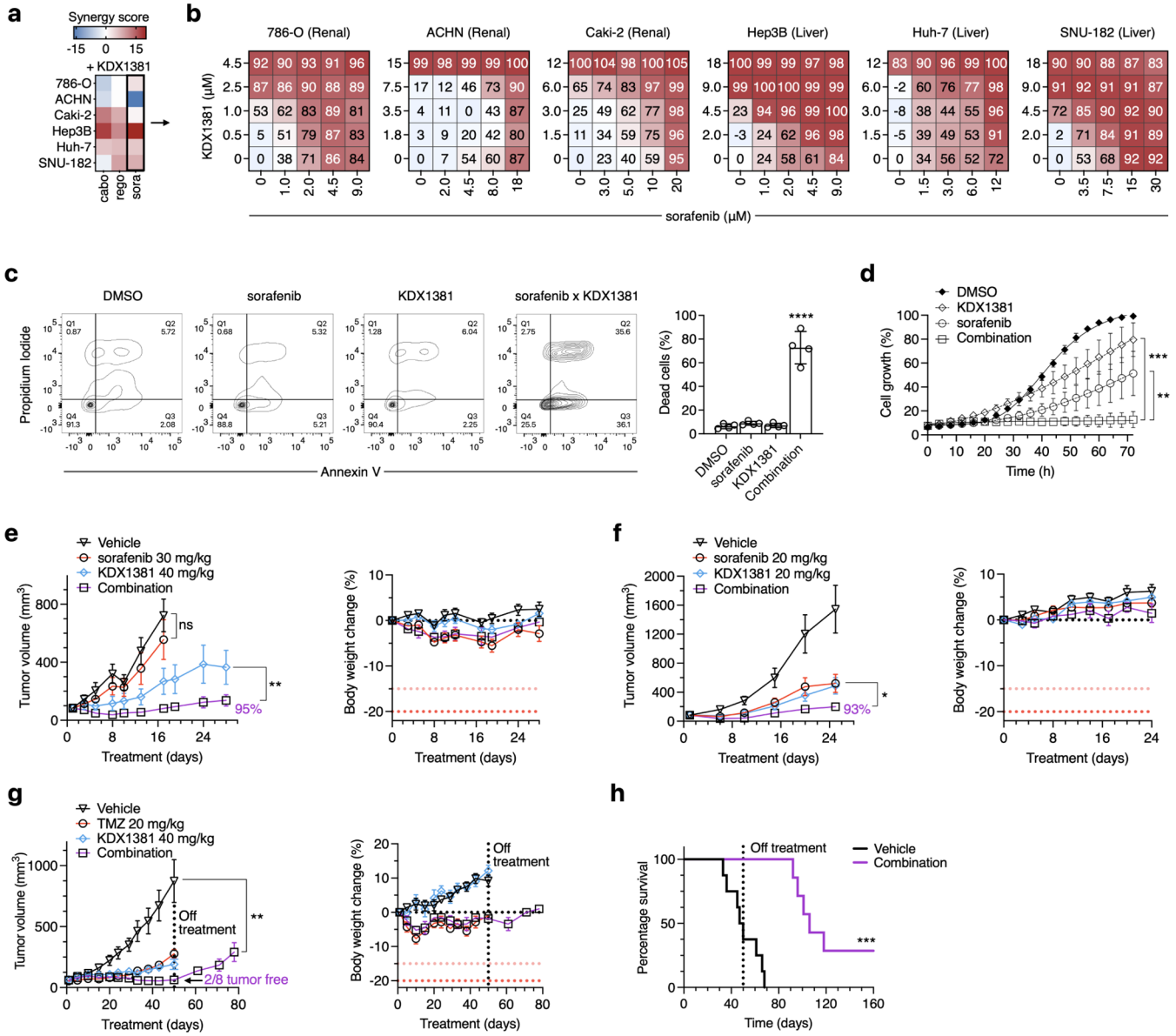


Figure 6. (a) Synergy scores for KDX1381 in combination with cabozantinib (cabo.), regorafenib (rego.), or sorafenib (sora.) are visualized as a heat map, where higher scores (darker red) indicate stronger synergy. (b) Heat maps illustrate KDX1381−sorafenib interactions. After a 3-day incubation period, cell viability (%) was measured and normalized against dimethyl sulfoxide (DMSO)-treated controls. Redder shades indicate grater reductions in viability. (c, d) Flow cytometric analysis (c) and proliferation assays (d) of 786-O cells following 3-day treatment with sorafenib (4.5 μM), KDX1381 (1.0 μM), or their combination. For the cell death assay, cells were stained with Annexin V and propidium iodide (PI), and representative dot plots illustrate the distribution of necrotic (Q1, Annexin V−/PI+), late apoptotic/necrotic (Q2, Annexin V+/PI+), early apoptotic (Q3, Annexin V^+/PI−), and viable (Q4, Annexin V−/PI−) populations. Classification is based on fluorescence intensity. Proliferation was monitored in real-time via live-cell imaging. Data are mean ± s.d. (n = 4) and statistical significance was determined using one-way ANOVA followed by Dunnett's multiple comparisons test (***p < 0.001, ****p < 0.0001). (e, f) Tumor growth inhibition was evaluated in response to treatment with sorafenib, KDX1381 or their combination in mice bearing (e) Hep3B and (f) 786-O xenografts (n = 8 mice/group). Data are mean tumor volume ± s.e.m., with combination treatment demonstrating statistically significant inhibition compared to KDX1381 monotherapy, as analyzed by a two-tailed Student's t test (*p < 0.05, **p < 0.01). (g) Tumor growth inhibition in SF-767 xenografts was evaluated following treatment with temozolomide (TMZ), KDX1381, or their combination (n = 8 mice/group). Data are mean tumor volume ± s.e.m. Tumor volumes for the combination group were statistically significant versus KDX1381 single agent using a two-tailed Student's t test (**p < 0.01). (h) Treatments were discontinued on day 48, and survival was monitored until tumor volumes reached 800 mm^3. Statistical differences in survival between the combination arm and the control group were evaluated using the log-rank (Mantel−Cox) test. (***p < 0.001). s.d., standard deviation; s.e.m., standard error of the mean.

transfected LLC-PK1 cell permeability assay, **KDX1381** displayed limited permeability, suggesting potential challenges in intestinal absorption. Following intravenous (IV) administration of **KDX1381** at 1.0 mg/kg in CD-1 mice, the compound exhibited a clearance (CL) of 60.5 mL/min/kg, approaching the hepatic blood flow in this species and consistent with extensive first-pass metabolism. However, its high plasma protein binding (99.1%) substantially limited the fraction of unbound drug available for hepatic extraction. The observed terminal half-life ($t_{1/2}$) of 1.13 h is thus largely

https://doi.org/10.1021/acs.jmedchem.5c00695
J. Med. Chem. XXXX, XXX, XXX−XXX

determined by this strong binding, together with a moderate-to-high steady-state volume of distribution (Vss 5.90 L/kg), indicative of significant extravascular partitioning. Collectively, these properties contribute to a systemic exposure profile that remains prolonged relative to the compound's clearance capacity.[56] Following oral administration (PO) at 100 mg/kg, **KDX1381** reached a peak plasma concentration (Cmax) of 0.26 μg/mL and exhibited low bioavailability (F 8%) (Figure S5). Given this limited systemic exposure, efficacy studies were pursued using intraperitoneal (IP) administration. At 40 mg/kg IP, the compound was fully absorbed, yielding a Cmax of 2.70 μg/mL (~5.4 μM total plasma concentration) and an area under the curve (AUCinf) of 8.64 μg·h/mL. As free plasma concentrations remained below the *in vitro* IC_{50} range, and considering the short terminal half-life, a single administration was not expected to maintain pharmacologically active exposure over 24 h. A twice-daily (BID) dosing schedule was therefore adopted to sustain robust target engagement throughout the dosing interval and support *in vivo* efficacy.

The antitumor efficacy and tolerability of **KDX1381** were first assessed in immunocompromised mice bearing 786-O tumor xenografts (Figure 5b). Once tumors reached ~ 100 mm^3, animals were randomized and treated BID with either vehicle or **KDX1381** at 40 mg/kg. Tumors in the control group grew without restriction, while **KDX1381** treatment resulted in a striking 90% tumor growth inhibition (TGI) after three treatment cycles. Importantly, no signs of toxicity, including weight loss or adverse clinical symptoms, were observed throughout the treatment period, underscoring the favorable tolerability of **KDX1381**. Pharmacodynamic analysis of 786-O tumors excised following a single IP dose of **KDX1381** (40 mg/kg) revealed a time-dependent attenuation of CK2 signaling. Immunoblot analysis using a phospho-substrate antibody recognizing the canonical CK2 consensus motif (phospho-Ser/Thr-D/E-X; [(pS/pT)DXE]), demonstrated a ~ 40% reduction in global CK2-mediated phosphorylation at 6- and 12 h postdose, with suppression remaining evident at 24 h (Figure 5c). In parallel, phosphorylation of known CK2 targets, p-AKT^{129} and p-$p21^{T145}$, was reduced following a single administration, with maximal suppression observed at 12 h and partial recovery by 24 h (Figure 5d). To extend these findings, **KDX1381** was tested in $BRAF^{V600E}$ mutant A375 xenografts, a melanoma model driven by a common oncogenic kinase mutation. Twice-daily administration (5.0 or 40 mg/kg) was well tolerated and led to dose-dependent tumor growth inhibition (Figure S5).

Bivalent CK2α Inhibitor Improves Efficacy of Targeted Agents. As CK2α expression is instrumental in driving oncogenic pathways and regulating essential processes that support tumor survival, we reasoned that combining **KDX1381** with other targeted therapies could enhance tumor cell eradication. To evaluate potential additive or synergistic effects, we conducted a 3-day *in vitro* viability screen using a focused set of compounds targeting key cancer-related signaling nodes across a panel of cancer cell lines. These compounds were selected for their relevance to CK2-dependent signaling pathways and their established clinical use in the systemic treatment of colorectal, hepatocellular, and renal cancers. All combinations were initially tested using dose–response matrices of **KDX1381** and inhibitors, each in technical triplicate. A heterologous compound combination (AxB) was considered synergistic only if its synergy scores significantly exceeded those of both the individual self-crosses (AxA and BxB), as determined by the Loewe additivity model.[57,58] In this analysis, inhibitors of the VEGFR family – specifically cabozantinib, regorafenib, and sorafenib – demonstrated synergy with **KDX1381** in a significant proportion of the evaluated cell lines (Figure 6a, b). To further elucidate the underlying mechanisms of the observed reductions in cell viability, we assessed whether these effects were driven by enhanced cell death or a reduction in cell proliferation. Exemplified here with sorafenib (Figure 6c), flow cytometry-based Annexin V and PI staining revealed a marked synergistic induction of cell death with the combination of **KDX1381** and VEGFR-tyrosine kinase inhibitors (TKIs), even at subtherapeutic concentrations where individual agents exhibited negligible activity. In contrast, live-cell imaging studies assessing recovery demonstrated substantial activity of the VEGFR inhibitor as individual treatment, with modest cooperative effects upon combination (Figure 6d). This dichotomy underscores that the observed synergy is primarily driven by enhanced cell death rather than by cumulative cytostatic effects. Mechanistically, combination treatment elicited a sustained modulation of AKT and p21 phosphorylation, with changes significantly surpassing those induced by either agent alone (Figure S6). VEGFR-TKIs, while integral in the management of HCC and RCC, frequently demonstrate limited durability due to acquired resistance, often mediated by activation of the PI3K/AKT signaling axis.[59,60] Protein p21 plays a central role in RCC resistance,[61] acting via cytoplasmic sequestration of pro-caspase-3 (CASP3) and other apoptotic mediators. Notably, p21 phosphorylation at T145 by AKT enhances its cytoplasmic retention, amplifying its antiapoptotic properties and compounding therapeutic resistance.[62] These findings suggest that concurrent inhibition of AKT and p21 by **KDX1381** offers a mechanistic rationale for its synergy with VEGFR-targeted therapies. To evaluate the therapeutic potential of this combination, an *in vivo* study was conducted using subcutaneous Hep3B xenografts. Once tumors reached ~ 90 mm^3, mice were treated for 28 days with either vehicle, sorafenib, **KDX1381**, or combination sorafenib plus **KDX1381**. Sorafenib was administered at 30 mg/kg once daily (QD), a regimen calibrated to achieve exposures comparable to the standard clinical dose of 400 mg BID.[63] After four treatment cycles, the combination arm demonstrated superior antitumor activity, achieving a TGI of 95%, significantly prolonging time to end point compared to either monotherapy (Figure 6e). Sorafenib alone exhibited modest efficacy with 29% TGI, while **KDX1381** showed a moderate response (74% TGI). Crucially, no significant weight loss was observed across treatment groups, emphasizing the tolerability of these regimens. The combinatorial advantage was further validated in a second 786-O RCC xenograft model (Figure 6f). Here, the combination of sorafenib plus **KDX1381** yielded markedly stronger and more sustained tumor suppression than either agent alone. Notably, to delineate the specific contribution of each component, suboptimal doses of sorafenib and **KDX1381** were employed, demonstrating that their efficacy extends across a range of dosages. Encouraged by its promising activity, we hypothesized that **KDX1381** could potentiate the efficacy of standard-of-care (SOC) chemotherapeutics. CK2's established role in coordinating multiple DNA repair pathways provides a strong mechanistic basis for such combinations.[18] This rationale is supported by prior clinical data, including a Phase IB study (NCT02128282) demonstrating synergistic antitumor activity between **CX-4945**

https://doi.org/10.1021/acs.jmedchem.5c00695
J. Med. Chem. XXXX, XXX, XXX–XXX

and the DNA-damaging agents gemcitabine and cisplatin. Given the prevalence of chemoresistance in cancer, identifying effective combination regimens and predictive biomarkers remains a priority. To explore this, we evaluated the combination of **KDX1381** with a panel of chemotherapeutics, including cisplatin, fluorouracil, oxaliplatin, and temozolomide (TMZ), using the same methodology previously employed with VEGFR-TKIs. Notably, TMZ and **KDX1381** demonstrated robust synergistic cytotoxicity across multiple glioblastoma multiforme (GBM) and glioma cell lines. While TMZ effectively impaired cell viability in A172 and SF767 glioma cells, it failed to fully eliminate the tumor cell population. In contrast, combining TMZ with **KDX1381** achieved a more sustained tumoricidal effect, indicating enhanced therapeutic potential (Figure S6). Building on these findings, the combination of TMZ and **KDX1381** was further evaluated *in vivo* using a subcutaneous SF-767 xenograft model (Figure 6g). **KDX1381** was administered at 40 mg/kg BID and was combined with the maximum tolerated dose of TMZ in mice (20 mg/kg, administered three times weekly). After 48 days of treatment, TMZ monotherapy achieved significant tumor growth inhibition (67% TGI), although moderate tumor regrowth occurred following cessation of therapy. **KDX1381** alone demonstrated slightly greater activity compared to TMZ, achieving 77% TGI by day 48 (D48), but similarly showed tumor regrowth post-treatment. Strikingly, the combination arm achieved complete tumor growth inhibition (103% TGI) at D48, with tumor volumes reduced by more than 50% relative to baseline. Notably, two animals in the combination group exhibited complete tumor regression, remaining tumor-free at the study end point (D160; Figure 6h). While moderate regrowth was observed in other combination-treated mice after drug withdrawal, the durability of the response in these two animals highlights the potential for achieving long-term disease control. Throughout the study, no significant body weight changes were observed across treatment groups, indicating that the combination was well-tolerated at the administered doses and schedules.

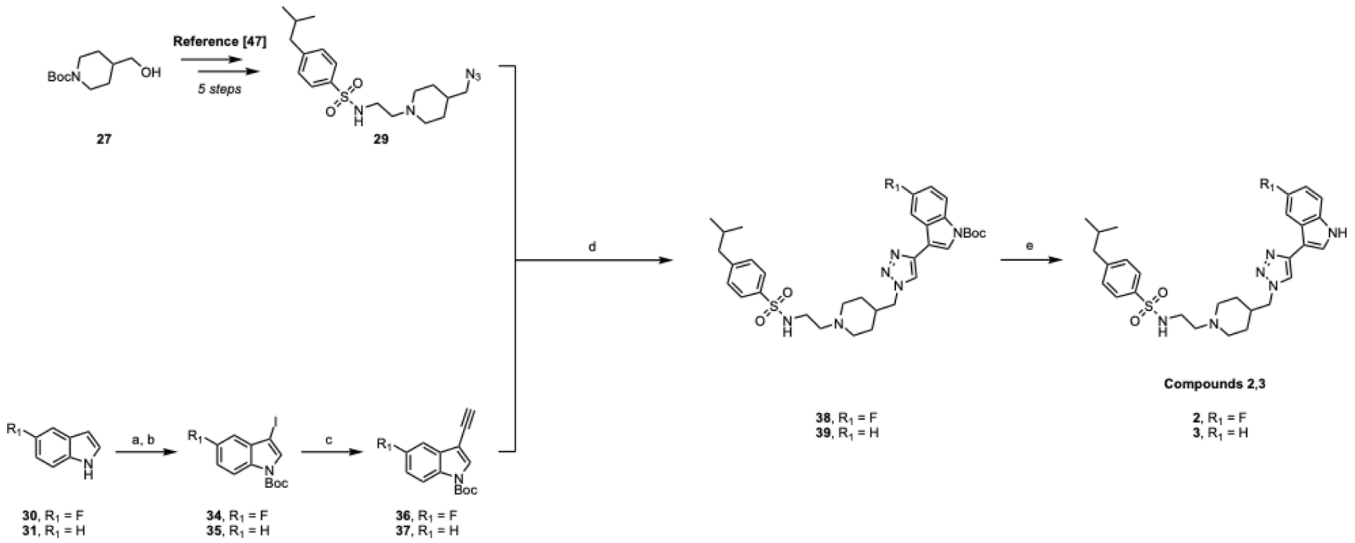
CONCLUSIONS

This study reports the discovery and preclinical characterization of **KDX1381**, a bivalent CK2α inhibitor derived from rational SAR optimization of the chemical probe **AB668**. Efforts focused on improving solubility and metabolic stability, resulting in a compound with 10- to 15-fold greater cellular potency than its predecessor. Co-crystal structures confirmed selective engagement of CK2α, and **KDX1381** modulated CK2 signaling in a concentration-dependent manner across multiple tumor cell lines. Treatment modulated the PI3K/AKT axis − a key oncogenic driver in solid tumors − and was associated with pronounced cell death and reduced malignant regrowth. Compared to **CX-4945**, a clinical-stage ATP-competitive CK2 inhibitor, **KDX1381** demonstrated improved efficacy in relevant models, suggesting a differentiated pharmacological profile. Notably, **KDX1381** impaired the viability of cancer cells while sparing nontransformed counterparts, supporting a selective mode of action. It further distinguishes itself from earlier bivalent CK2 inhibitors[44−47] through improved physicochemical and PK properties that enable *in vivo* evaluation. Intraperitoneal dosing at 40 mg/kg achieved sufficient systemic exposure to induce robust tumor growth inhibition (TGI, 70−90%) as monotherapy across multiple xenograft models, including glioma, HCC, and RCC. Importantly, the time-dependent suppression of CK2 signaling observed in tumor tissues supports an on-target activity of **KDX1381** in mice. The compound was well tolerated and potentiated the efficacy of SOC therapies − including VEGFR-TKIs and DNA-damaging agents − leading to durable responses beyond the treatment period. Collectively, these results represent an initial preclinical validation for selective bivalent CK2α inhibition as a therapeutic strategy. Nonetheless, given the reliance on micromolar exposures and the broad involvement of CK2 in survival signaling, the contribution of additional pharmacological interactions with **KDX1381** at higher concentrations cannot be excluded and warrants further mechanistic dissection. To that end, validation using inactive analogues or engineered resistance models would help clarify CK2 dependency and refine the therapeutic rationale. Evaluation in immunocompetent models is also justified to determine whether bivalent CK2α inhibition can elicit immunogenic responses. While **KDX1381** exhibits promising activity, its PK profile− specifically limited oral bioavailability and rapid clearance in mice − remains a limitation for broader preclinical investigation. Further optimization to improve drug-like properties is ongoing and will be reported in due course.

Chemistry Details. The synthetic strategies employed to construct the 1,2,3-triazole-based inhibitors are depicted in Schemes 1−3. These compounds were synthesized via a convergent sequence involving copper-catalyzed azide−alkyne cycloaddition ("click" reaction)[64] between two key precursors: azide analogs and heteroaryl alkynes. Scheme 1 outlines the synthesis of inhibitors **2** and **3**, starting from intermediate **29**, which was derived from *tert*-butyloxycarbonyl (Boc)-4-piperidinemethanol (**27**).[47] Conversely, the preparation of advanced intermediates **36** and **37**, began with iodination of commercially available precursors **30** and **31** under basic conditions. Potassium hydroxide (KOH) was employed to activate the heterocyclic ring, facilitating the formation of iodinated intermediates. To enhance stability and reactivity, a Boc protecting group was introduced. The resulting derivatives **34** and **35** were subjected to a Sonogashira[65] coupling with trimethylsilylacetylene (TMSA) under standard conditions, with bis(triphenylphosphine)palladium(II) chloride and copper(I) iodide as catalysts with an excess of triethylamine (TEA). Subsequent deprotection of the trimethylsilyl group using tetra-*n*-butylammonium fluoride (TBAF) afforded the desired terminal alkynes. The 1,3-dipolar cycloaddition reactions with azide **29** and heteroaryl derivatives **36** or **37**, were catalyzed *in situ* using Cu(II) salts reduced with sodium ascorbate, affording inhibitors **2** and **3** after Boc deprotection under basic conditions. Scheme 2 describes the derivation of C2-functionalized indole analogues **41**, **42**, and **44** from 5-fluoro-1*H*-indole-2-carboxylic acid (**40**). The ester derivative **41** was synthesized under Mitsunobu reaction conditions,[66] whereas intermediate **42** was obtained via amidation using hexafluorophosphate azabenzotriazole tetramethyl uronium (HATU) in the presence of pyrrolidine. A two-step sequence was employed to introduce the acetyl group at C2: Weinreb amidation yielded intermediate **43**, followed by reduction with methyllithium to furnish the methyl ketone **44**. In a parallel pathway, 5-fluoroindole (**31**) was tosyl-protected to yield intermediate **45**, which was then treated with *n*-butyllithium (*n*-BuLi). The resulting lithium anion was subsequently reacted with alkyl aldehydes, affording alcohol derivatives **46**, **47**, and **48**. These intermediates were deprotected under basic

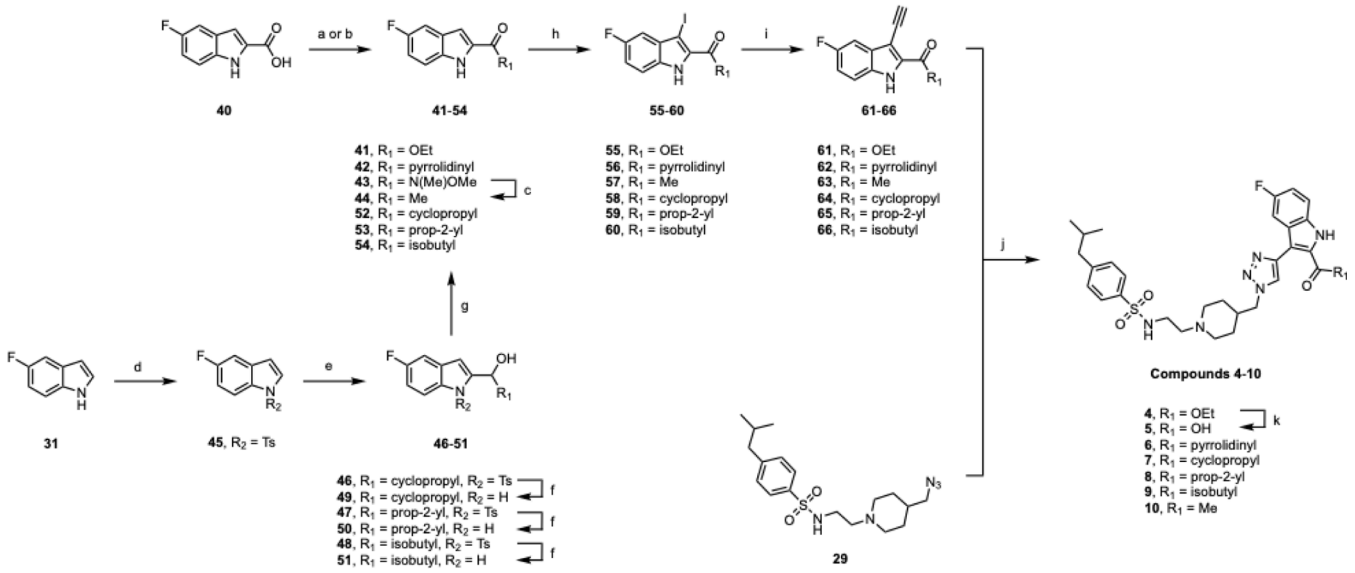
https://doi.org/10.1021/acs.jmedchem.5c00695
J. Med. Chem. XXXX, XXX, XXX−XXX

Scheme 1. Synthesis of Compounds 2 and 3[a]



[a]*Reagents and conditions: (a)* I_2, KOH, DMF, rt, 1−3h; (b) Boc_2O, 10 mol % DMAP, DCM, rt, 1h; (c) 2 mol % $PdCl_2(PPh_3)_2$, 4 mol % CuI, TMSA, THF, rt, 6−12h then 1M TBAF, THF, 0°C to rt, 0.5−1h; (d) 5 mol % $CuSO_4.5H_2O$, 10 mol % Na ascorbate THF/H_2O/*t*-BuOH (3:1:1), rt, 6−12h; (e) K_2CO_3, MeOH, rt, 12h

Scheme 2. Synthesis of Compounds 4−10[a]

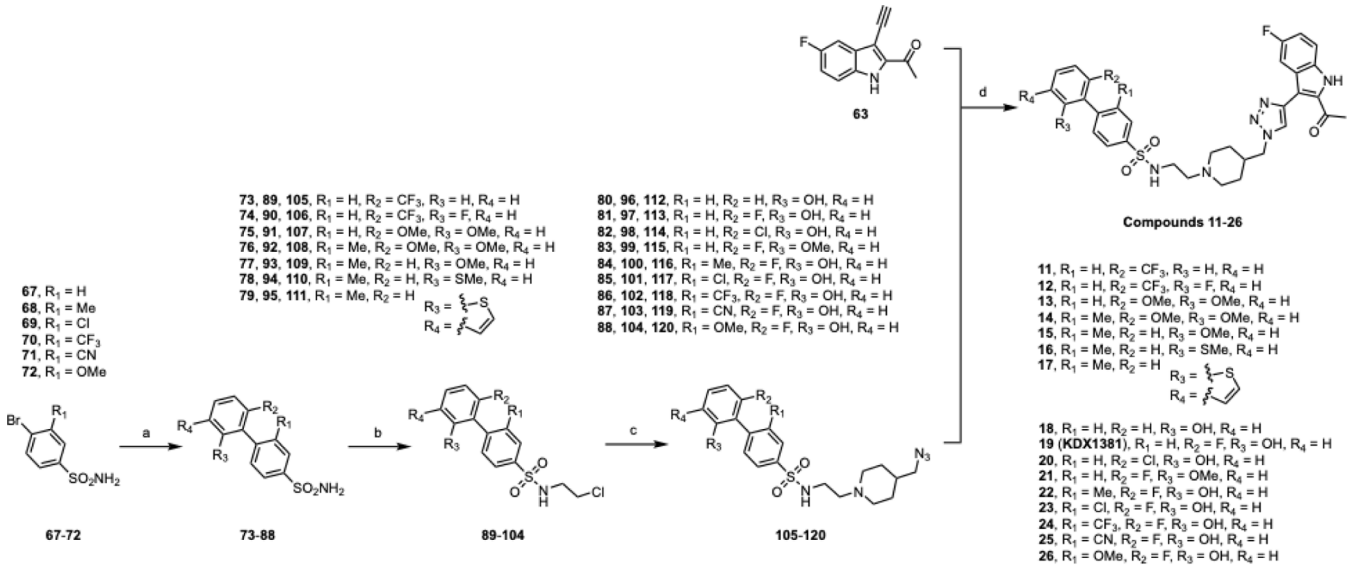


[a]*Reagents and conditions: (a) EtOH, PPh*$_3$, DIAD, THF, 0°C to rt, 48h or pyrrolidine, DIPEA, HATU, DMF, rt, 18h; (b) *N*,O-dimethylhydroxylamine hydrochloride, DIPEA, EDCI, 10 mol % DMAP, DCM, 0°C to rt, 18h; (c) MeLi, Et_2O, THF −78°C, 3h; (d) TsCl, NaH, THF, 0°C, 0.5h then rt, 18h; (e) *n*-BuLi, THF, −78°C, 1h, then R_1CHO, THF, −78°C; (f) KOH, THF/EtOH (1:10), 80°C, 2−4h; (g) MnO_2, $CHCl_3$, 80°C, 4−8h; (h) I_2, KOH, DMF, rt, 2−4h; (i) 5 mol % $PdCl_2(PPh_3)_2$, 10 mol % CuI, TMSA, TEA/THF (1:1), 60°C, 18h then 1M TBAF, THF, 0°C to rt, 0.5−1h; (j) 7.5 mol % $CuSO_4.5H_2O$, 15 mol % Na ascorbate THF/*t*-BuOH/H_2O (3:1:1), rt, 48h. (k) LiOH, THF/H_2O (1:1) 70°C, 12h then 0.1 N HCl

conditions and then oxidized to generate ketone analogues **52**−**54**. Subsequent 3-iodination and Sonogashira coupling with TMSA, followed by one-pot deprotection of the organosilyl group, efficiently provided terminal alkynes **61**−**66**. The steric constraints imposed by the C2 substituents necessitated more rigorous reaction conditions compared to those used for the analogues **36** and **37**, such as elevated temperatures and increased catalytic charges. Final 1,3-dipolar cycloadditions between azide **29** and heteroaryl alkynes **61**−**66** yielded inhibitors **4** and **6**−**10**. Acid **5** was synthesized from precursor **4** via hydrolysis of the ethyl ester using excess lithium hydroxide. Scheme 3 illustrates the synthesis of **19** (**KDX1381**), following the same sequence used for other 1,2,3-triazole-based inhibitors (**11**−**18**, **20**−**26**) via coupling of intermediate **63** with azide derivatives **105**−**120**. These azides were prepared via Suzuki coupling[67] of boronic acids with 4-bromobenzenesulfonamide derivatives (**67**−**72**), followed by conversion of the resulting sulfonamide into sulfonyl chlorides using pyridinium tetrafluoroborate as activating reagents.[68] The sulfonyl chlorides were then condensed with 2-

https://doi.org/10.1021/acs.jmedchem.5c00695
J. Med. Chem. XXXX, XXX, XXX−XXX

Scheme 3. Synthesis of Compounds 11−26[a]



[a]Reagents and conditions: (a) $ArB(OH)_2$, 6.25−25 mol % $Pd(PPh_3)_4$, Na_2CO_3, DME, 85°C, 6−18h; (b) Pyry-BF_4, $MgCl_2$, *t*-BuOH, 60°C, 2−4h then 2-chloroethylamine hydrochloride, TEA, DCM, 0°C to rt, 2h; (c) 4-(azidomethyl)piperidine hydrochloride, KI (cat.), DIPEA, MeCN, 90°C, 18h; (d) 7.5 mol % $CuSO_4.5H_2O$, 15 mol % Na ascorbate THF/*t*-BuOH/H_2O (3:1:1), rt, 48h

chloroethylamine in the presence of triethylamine to yield intermediates **89−104**. Finally, a bimolecular nucleophilic substitution (S_N2) reaction was performed with 4-(azidomethyl)piperidine hydrochloride **28**[48] using Hünig's base and potassium iodide (KI), affording the azide analogues **105−120** required for the 1,3-dipolar cycloaddition.

EXPERIMENTAL SECTION

Kinase Assay and Profiling. Assays were conducted by Eurofins Discovery Services using full-length human CK2α, CK2α', and CK2β expressed in *Spodoptera frugiperda* (Sf21) insect cells. CK2α isoforms carried a C-terminal His_6, while CK2β was expressed as a GST-His_6 fusion. Enzymatic reactions were performed using 18.3 nM CK2$\alpha_2\beta_2$ (holoenzyme), 5.2 nM CK2α, or 3.6 nM CK2α' in assay buffer containing 20 mM HEPES (pH 7.4), 150 mM NaCl, 0.1 mM EDTA, 5.0 mM DTT, 0.1% Triton X-100, 165 μM synthetic peptide substrate (RRREDEESDDE), 10 mM $Mg(OAc)_2$ and [γ-^{33}P]-ATP (final ATP concentration 10 μM, unless otherwise stated). Reactions were initiated by the addition of the Mg/ATP mixture and incubated at room temperature for 40 min. Termination was achieved by addition of phosphoric acid to a final concentration of 0.5%. Aliquots were spotted onto a filter, washed four times (4 min each) with 0.425% phosphoric acid, followed by a single wash with methanol before drying and scintillation counting. For IC_{50} determination, the inhibitory effect of test compounds at various concentrations was measured relative to a dimethyl sulfoxide (DMSO) vehicle control. Measurements were performed in duplicate, and IC_{50} values were determined by nonlinear regression using Prism 9 (v9.5.0, GraphPad Software, LLC). K_i values for compound 1 and KDX1381 were estimated from IC_{50} measurements using a tight-binding correction model appropriate for high affinity inhibitor.[69] Specifically, the following adapted form was applied:

$$IC_{50} = K_i\left(1 + \frac{[ATP]}{K_m}\right) + \frac{[enzyme]}{2}$$

Where Km,ATP values of 10 μM for CK2α and 81.6 ± 0.2 μM for CK2$\alpha_2\beta_2$ were used.[70] Kinase selectivity profiling was performed against a panel of 413 kinases at a fixed concentration of 5.0 μM KDX1381, using standardized protocols from Eurofins Discovery Services, with ATP concentrations individually adjusted to the Km value of each kinase. Percent inhibition was calculated from duplicate measurements, and the resulting data were visualized on a kinome tree using CORAL.[49]

KINOMEscan Profiling Assay. Kinase binding assays were performed by Eurofins Discovery Services following their standardized protocols, with human recombinant kinases including CK2α and CK2α' catalytic subunits. For affinity enrichment, streptavidin-coated magnetic beads were incubated with biotinylated small-molecule ligands for 30 min at room temperature. Following ligand conjugation, beads were blocked with excess biotin and washed with blocking buffer (SeaBlock, 1% BSA, 0.05% Tween-20, 1.0 mM DTT) to minimize nonspecific interactions. Binding reactions were assembled in a final volume of 20 μL by combining kinases, ligand-bound affinity beads, and test compounds in 1× binding buffer (20% SeaBlock, 0.17× PBS, 0.05% Tween-20, 6.0 mM DTT). Compounds were prepared as 111× stock solutions in DMSO, dispensed by acoustic transfer, and diluted directly into the assay (final DMSO concentration: 0.9%). Assays were conducted in polypropylene 384-well plates, incubated at room temperature with shaking for 1 h. Following incubation, beads were washed with PBS containing 0.05% Tween-20 and resuspended in elution buffer (1× PBS, 0.05% Tween-20, 0.5 μM nonbiotinylated affinity ligand) before an additional 30 min incubation at room temperature. The concentration of kinase in the eluates was quantified via qPCR. Binding dissociation constants (K_D) were derived from 11-point, 3-fold serial dilution curves fitted to the Hill equation:

$$\text{Response} = \text{Background} + \frac{\text{Signal} - \text{Background}}{1 + \left(\frac{K_D^{\text{Hill Slope}}}{\text{Dose}^{\text{Hill Slope}}}\right)}$$

where the Hill slope was fixed at −1. Curve fitting was performed using a nonlinear least-squares regression with the Levenberg−Marquardt algorithm.

Solubility Assay and Formulation Screening. Solubility assays were performed by Pharmaron following their standardized protocols. Briefly, test compounds, including the reference compound amprenavir, were dissolved in DMSO at a concentration of 10 mM. Stock solutions were subsequently diluted into test media (PBS, pH 7.4, FaSSIF, pH 6.5, and 0.1 N HCl, pH 1.0, used as a surrogate for simulated gastric fluid) to a final concentration of 200 μM, maintaining a total DMSO content of 1% (v/v). The solutions

https://doi.org/10.1021/acs.jmedchem.5c00695
J. Med. Chem. XXXX, XXX, XXX−XXX

were incubated at 37 °C under continuous agitation (1,100 rpm) for 24 h using an Eppendorf Thermomixer Comfort plate shaker, followed by centrifugation to remove insoluble material. Supernatants were analyzed via high-performance liquid chromatography (HPLC) coupled with diode array UV/vis detection. Solubility values were determined by comparing chromatographic peak areas of the compound in test solutions against those of an unextracted reference standard. In parallel, chemical stability was assessed under identical incubation conditions in PBS and 0.1 N HCl at 37 °C for 24 h. Compound integrity was evaluated by HPLC, with degradation profiles analyzed to determine stability under physiologically relevant conditions.

For formulation screening, compound saturation was achieved by adding an excess of KDX1381 to a defined volume of test medium. The suspension was stirred magnetically for 24 to 48 h at 20 °C, protected from light. The supernatant was then isolated via centrifugation (double centrifugation for 15 min at 15,000 rpm, 20 °C) and/or filtration, followed by dilution in a solvent mixture compatible with chromatographic analysis. The concentration of KDX1381 in each medium was quantified by HPLC using external standardization.

Mouse Hepatocyte Stability Assay. Test compounds, including the reference compound verapamil, were prepared as 10 mM stock solutions in DMSO. Working solutions (100 μM) were generated by diluting 5.0 μL of each stock solution into 495 μL of an acetonitrile/water mixture (1:1). Cryopreserved mouse hepatocytes (male CD-1, BioIVT) were thawed according to Pharmaron's standardized protocols. Briefly, hepatocyte thawing medium and incubation medium (William's E Medium supplemented with GlutaMAX, Life Technologies) were prewarmed to 37 °C for 15 min. Cryogenic vials containing hepatocytes were retrieved from storage and thawed in a 37 °C water bath with gentle agitation for 2 min. Vials were then decontaminated with 70% ethanol and transferred to a biosafety cabinet. The thawed cell suspension was gently pipetted into a 50 mL conical tube containing thawing medium and centrifuged at 945 rpm for 10 min. After aspiration of the supernatant, the cell pellet was resuspended in incubation medium to achieve a final concentration of $\sim 1.5 \times 10^6$ cells/mL. Cell viability was assessed using acridine orange (AO) and PI staining, with only samples exhibiting $\geq$ 75% viability proceeding to further analysis. The hepatocyte suspension was then diluted to a final working concentration of 0.5×10^6 viable cells/mL. As a negative control, a subset of the hepatocyte suspension was heat-inactivated by boiling for 5 min to eliminate enzymatic activity. Hepatocytes (198 μL, 0.5×10^6 viable cells/mL) were seeded into each well of a 96-well noncoated plate and equilibrated for 10 min under continuous orbital shaking at 37 °C. Reactions were initiated by adding 2.0 μL of 100 μM test compound or reference compound, resulting in a final concentration of 1.0 μM. Plates were returned to the incubator with continuous shaking. At predefined time points (0, 15, and 30 min), 25 μL aliquots were collected and quenched with 150 μL of acetonitrile containing internal standards (100 nM alprazolam, 200 nM labetalol, 200 nM caffeine, and 2.0 μM ketoprofen) to terminate enzymatic activity. Samples were centrifuged at 5,400 rpm for 20 min, and 100 μL of the resulting supernatant was diluted with an equal volume of ultrapure water before LC-MS/MS analysis. All incubations were performed in duplicate. Quantification of test compounds and internal standards was conducted via LC-MS/MS, and extracted ion chromatograms were analyzed using Microsoft Excel. Peak areas were measured at each time point to evaluate compound stability over time.

X-ray Crystallography. Recombinant human CK2α was expressed and purified following established protocols.[32] Briefly, *Escherichia coli* BL21(DE3) cells were cultured in Terrific Broth supplemented with 50 mg/mL kanamycin. Protein expression was induced at an optical density at 600 nm (OD600) of 2.0 by adding 0.5 mM isopropyl β-D-1-thiogalactopyranoside (IPTG), followed by incubation at 18 °C for 12 h. Cells expressing His_6-tagged CK2α were harvested and lysed in buffer containing 50 mM HEPES (pH 7.5), 500 mM NaCl, 25 mM imidazole, 5% glycerol, and 0.5 mM tris(2-carboxyethyl)phosphine (TCEP) via sonication. Lysates were cleared by centrifugation, and the soluble fraction was applied to a Nickel-Sepharose affinity column pre-equilibrated with lysis buffer. The column was washed with 60 mL of lysis buffer before protein elution using an imidazole step gradient (50, 100, 200, and 300 mM). Eluted protein fractions were pooled and dialyzed overnight at 4 °C in 1.0 L of final buffer (25 mM HEPES, pH 7.5, 500 mM NaCl, 0.5 mM TCEP). The His_6 tag was removed by cleavage with TEV protease (1:20 protein-to-TEV molar ratio). The sample was then passed through a second Nickel-Sepharose column to remove both TEV protease and the cleaved tag. The flow-through and wash fractions (25 mM imidazole) containing CK2α were concentrated to 4−5 mL and further purified by size-exclusion chromatography using a Superdex 75 16/60 Hi-Load column pre-equilibrated with final buffer. The purified protein was concentrated to $\sim$ 9 mg/mL and stored for downstream applications. CK2α was crystallized using the hanging-drop vapor-diffusion method at 20 °C, with the protein concentrated to 9 mg/mL. The reservoir solution consisted of 33% polyethylene glycol methyl ether 5000, 0.2 M ammonium sulfate, and 0.1 M MES (pH 6.5). Crystals were obtained by mixing 1.0 μL of reservoir solution with 1.0 μL of protein solution. Ligand soaking was performed by adding 0.2 μL of a 50 mM ligand solution in DMSO directly to the drops. Crystals were cryoprotected using the reservoir solution supplemented with 20% glycerol before being flash-cooled in liquid nitrogen. Diffraction data were collected at the European Synchrotron Radiation Facility (ESRF), beamline ID30B (Grenoble, France). Data processing and scaling were performed using the program suites available at ESRF.[71] The crystals belonged to the $P4_32_12$ space group, with two monomers in the asymmetric unit. Structural determination was carried out by molecular replacement, using the CK2α structure (PDB 6Z84) as a search model. Ligands were manually fitted into Fo−Fc electron density maps using Coot,[72] and ligand parametrization was performed with grade Server (http://grade.globalphasing.org/cgi-bin/grade/server.cgi). Iterative model building and refinement were performed using Coot and Phenix.[73] Data collection and refinement statistics are summarized in Table S1 and structural figures were generated using the PyMOL Molecular Graphics System (v2.5.7, Schrödinger, LLC).

Cell Culture. Human colorectal cancer (HT-29, HCT116, LoVo, SW620, SW1116), melanoma (A375), renal (786-O, ACHN, Caki-1, Caki-2), and liver (Hep3B, SNU-182) cancer cell lines were obtained from the American Type Culture Collection (ATCC, US). Human glioma (A-172, SF-767) and liver cancer (Huh-7, JHH4) cell lines were generously provided by the "Cancer Cell Death" team at the Cancer Research Center of Lyon. All cell lines were cultured according to supplier-recommended protocols. HCT116, LoVo, SW620, SW1116, 786-O, ACHN, SNU-182, A-172, and SF-767 were maintained in RPMI 1640 medium supplemented with GlutaMAX (Gibco, Thermo Fisher Scientific). Caki-1, Caki-2, Hep3B, Huh-7, and JHH4 were cultured in high-glucose Dulbecco's modified Eagle's medium (DMEM) (Gibco, Thermo Fisher Scientific), supplemented with 1% GlutaMAX, 1% NEAA and 1% sodium pyruvate (Gibco, Thermo Fisher Scientific). Human melanoma A375 and colorectal cancer HT29 cells were maintained in DMEM. All media were supplemented with 10% FBS (Gibco, Thermo Fisher Scientific). Cells were incubated at 37 °C in a humidified atmosphere containing 5% CO_2 and were routinely tested for mycoplasma contamination using the MycoAlert detection kit (Lonza). Unless stated otherwise, cells were seeded at a density of $\sim$ 5000 cells/well in 96-well plates 24 h prior to treatment. Experimental conditions included treatment with CK2 inhibitors (KDX1381, Kairos Discovery; CX-4945, Cat. #A103748, Ambeed), VEGFR-TKIs (cabozantinib, Cat. #A200488; lenvatinib, Cat. #A336250; pazopanib, Cat. #A135375; regorafenib, Cat. #A177150; sorafenib, Cat. #A316727; sunitinib, Cat. #A157426, Ambeed), chemotherapeutic agents (cisplatin, Cat. #A210558; fluorouracil, Cat. #A370752; oxaliplatin, Cat. #A100048; Temozolomide, Cat. #A137834, Ambeed), either as monotherapies or in combination. Control wells were treated with 0.5% DMSO unless stated otherwise.

Cell Viability Assays. For WST-1 viability assays, cells were treated for 72 h, after which WST-1 reagent (Roche) was added

https://doi.org/10.1021/acs.jmedchem.5c00695
J. Med. Chem. XXXX, XXX, XXX−XXX

following the manufacturer's protocol. Absorbance was measured at 440 nm, with a reference wavelength of 660 nm, using an Infinite M1000 Pro microplate reader (Tecan). Live-cell imaging was performed using the IncuCyteZOOM system (Essen BioScience) to monitor proliferation and cell death dynamics over 72 h. Cells were treated with 30 nM Sytox Green nucleic acid stain (Invitrogen) for real-time visualization of cell viability. For flow cytometry analysis, cells and supernatants were collected after 72 h of treatment, following trypsinization and centrifugation at 800 rcf for 5 min. Cells were resuspended in DPBS (without calcium or magnesium) and counted using the NucleoCounter NC-3000 (ChemoMetec). Approximately 200,000 cells were stained with APC-Annexin V and PI (BioLegend), vortexed, and incubated for 15 min at room temperature in the dark. Flow cytometric analysis was performed using a BD LSRFortessa cell analyzer (BD Biosciences).

Multiplexed Cytotoxicity Assay. Cancer cells screening was performed by Eurofins Discovery Services following their standardized protocols. Briefly, cells were cultured in RPMI 1640 medium supplemented with 10% FBS, 2.0 mM L-alanyl-L-glutamine, and 1.0 mM sodium pyruvate, or in a specialized medium where indicated. Cells were seeded into 384-well plates and incubated at 37 °C in a humidified atmosphere with 5% CO_2. KDX1381 was added the following day, and a parallel untreated time-zero control plate was prepared. Following a 72-h incubation, cells were fixed and stained with fluorescently labeled antibodies and nuclear dyes to facilitate imaging of nuclei, apoptotic cells, and mitotic cells. KDX1381 was serially diluted in 2-fold steps, tested across ten concentrations, with a maximum assay concentration of 0.1% DMSO. Automated fluorescence microscopy was performed using a Molecular Devices ImageXpress Micro XL high-content imager, equipped with a 4× objective. High-resolution 16-bit TIFF images were acquired and analyzed using MetaXpress 5.1.0.41 software. Cell proliferation was assessed by quantifying the fluorescence intensity of an incorporated nuclear dye. The relative cell count was expressed as a percentage of control (POC) using the following equation:

$$\mathrm{POC} = \frac{I_x}{I_0} \times 100$$

where I_X represents the nuclear fluorescence intensity at compound concentration x, and I_0 corresponds to the mean nuclear fluorescence intensity of vehicle-treated wells. Dose−response relationships were analyzed using a sigmoidal single-site nonlinear regression model:

$$y = \mathrm{A} + \frac{\mathrm{B} - \mathrm{A}}{1 + (\mathrm{C}/x)^{\mathrm{D}}}$$

where y represents the measured cellular response at concentration x, A and B denote the lower and upper asymptotes of the response curve, C corresponds to the half-maximal effective concentration (EC_{50}), and D is the Hill slope. Cellular proliferation during the assay period was quantified by determining the number of population doublings using the following formula:

$$\mathrm{Doublings} = \log_2\left(\frac{N}{N_{\mathrm{T0}}}\right)$$

where N represents the final cell count in untreated control wells, and N_{T0} is the initial cell count at the time of compound addition. The IC_{50} value was defined as the concentration of test compound required to reduce the cell count to 50% of the maximum possible response. To provide an integrated assessment of drug activity, the activity area was computed as the area under the dose−response curve, ranging from 0 to 10. An activity area of 0 indicated no proliferation inhibition at any tested concentration, whereas a value of 10 corresponded to complete inhibition at all concentrations. In rare cases, values below 0 or above 10 were observed; negative values were considered equivalent to 0, while values exceeding 10 were treated as equivalent to 10.

Immunoblot Analyses. 786-O, HCT116 and Hep3B were treated with CK2 inhibitors (KDX1381, CX-4945), VEGFR-TKIs (regorafenib, sorafenib), their corresponding combination, or 0.5% DMSO as a control. Cells were incubated for the indicated durations, after which plates were placed on ice. Cells were washed with ice-cold PBS, harvested by scraping, pelleted by centrifugation, and lysed in RIPA buffer (50 mM Tris-HCl, pH 7.5, 1% Igepal, 0.5% sodium deoxycholate, 150 mM NaCl, 0.1% sodium dodecyl sulfate) supplemented with cOmplete Protease Inhibitor Cocktail and Phosphatase Inhibitor Cocktails 1 and 2 (Sigma-Aldrich). Lysates were centrifuged at 14,000 rcf for 15 min at 4 °C, and supernatants were collected for protein analysis. Protein concentrations were determined using the Bio-Rad Protein Assay Kit II according to the supplier's recommendations. Equal amounts of protein were resolved by SDS-PAGE and transferred onto nitrocellulose membranes. After blocking with 5% bovine serum albumin (BSA, Sigma-Aldrich) in TBS-T (Tris-buffered saline, Euromedex and 0.1% Tween-20, ThermoFisher Scientific), membranes were incubated overnight at 4 °C with primary antibodies targeting AKT (Cat. #9272S, Cell Signaling Technology), p-AKT^{S129} (Cat. #ab133458, Abcam), p21 (Cat. #2947S, Cell Signaling Technology), p-$p21^{T145}$ (Cat. #ab47300, Abcam), and p-CK2 substrates [(pS/pT)DXE] MultiMab Rabbit mAb mix (Cat. #8738S, Cell Signaling Technology), along with β-actin-HRP (Cat. #664804, BioLegend) as a loading control. Primary antibodies were diluted at 1:1000 in blocking buffer. Following three washes in TBS-T, membranes were incubated at room temperature for 1 h with a secondary horseradish peroxidase (HRP)-conjugated AffiniPure Goat Anti-Rabbit IgG antibody (Cat. #11−035−003, Jackson ImmunoResearch) diluted 1:10,000 in blocking buffer, except for β-actin, which was directly detected. Membranes were subsequently washed three times in TBS-T and visualized using the Chemidoc Touch Imaging System (Bio-Rad) following incubation with SuperSignal West Pico PLUS chemiluminescent substrate (ThermoFisher Scientific). Densitometric quantification was performed using ImageLab software (v4.1 or v5.2.1, Bio-Rad), ensuring precise measurement of protein expression levels.

Long-Term Proliferation Assay. 786-O and HCT116 cells were treated with CK2 inhibitors (KDX1381, CX-4945) or 0.5% DMSO as a control. After 72 h of incubation, treatments were removed and replaced with fresh culture medium. Cells were maintained for 14 days, with media replenished every 4 to 5 days. Throughout the experiment, cell proliferation dynamics were continuously monitored using the IncucyteZOOM system (Essen BioScience), allowing real-time assessment of growth kinetics under each treatment condition.

Colony Formation Assay. 786-O and HCT116 cells were treated with CK2 inhibitors (KDX1381, CX-4945) or 0.5% DMSO as a control. Following treatment, drug-containing media were removed and replaced with fresh drug-free culture media. Cells were maintained under standard conditions for an additional 7 to 10 days to allow colony formation. Colonies were subsequently fixed and stained with a crystal violet solution (1% crystal violet, Sigma-Aldrich, 50% methanol, 50% distilled water). Images were captured using an Axiovert 25 microscope (Zeiss), and colony formation was quantified using ImageJ software (v1.54, National Institutes of Health).

Combination Studies. For two-way compound combination studies, cells were treated in a matrixed format, with one agent titrated along the x-axis and the second along the y-axis. The starting concentrations and dilution factors were optimized for each compound to ensure well-defined dose−response curves, capturing the curve maximum, minimum, and slope across the selected dose range. Cell viability was assessed using WST-1 reagent (Roche), following the manufacturer's protocol. Absorbance was measured at 440 nm, with a reference wavelength of 660 nm, using an Infinite M1000 Pro microplate reader (Tecan). Synergy analysis was performed using SynergyFinder Software, which calculates synergy scores based on the Loewe additivity model (https://synergyfinder.fimm.fi). Data processing followed the supplier's protocol, available at https://synergyfinder.fimm.fi/synergy/synfin_docs/.

Physical Characterization. Preliminary physical analyses of KDX1381 was conducted using optical microscopy, X-ray powder diffraction (XRPD), and differential scanning calorimetry (DSC). Optical microscopy analysis was performed using a LEICA DMIRB

https://doi.org/10.1021/acs.jmedchem.5c00695
J. Med. Chem. XXXX, XXX, XXX−XXX

microscope equipped with a digital camera and a motorized stage. Microscopy images were acquired with a Microvision Instruments image analysis station under transmitted and cross-polarized light. A few milligrams of KDX1381 were placed onto a microscope glass slide with silicon oil, covered with a coverslip, and dispersed by gentle pressure before imaging. XRPD analysis was performed using a Brüker−AXS D2 Phaser equipped with a copper anticathode, a monocrystalline silicon sample holder, and a position-sensitive detector (LynxEye). Powder samples were loaded onto a flat monocrystalline silicon sample holder to minimize preferred orientation and ensure planarity of the specimen surface. DSC analysis was conducted using a Q2000 TA Instruments analyzer. KDX1381 was weighed into an aluminum capsule, which was then crimped and placed into the calorimeter oven for thermal analysis.

Pharmacokinetics Studies. Male CD-1 mice (6−8 weeks, 20−30 g) were administered KDX1381 via IV injection (1.0 mg/kg in 100% DMSO, 0.5 mL/kg), IP injection (40 mg/kg, formulated in 2.5% DMSO, 15% Cremophor EL, and 82.5% water, 5.0 mL/kg), or oral gavage (100 mg/kg, formulated as above, 5.0 mL/kg). Animals had ad libitum access to an irradiated rodent diet (Beijing Keaoxieli, Cobalt-60). Blood samples (~30 μL) were collected from the dorsal metatarsal vein at predefined time points (0.083, 0.25, 0.5, 1, 2, 4, 8, 12, and 24 h postdosing) and transferred into plastic microcentrifuge tubes containing EDTA-K2 as an anticoagulant. Samples were mixed thoroughly, placed on ice, and centrifuged at 6,000 rpm for 5 min at 4 °C to obtain plasma, which was subsequently stored at − 75 ± 15 °C until analysis. Working solutions of KDX1381 were prepared by diluting stock solutions with an acetonitrile/water (1:1) mixture to obtain concentrations of 1, 2, 4, 20, 100, 200, 1000, and 2000 ng/mL. Calibration standards were prepared by adding 5.0 μL of working solution to 10 μL of blank CD-1 mouse plasma, yielding final concentrations of 0.5, 1, 2, 10, 50, 100, 500, and 1000 ng/mL in a total volume of 15 μL. Four quality control (QC) samples (1, 2, 50, and 800 ng/mL) were independently prepared following the same procedure. On the day of analysis, 15 μL of calibration standards, QC samples, and unknown plasma samples (10 μL plasma +5.0 μL blank solution) were added to 200 μL of acetonitrile containing internal standard mixture for protein precipitation, vortexed for 30 s, and centrifuged at 4,000 rpm for 15 min at 4 °C. The resulting supernatant was diluted 3-fold with water, and a 5.0 μL aliquot was injected into the LC-MS/MS system for quantitative analysis. PK parameters were derived from the mean plasma concentration−time profile using a noncompartmental model in WinNonlin (v8.3, Phoenix Software, Certara).

Animals Studies. All animal experiments were performed in compliance with European and French regulations for animal experimentation and were approved by the French Ministries of Agriculture and Research under protocol APAFIS#31777−2021042111599650. All experiments were performed using female NMRI-Foxn1nu/nu mice (Janvier Laboratories, France) aged 5 to 6 weeks. Mice were housed in an environmentally controlled facility under standardized conditions, including a temperature of 23 ± 2 °C, relative humidity of 50 ± 20%, and a 12-h light/dark cycle. Animals were provided with commercial rodent chow and water ad libitum. Throughout the study, animals were monitored for tumor growth as well as general health parameters, including mobility, food and water consumption, body weight, eye condition, and any other signs of distress. Any mortality or abnormal clinical signs were recorded. Body weights were measured three times per week, and changes were expressed as a percentage using the formula %Bw change = (Bw_{D1}/Bw_{D0}) × 100, where Bw_{D1} represents body weight on a given day and Bw_{D0} corresponds to the initial body weight at the start of treatment.

Xenograft Studies. A375, Hep3B, 786-O, and SF-767 tumor models were established by subcutaneously implanting 5.0 × 10^6 cells into the flank of immunocompromised mice. For 786-O and SF-767 models, cells were suspended in a 50% Matrigel (Corning) solution prior to injection. Tumor progression was monitored, and treatment was initiated upon randomization once tumors reached a volume of 100−150 mm^3. KDX1381 was formulated in 2.5% DMSO, 15% Cremophor EL, and 82.5% water. Sorafenib was prepared in 10% ethanol, 10% Cremophor EL, and 80% water, while TMZ was dissolved in 100% water. For the 786-O and A375 models, mice received IP injections of either vehicle (BID) or KDX1381 (5.0 or 40 mg/kg, BID) at a dose volume of 5.0 mL/kg. In combination studies with sorafenib, mice were randomized (n = 8/group) and received vehicle (BID), KDX1381 (20 or 40 mg/kg BID, IP), sorafenib (20 or 30 mg/kg QD, PO), or KDX1381 (20 or 40 mg/kg BID, IP) in combination with sorafenib (20 or 30 mg/kg QD, PO). For combination studies with TMZ, randomized mice (n = 8/group) received vehicle (BID), KDX1381 (40 mg/kg BID, IP), TMZ (20 mg/kg, three times per week, PO), or KDX1381 (40 mg/kg BID, IP) in combination with TMZ (20 mg/kg, three times per week, PO). Tumor size was measured three times per week using a caliper, and tumor volume (TV) was calculated using the formula: TV (mm^3) = (a × b)^2/2, where a and b represent the longest and shortest tumor diameters, respectively. TGI was calculated using the formula: TGI (%) = (1 − T/C) × 100, where T and C denote the mean relative tumor volumes in the treated and control groups, respectively. Study end points were established based on ethical guidelines, with termination criteria including a mean tumor volume exceeding 2000 mm^3 or the development of tumor ulceration in necrotic models.

Tumor Pharmacodynamic Assays. The effects of KDX1381 on CK2α pathway activity were assessed in a 786-O tumor xenograft model. 786-O tumor cells (5.0 × 10^6 cells) were injected subcutaneously into the flank of NMRI-Foxn1nu/nu mice in a mixture with Matrigel (Corning). Treatment was initiated when tumors reached an average size of ~ 250 mm^3, with mice receiving a single IP dose of either vehicle or KDX1381 (40 mg/kg). Experimental groups consisted of 6−8 mice for the vehicle control group and 3 mice per treated group. Tumor samples were collected at the indicated times and transferred into Protein Safe Soft Tissue Homogenizing CK14 tubes (Bertin Technologies) containing RIPA lysis buffer supplemented with cOmplete Protease Inhibitor Cocktail (Roche) and Phosphatase Inhibitor Cocktails 1 and 2 (Sigma-Aldrich). Samples were homogenized using a Precellys homogenizer (Bertin Technologies) precooled to 4 °C, with the following settings: two cycles of 20-s centrifugation at 2,500 rpm, with a 20-s interval between cycles. Following homogenization, lysates were incubated on ice for 15 min, then centrifuged at 14,000 g for 15 min at 4 °C to separate cellular debris. Supernatants containing protein extracts were collected for subsequent analysis. Immunoblot analyses were performed following the same protocol as described in the Immunoblotting Assay section.

Statistic and Reproducibility. *In vitro* experiments were repeated the indicated number of times with similar results. Statistical analyses were conducted using Prism 9 (v9.5.0, GraphPad Software, LLC). Detailed statistical parameters for each experiment are provided in the corresponding figure legends. Data are presented as mean ± standard error of the mean (SEM) unless otherwise specified. For data sets following a normal distribution, statistical significance was assessed using a two-tailed Student's t test. For non-normally distributed data, one-way ANOVA followed by Dunnett's multiple comparisons test was applied. A P-value <0.05 was considered statistically significant (*p < 0.05, **p < 0.01, ***p < 0.001, ****p < 0.0001).

General Chemistry Method. All reactions were performed under an inert argon atmosphere using commercially available reagents and anhydrous solvents without further purification. Volatile solvents were removed by rotary evaporation, and residual traces were eliminated under high vacuum. Products were purified by silica gel column chromatography (35−70 μm, 60Å, manually packed). Reported yields refer to isolated materials. Reaction progress and compound purity were monitored by analytical thin-layer chromatography (TLC) on precoated silica gel plates (200 μm, F254 indicator), visualized under ultraviolet (UV) light (254 nm). Analytical HPLC-MS was performed on an Agilent 1290 Infinity system equipped with a Poroshell 120 SB-C18 column (2.7 μm, 2.1 × 50 mm), using positive electrospray ionization (ESI) mode under the following parameters: gas temperature, 350 °C; drying gas flow, 12.0 L/min; nebulizer pressure, 35 psig; capillary voltage, 3000 V; fragmentor voltage, 60 V. The purity

https://doi.org/10.1021/acs.jmedchem.5c00695
J. Med. Chem. XXXX, XXX, XXX−XXX

of all final compounds was determined by HPLC and confirmed to be ≥ 95%, unless otherwise stated. Nuclear magnetic resonance (NMR) spectra were recorded on Bruker DRX400 or AV500 Fourier-transform spectrometers, operating at 400 or 500 MHz for ^{1}H NMR, at 125 MHz for ^{13}C NMR, and 471 MHz for ^{19}F NMR. Chemical shifts (δ) are reported in parts per million (ppm), relative to residual solvent peaks as internal standards. Coupling constants (J) are given in hertz (Hz). The following abbreviations denote spin multiplicities: s, singlet; br s, broad singlet; d, doublet; t, triplet; q, quartet; p, pentet; and m, multiplet. Data acquisition and spectral analysis using Mnova (v.15.1, Mestrelab Research). All experimental procedures for the synthesis of target compounds **2**–**26**, including each step involving synthetic intermediates, are described below using generalized protocols. Analytical characterization data and reaction scales for intermediates are provided in the Supporting Information. Pyridinium tetrafluoroborate,[68] key synthetic intermediates **28**, **29**, and compound **1** were prepared according to previously reported procedures,[47] as were intermediates **41**–**45**.[74] All were obtained without modification, and their analytical data were consistent with the literature.

General Procedure A for Intermediates **32**, **33** and **55**–**60.** Heterocyclic compound (1.0 equiv) was dissolved in dimethylformamide (C ∼ 0.6 M), and treated with potassium hydroxide (2.5–3.5 equiv) at room temperature for 10 min. A solution of iodine (1.01 equiv) in dimethylformamide (C ∼ 0.7 M) was added dropwise, and the reaction mixture was stirred at room temperature for 1–4 h, monitored by TLC. The reaction was quenched by adding the mixture to ice water (C ∼ 0.1 mM) containing sodium bisulfite (0.5%) and ammonia (2.5%). The resulting solution was refrigerated to ensure complete precipitation. The precipitate was filtered, washed with ice-cold water, and dried under vacuum to afforded the product, used without further purification.

General Procedure B for Intermediates **34** and **35**. Iodinated derivative (1.0 equiv) was combined with 4-dimethylaminopyridine (10 mol %) and di*tert*-butyldicarbonate (1.5 equiv) in dry dichloromethane (C ∼ 0.5 M). The reaction was stirred at room temperature for 0.5 h, monitored by TLC. The organic layer was washed with 10% aqueous hydrochloric acid, and the aqueous phase was extracted three times with dichloromethane. Combined organic extracts were washed with brine, dried over $MgSO_4$, filtered, and evaporated. Purification by column chromatography on silica gel afforded the desired compound.

General Procedure C for Intermediates **36** and **37**. Iodinated derivative (1.0 equiv), $PdCl_2(PPh_3)_2$ (2 mol %), and copper(I) iodide (4 mol %) were combined in dry tetrahydrofuran (C ∼ 0.2 M) under argon in an oven-dried round-bottom flask. The reaction mixture was degassed for 5 min, followed by the addition of trimethylsilylacetylene (1.5 equiv) and dry triethylamine (2.0 equiv). The reaction was stirred at room temperature for 18 h (monitored by TLC), then tetrabutylammonium fluoride (1.5 equiv., 1.0 M in tetrahydrofuran) was added dropwise. Stirring continued for 0.5 h until complete deprotection. The reaction was quenched with saturated aqueous ammonium chloride, extracted three times with ethyl acetate, washed with brine, dried over $MgSO_4$, filtered, and evaporated. Purification by column chromatography on silica gel afforded the desired compound.

General Procedure D for Intermediates **61**–**66** followed the same protocol as General Procedure C but was modified by employing $PdCl_2(PPh_3)_2$ (5 mol %), copper(I) iodide (10 mol %), and conducting the reaction at 60 °C in a preheated oil bath for 18 h. After cooling to room temperature, TMS deprotection was then performed as described above.

General Procedure E for Intermediates **46**–**48**. The corresponding indole (1.8 equiv) was dissolved in dry tetrahydrofuran (C ∼ 0.15 M) under an argon atmosphere and cooled to −78 °C. *n*-butyllithium (1.8 equiv., 2.5 M in hexane) was added dropwise over 15 min. After stirring for 1 h at −78 °C, the aldehyde (1.0 equiv) in dry tetrahydrofuran (C ∼ 0.1 M) was added slowly. The reaction was stirred for another 1 h, then quenched with aqueous ammonium chloride. The mixture was extracted three times with ethyl acetate, washed with brine, dried over $MgSO_4$, filtered, and evaporated. Purification by column chromatography on silica gel afforded the desired compound.

General Procedure F for Intermediates **49**–**51**. The N-Ts protected indole (1.0 equiv) was dissolved in dry tetrahydrofuran/ethanol mixture (1:10, C ∼ 0.1 M). Potassium hydroxide (5.0 equiv) was added, and the reaction was heated to 80 °C (preheated oil bath) for 2–4 h, monitored by TLC. After cooling to room temperature, the mixture was poured into water and extracted three times with ethyl acetate, washed with brine, dried over $MgSO_4$, filtered, and evaporated. Purification by column chromatography on silica gel afforded the desired compound.

General Procedure G for Intermediates **52**–**54**. The corresponding alcohol (1.0 equiv) was dissolved in dry chloroform (C ∼ 0.1 M) in an oven-dried round-bottom flask, under an argon atmosphere, equipped with a reflux condenser. Manganese(IV) oxide (20 equiv) was added, and the reaction was heated to 80 °C (preheated oil bath) for 4–8 h, monitored by TLC. After cooling to room temperature, the mixture was filtered through a Celite pad, and washed with ethyl acetate. The combined filtrates were evaporated, and the residue was purified by column chromatography on silica gel to afforded the desired compound.

General Procedure H for Intermediates **73**–**88**. Aryl bromide (1.0 equiv), the appropriate boronic acid (3.0 equiv), and potassium carbonate (3.0 equiv) were combined in a mixture of dimethoxyethane/water (4:1, C ∼ 0.4 M), in an oven-dried round-bottom flask equipped with a reflux condenser under an argon atmosphere. The reaction mixture was degassed by bubbling argon through the solution for 15 min before the addition of $Pd(PPh_3)_4$ (10 mol %). The solution was further degassed for 5 min, then heated to 90 °C (preheated oil bath) for 18 h, monitored by TLC. The reaction was cooled to room temperature, filtered through a Celite pad, and washed with ethyl acetate. The combined filtrates were evaporated, and the residue was purified by column chromatography on silica gel to afforded the desired compound.

General Procedure I for Intermediates **89**–**104**. Step 1, the respective sulfonamide was dissolved in tert-butanol (C ∼ 0.1 M) in an oven-dried round-bottom flask. Pyridinium tetrafluoroborate (2.0 equiv) and magnesium chloride (2.55 equiv) were added, and the reaction was heated to 65 °C (preheated oil bath) for 2–6 h, monitored by TLC. The reaction mixture was filtered through a short Celite plug and washed with ethyl acetate. The filtrates were evaporated, and the residue was used without further purification. Step 2, the crude residue was dissolved in dichloromethane (C ∼ 0.2 M) in an oven-dried round-bottom flask, treated with triethylamine (3.0 equiv), followed by the slow addition of 2-chloroethylamine hydrochloride (1.5 equiv). The reaction mixture was stirred for ∼ 2 h, then extracted three times with dichloromethane. The combined organic layers were washed with brine, dried over $MgSO_4$, filtered, and evaporated. Purification by column chromatography on silica gel afforded the desired compound.

General Procedure J for Intermediates **105**–**120.** The corresponding alkyl chloride (1.0 equiv) and ammonium salt **32** (1.5 equiv) were dissolved in dry acetonitrile (C ∼ 0.15 M) under an argon atmosphere. The reaction was stirred for 10 min at room temperature before the dropwise addition of diisopropylethylamine (3.0 equiv), then heated to 82 °C (preheated oil bath) for 48 h, monitored by TLC. The reaction was cooled to room temperature, quenched with water, extracted three times with dichloromethane, washed with brine, dried over $MgSO_4$, filtered, and evaporated. Purification by column chromatography on silica gel afforded the desired compound.

General Procedure K for Compounds **2**–**26.** A solution of the ethynyl derivative (1.0 equiv) and corresponding azide (1.05 equiv) in tetrahydrofuran/tert-butanol/water (2:1:1, C ∼ 0.2 M) was prepared in an oven-dried flask. Freshly prepared sodium ascorbate (2.0 M, 1.0–5.0 equiv) and copper(II) sulfate pentahydrate (0.6 M, 0.25–0.87 equiv) were added, and the reaction mixture was stirred vigorously at room temperature for 12–48 h (monitored by TLC). The reaction was then extracted three times with ethyl acetate, washed with brine, dried over $MgSO_4$, filtered, and evaporated. Purification by silica gel column chromatography afforded the desired

https://doi.org/10.1021/acs.jmedchem.5c00695
J. Med. Chem. XXXX, XXX, XXX−XXX

product. For compounds **2** and **3**, the N-Boc-protected triazolyl derivatives (1.0 equiv) were dissolved in methanol (C ~ 0.2 M) and treated with potassium carbonate (2.5 equiv). The reaction was stirred at room temperature for ~ 2 h (monitored by TLC). The solvents were evaporated, and the crude product was purified by silica gel column chromatography.

N-(2-(4-((4-(5-fluoro-1H-indol-3-yl)-1H-1,2,3-triazol-1-yl)methyl)-piperidin-1-yl)ethyl)-4-isobutylbenzenesulfonamide (2). Step 1: Following General Procedure K, a solution of indole **36** (98 mg, 0.38 mmol), and azide **29** (153 mg, 0.40 mmol) in tetrahydrofuran/*tert*-butanol/water (2.4 mL) was treated with 2.0 M aqueous sodium ascorbate (0.38 mL, 0.76 mmol) and 15% aqueous copper(II) sulfate pentahydrate (0.37 mL, 0.22 mmol). The crude product was purified via flash column chromatography on silica gel (methanol/dichloromethane, 2:98 → 10:90) to provide compound **38** as yellow solid (234 mg, 0.37 mmol, 97% yield). MS (ESI) *m/z* 639.3 $[M + H]^+$. Step 2: Compound **38** was dissolved in methanol (2.0 mL) and treated with potassium carbonate (128 mg, 0.92 mmol). The crude product was purified via flash column chromatography on silica gel (methanol/dichloromethane, 2:98 → 15:85) to provide compound **2** as white solid (136 mg, 0.25 mmol, 68% yield, 66% overall yield over two steps). ^{1}H NMR (500 MHz, DMSO-d_6) δ 11.44 (d, J = 2.7 Hz, 1H), 8.42 (s, 1H), 7.86 (d, J = 2.6 Hz, 1H), 7.78 (dd, J = 10.2, 2.6 Hz, 1H), 7.73−7.65 (m, 2H), 7.45−7.41 (m, 1H), 7.35 (dd, J = 8.9, 6.9 Hz, 3H), 7.00 (td, J = 9.1, 2.6 Hz, 1H), 4.26 (d, J = 7.0 Hz, 2H), 2.82 (q, J = 6.2 Hz, 2H), 2.65 (dt, J = 11.8, 3.5 Hz, 2H), 2.49 (s, 3H), 2.31−2.20 (m, 2H), 1.87−1.74 (m, 4H), 1.49−1.39 (m, 2H), 1.24−1.15 (m, 2H), 0.82 (d, J = 6.6 Hz, 6H). ^{13}C RMN (126 MHz, DMSO-d_6) δ 157.3 (d, J = 234.4 Hz, C_{quat}), 146.0 (C_{quat}), 142.0 (C_{quat}), 138.0 (C_{quat}), 133.0 (C_{quat}), 129.5 (CH), 126.4 (CH), 124.9 (CH), 124.8 (C_{quat}), 119.8 (CH), 112.8 (d, J = 9.8 Hz, CH), 109.8 (d, J = 26.2 Hz, CH), 106.6 (d, J = 4.6 Hz, C_{quat}), 104.6 (d, J = 23.8 Hz, CH), 56.8 (CH_2), 54.5 (CH_2), 52.5 (CH_2), 44.1 (CH_2), 40.2 (CH_2), 36.4 (CH), 29.5 (CH), 29.1 (CH_2), 22.0 (CH_3). ^{19}F NMR (471 MHz, DMSO-d_6) δ −124.3 (td, J = 9.7, 4.8 Hz). MS (ESI) *m/z* 539.3 $[M + H]^+$.

N-(2-(4-((4-(1H-indol-3-Yl)-1H-1,2,3-triazol-1-yl)methyl)-piperidin-1-yl)ethyl)-4-isobutylbenzenesulfonamide (3). Step 1: Following General Procedure K, a solution of indole **37** (92 mg, 0.38 mmol), and azide **29** (153 mg, 0.40 mmol) in tetrahydrofuran/*tert*-butanol/water (2.4 mL) was treated with 2.0 M aqueous sodium ascorbate (0.38 mL, 0.76 mmol) and 15% aqueous copper(II) sulfate pentahydrate (0.37 mL, 0.22 mmol). The crude product was purified via flash column chromatography on silica gel (methanol/dichloromethane, 2:98 → 10:90) to provide compound **39** as orange oil (120 mg, 0.19 mmol, 50% yield). MS (ESI) *m/z* 621.3 $[M + H]^+$. Step 2: Compound **39** was dissolved in methanol (1.0 mL) and treated with potassium carbonate (65 mg, 0.47 mmol). The crude product was purified via flash column chromatography on silica gel (methanol/dichloromethane, 2:98 → 15:85) to provide compound **3** as white solid (120 mg, 0.23 mmol, 58% yield, 29% overall yield over two steps). ^{1}H NMR (500 MHz, DMSO-d_6) δ 11.32 (d, J = 2.6 Hz, 1H), 8.38 (s, 1H), 8.05−7.98 (m, 1H), 7.77 (d, J = 2.6 Hz, 1H), 7.74−7.63 (m, 2H), 7.44 (dt, J = 8.1, 1.0 Hz, 1H), 7.39−7.32 (m, 3H), 7.15 (ddd, J = 8.2, 7.0, 1.3 Hz, 1H), 7.10 (ddd, J = 8.0, 6.9, 1.1 Hz, 1H), 4.27 (d, J = 7.0 Hz, 2H), 2.83 (q, J = 5.2, 4.4 Hz, 2H), 2.66 (dt, J = 11.8, 3.6 Hz, 2H), 2.27−2.19 (m, 2H), 1.90−1.74 (m, 4H), 1.48−1.37 (m, 2H), 1.24−1.15 (m, 2H), 0.83 (d, J = 6.6 Hz, 6H). ^{13}C RMN (126 MHz, DMSO-d_6) δ 142.4 (C_{quat}), 138.0 (C_{quat}), 136.3 (C_{quat}), 129.6 (CH), 126.4 (CH), 124.7 (C_{quat}), 122.9 (CH), 121.6 (CH) 119.9 (CH), 119.8 (CH), 119.4 (CH), 111.7 (CH), 106.3 (C_{quat}), 56.8 (CH_2), 54.5 (CH_2), 52.5 (CH_2), 44.1 (C_{quat}), 40.2 (CH_2), 36.4 (CH), 29.5 (CH), 29.1 (CH), 22.0 (CH_3). MS (ESI) *m/z* 521.3 $[M + H]^+$.

Ethyl 5-fluoro-3-(1-((1-(2-((4-isobutylphenyl-sulfinamido) ethyl)-piperidin-4-yl)methyl)-1H-1,2,3-triazol-4-yl)-1H-indole-2-carboxylate (4). Following General Procedure K, a solution of indole **61** (175 mg, 0.76 mmol) and azide **29** (306 mg, 0.80 mmol) in tetrahydrofuran/*tert*-butanol/water (2.4 mL) was treated with 2.0 M aqueous sodium ascorbate (751 μL, 1.52 mmol) and 15% aqueous copper(II) sulfate pentahydrate (750 μL, 0.45 mmol). The crude product was purified via flash column chromatography on silica gel (methanol/dichloromethane, 0:100 → 10:90) to provide compound **4** as yellow solid (211 mg, 0.35 mmol, 46% yield). ^{1}H NMR (500 MHz, DMSO-d_6) δ 12.07 (s, 1H), 8.56 (s, 1H), 8.08 (dd, J = 10.3, 2.6 Hz, 1H), 7.71−7.68 (m, 2H), 7.54−7.50 (m, 1H), 7.38−7.32 (m, 3H), 7.22 (td, J = 9.1, 2.7 Hz, 1H), 4.41−4.31 (m, 4H), 2.85−2.79 (m, 2H), 2.68−2.62 (m, 2H), 2.50−2.48 (m, 2H), 2.24 (t, J = 6.9 Hz, 2H), 1.87−1.75 (m, 4H), 1.48−1.41 (m, 2H), 1.35 (t, J = 7.1 Hz, 3H), 1.24−1.15 (m, 2H), 0.82 (d, J = 6.6 Hz, 6H). ^{13}C RMN (126 MHz, DMSO-d_6) δ 160.9 (C_{quat}), 157.5 (d, J = 233.8 Hz, C_{quat}), 146.0 (C_{quat}), 140.3 (C_{quat}), 138.0 (C_{quat}), 133.1 (C_{quat}), 129.5 (CH), 126.4 (CH), 126.0 (d, J = 10.8 Hz, C_{quat}), 124.8 (CH), 123.8 (C_{quat}), 114.4 (d, J = 26.8 Hz, CH), 114.0 (d, J = 9.5 Hz, CH), 111.7 (d, J = 5.5 Hz), 107.5 (d, J = 24.5 Hz), 60.9 (CH_2), 56.8 (CH_2), 54.4 (CH_2), 52.5 (CH_2), 44.1 (CH_2), 40.2 (CH_2), 36.5 (CH), 29.47 (CH), 29.0 (CH_2), 22.0 (CH_3), 14.2 (CH_3). ^{19}F NMR (471 MHz, DMSO-d_6) δ −122.4 (td, J = 9.7, 4.7 Hz). MS (ESI) *m/z* 611.3 $[M + H]^+$.

Ethyl 5-fluoro-3-(1-((1-(2-((4-isobutylphenyl-sulfinamido) ethyl)-piperidin-4-yl)methyl)-1H-1,2,3-triazol-4-yl)-1H-indole-2-carboxylic acid (5). In an oven-dried round-bottom flask were combined compound **4** (100 mg, 0.16 mmol, 1.0 equiv) in tetrahydrofuran/water (1:1, 4 mL, C ~ 0.08 M). Then lithium hydroxide (15 mg, 0.64 mmol, 4.0 equiv) was added. The reaction mixture was stirred for 18 h at 70 °C and after the complete consumption of the starting material (monitored by TLC), the mixture was cooled to room temperature and adjusted to pH 1 with aqueous hydrogen chloride solution (1M). The mixture was partitioned into water and extracted with ethyl acetate three times. The combined organics extracts were washed with water, brine, dried over $MgSO_4$ and filtered. The solvents were evapored to dryness to provide the compound **5** as yellow solid (58 mg, 0.10 mmol, 63% yield). ^{1}H NMR (500 MHz, DMSO-d_6) δ 12.03 (s, 1H), 8.74 (s, 1H), 8.10 (dd, J = 10.4, 2.6 Hz, 1H), 8.02−7.97 (m, 1H), 7.76−7.71 (m, 2H), 7.53−7.49 (m, 1H), 7.40−7.34 (m, 2H), 7.20 (td, J = 9.1, 2.6 Hz, 1H), 4.44 (d, J = 7.0 Hz, 2H), 3.36−3.27 (m, 2H), 3.16−3.09 (m, 2H), 3.02−2.96 (m, 2H), 2.83 (s, 1H), 2.53−2.50 (m, 4H), 2.15 (s, 1H), 1.84 (dt, J = 13.5, 6.8 Hz, 1H), 1.75−1.68 (m, 2H), 1.65−1.55 (m, 2H), 1.28−1.15 (m, 1H), 0.83 (d, J = 6.6 Hz, 6H). ^{13}C RMN (126 MHz, DMSO-d_6) δ 162.4 (C_{quat}), 157.5 (d, J = 233.5 Hz, C_{quat}), 146.4 (C_{quat}), 140.7 (C_{quat}), 137.2 (C_{quat}), 132.8 (C_{quat}), 129.7 (CH), 126.6 (CH), 125.8 (d, J = 10.8 Hz, C_{quat}), 125.5 (CH), 124.7 (C_{quat}), 114.0 (d, J = 9.0 Hz, CH), 113.9 (d, J = 7.9 Hz, CH), 110.2 (d, J = 5.4 Hz, C_{quat}), 107.2 (d, J = 24.4 Hz, CH), 59.7 (CH_2), 55.6 (CH_2), 50.5 (CH_2), 44.2 (CH_2), 37.5 (CH_2), 29.5 (CH), 25.9 (CH_2), 22.0 (CH_3). ^{19}F NMR (471 MHz, DMSO-d_6) δ −122.5 (dt, J = 13.3, 6.5 Hz). MS (ESI) *m/z* 583.2 $[M + H]^+$.

N-(2-(4-((4-(5-fluoro-2-(pyrrolidine-1-carbonyl)-1H-indol-3yl)-1,2,3-triazol-1-yl)methyl)piperidin-1-yl)ethyl)-4-isobutyl benzene-sulfonamide (6). Following General Procedure K, a solution of indole **62** (100 mg, 0.39 mmol) and azide **29** (155 mg, 0.41 mmol) in tetrahydrofuran/*tert*-butanol/water (2.4 mL) was treated with 2.0 M aqueous sodium ascorbate (683 μL, 1.37 mmol) and 7.5% aqueous copper(II) sulfate pentahydrate (566 μL, 0.34 mmol). The crude product was purified via flash column chromatography on silica gel (methanol/dichloromethane, 0:100 → 10:90) to provide compound **6** as pale yellow solid (128 mg, 0.20 mmol, 52% yield). ^{1}H NMR (500 MHz, DMSO-d_6) δ 11.86 (s, 1H), 8.20 (s, 1H), 7.82 (dd, J = 10.1, 2.6 Hz, 1H), 7.75−7.67 (m, 2H), 7.41 (dt, J = 10.0, 5.1 Hz, 1H), 7.40−7.25 (m, 3H), 7.08 (td, J = 9.1, 2.6 Hz, 1H), 4.30 (d, J = 6.9 Hz, 2H), 3.54 (t, J = 7.0 Hz, 2H), 3.10 (t, J = 6.8 Hz, 2H), 2.82 (dt, J = 10.6, 5.4 Hz, 2H), 2.72−2.59 (m, 2H), 2.24 (t, J = 6.9 Hz, 2H), 1.82 (dq, J = 17.0, 8.8 Hz, 6H), 1.69 (p, J = 6.8 Hz, 2H), 1.45−1.35 (m, 2H), 1.28−1.10 (m, 4H), 0.83 (d, J = 6.6 Hz, 6H). ^{13}C RMN (126 MHz, DMSO-d_6) δ 162.0 (C_{quat}), 155.2 (d, J = 233.8 Hz, C_{quat}), 146.0 (C_{quat}), 140.7 (C_{quat}), 138.0 (C_{quat}), 132.1 (C_{quat}), 131.5 (C_{quat}), 129.5 (CH), 126.4 (CH), 125.6 (d, J = 10.8 Hz, C_{quat}), 121.5 (CH), 118.2 (C_{quat}), 114.4 (d, J = 26.8 Hz, CH), 114.0 (d, J = 9.5 Hz, CH), 110.6 (d, J = 24.7 Hz, CH), 104.7 (d, J = 24.5 Hz, CH), 56.4 (CH_2), 54.4 (CH_2), 52.5 (CH_2), 47.3 (CH_2), 45.7 (CH_2), 44.1 (CH_2), 36.4

https://doi.org/10.1021/acs.jmedchem.5c00695
J. Med. Chem. XXXX, XXX, XXX−XXX

(CH), 29.4 (CH), 29.0 (CH_2), 23.9 (CH_2), 22.0 (CH_3).^{19}F NMR (471 MHz, DMSO-d_6) δ −122.5. MS (ESI) m/z 636.3 $[M + H]^+$.

N-(2-(4-((4-(2-(cyclopropanecarbonyl)-5-fluoro-1H-indol-3-yl)-1,2,3-triazol-1-yl)methyl)piperidin-1-yl)ethyl)-4-isobutylbenzenesulfonamide (7). Following General Procedure K, a solution of indole **64** (60 mg, 0.26 mmol) and azide **29** (105 mg, 0.28 mmol) in tetrahydrofuran/*tert*-butanol/water (2.4 mL) was treated with 2.0 M aqueous sodium ascorbate (462 μL, 0.92 mmol) and 15% aqueous copper(II) sulfate pentahydrate (382 μL, 0.23 mmol). The crude product was purified via flash column chromatography on silica gel (methanol/dichloromethane, 0:100 → 4:96) to provide compound **7** as white solid (103 mg, 0.17 mmol, 64% yield). ^{1}H NMR (500 MHz, DMSO-d_6) δ 12.20 (s, 1H), 8.57 (s, 1H), 7.81 (dd, J = 10.1, 2.6 Hz, 1H), 7.79−7.60 (m, 2H), 7.54 (dd, J = 8.9, 4.6 Hz, 1H), 7.50−7.32 (m, 3H), 7.24 (td, J = 9.1, 25 2.6 Hz, 1H), 4.33 (d, J = 6.9 Hz, 2H), 2.82 (d, J = 5.8 Hz, 2H), 2.73−2.58 (m, 5H), 2.23 (t, J = 6.9 Hz, 2H), 1.90−1.73 (m, 3H), 1.46−1.37 (m, 2H), 1.25−1.17 (m, 2H), 1.16 (d, J = 3.7 Hz, 1H), 1.13−1.09 (m, 2H), 1.00 (dt, J = 8.1, 3.4 Hz, 2H), 0.83 (d, J = 6.7 Hz, 6H). ^{13}C RMN (126 MHz, DMSO-d_6) δ 193.0 (C_{quat}), 157.6 (d, J = 234.3 Hz, C_{quat}), 146.0 (C_{quat}), 140.1 (C_{quat}), 138.0 (C_{quat}), 133.2 (C_{quat}), 133.1 (C_{quat}), 129.5 (CH), 126.6 (d, J = 10.2 Hz, C_{quat}), 126.4 (CH), 125.1 (CH), 114.7 (d, J = 26.9 Hz, CH), 114.2 (d, J = 9.5 Hz, CH), 110.5 (d, J = 5.6 Hz, C_{quat}), 106.9 (d, J = 24.1 Hz, CH), 56.8 (CH_2), 54.5 (CH_2), 52.5 (CH_2), 44.1 (CH_2), 40.2 (CH_2), 36.4 (CH), 29.5 (CH), 29.0 (CH_2), 22.0 (CH_3), 18.9 (CH), 11.7 (CH_2). ^{19}F NMR (471 MHz, DMSO-d_6) δ −122.4. MS (ESI) m/z 607.3 $[M + H]^+$.

N-(2-(4-((4-(5-fluoro-2-isobutyryl-1H-indol-3-yl)-1H-1,2,3-triazol-1-yl)methyl)piperidin-1-yl)ethyl)-4-isobutylbenzene-sulfonamide (8). Following General Procedure K, a solution of indole **65** (60 mg, 0.26 mmol) and azide **29** (104 mg, 0.27 15 mmol) in tetrahydrofuran/*tert*-butanol/water (2.4 mL) was treated with 2.0 M aqueous sodium ascorbate (458 μL, 0.92 mmol) and 7.5% aqueous copper(II) sulfate pentahydrate (380 μL, 0.23 mmol). The crude product was purified via flash column chromatography on silica gel (methanol/dichloromethane, 0:100 → 4:96) to provide compound **8** as white solid (103 mg, 0.17 mmol, 65% yield). ^{1}H NMR (500 MHz, DMSO-d_6) δ 12.06 (s, 1H), 8.62 (s, 1H), 7.78 (dd, J = 10.1, 2.6 20 Hz, 1H), 7.74−7.65 (m, 2H), 7.54 (dd, J = 9.0, 4.6 Hz, 1H), 7.43−7.32 (m, 3H), 7.23 (td, J = 9.1, 2.6 Hz, 1H), 4.35 (d, J = 7.0 Hz, 2H), 3.49 (h, J = 6.8 Hz, 1H), 2.83 (q, J = 6.0 Hz, 2H), 2.73−2.62 (m, 2H), 2.25 (q, J = 6.6 Hz, 2H), 1.97−1.74 (m, 4H), 1.52−1.38 (m, 2H), 1.32−1.18 (m, 3H), 1.06 (d, J = 6.9 Hz, 6H), 0.97−0.87 (m, 1H), 0.82 (d, J = 6.6 Hz, 6H). ^{13}C NMR (126 MHz, DMSO-d_6) δ 197.7 (C_{quat}), 157.5 (d, J = 233.4 Hz, C_{quat}), 146.0 (C_{quat}), 140.1 (C_{quat}), 138.0 (C_{quat}), 133.0 (C_{quat}), 131.8 (C_{quat}), 129.5 (CH), 126.4 (CH), 126.0 (d, J = 10.2 Hz, C_{quat}), 124.9 (CH), 114.4 (d, J = 26.6 Hz, CH), 114.0 (d, J = 9.6 Hz, CH), 111.9 (d, J = 5.3 Hz, C_{quat}), 107.2 (d, J = 23.7 Hz, CH), 56.8 (CH_2), 54.4 (CH_2), 52.5 (CH_2), 44.1 (CH_2), 40.2 (CH_2), 29.5 (CH), 29.0 (CH_2), 22.0 (CH_3), 18.8 (CH_3). ^{19}F NMR (471 MHz, DMSO-d_6) δ −122.4. MS (ESI) m/z 609.3 $[M + H]^+$.

N-(2-(4-((4-(5-fluoro-2-(3-methylbutanoyl)-1H-indol-3-yl)-1H-1,2,3-triazol-1-yl)methyl)piperidin-1-yl)ethyl)-4-isobutyl-benzene-sulfonamide (9). Following General Procedure K, a solution of indole **66** (60 mg, 0.25 mmol) and azide **29** (98 mg, 0.26 mmol) in tetrahydrofuran/*tert*-butanol/water (2.4 mL) was treated with 2.0 M aqueous sodium ascorbate (432 μL, 0.86 mmol) and 7.5% aqueous copper(II) sulfate pentahydrate (358 μL, 0.21 mmol). The crude product was purified via flash column chromatography on silica gel (methanol/dichloromethane, 0:100 → 4:96) to provide compound **9** as white solid (94 mg, 0.15 mmol, 61% yield). ^{1}H NMR (500 MHz, DMSO-d_6) δ 12.04 (s, 1H), 8.60 (s, 1H), 7.71 (ddt, J = 10.4, 8.6, 2.4 Hz, 3H), 7.53 (dd, J = 9.0, 4.6 Hz, 1H), 7.41−7.31 (m, 3H), 7.22 (td, J = 9.1, 2.6 Hz, 1H), 4.36 (d, J 10 = 7.0 Hz, 2H), 2.89−2.80 (m, 2H), 2.77 (d, J = 6.9 Hz, 2H), 2.72−2.61 (m, 2H), 2.25 (q, J = 7.9 Hz, 2H), 2.20−2.02 (m, 1H), 1.81 (ddt, J = 13.8, 11.1, 4.6 Hz, 4H), 1.45 (dd, J = 13.3, 3.7 Hz, 2H), 1.31−1.09 (m, 3H), 1.03−0.92 (m, 1H), 0.93−0.78 (m, 12H). ^{13}C NMR (126 MHz, DMSO-d_6) δ 193.3 (C_{quat}), 157.6 (d, J = 233.4 Hz, C_{quat}), 145.9 (C_{quat}), 140.0 (C_{quat}), 138.3 (C_{quat}), 133.1 (C_{quat}), 132.9 (C_{quat}), 129.5 (CH), 126.7 (d, J = 10.1 Hz, C_{quat}), 126.4 (CH), 125.0 (CH), 114.7 (d, J = 25.8 Hz, CH), 114.2 (d, J = 9.9 Hz, CH), 110.5 (d, J = 6.0 Hz, C_{quat}), 107.2 (d, J = 25.8 Hz, CH), 56.8 (CH_2), 54.5 (CH_2), 52.5 (CH_2), 48.6 (CH_2), 44.1 (CH_2), 40.2 (CH_2), 29.5 (CH), 29.0 (CH_2), 24.5 (CH), 22.3 (CH_3), 22.0 (CH_3). ^{19}F NMR (471 MHz, DMSO-d_6) δ −122.5. MS (ESI) m/z 623.3 $[M + H]^+$.

N-(2-(4-((4-(2-acetyl-5-fluoro-1H-indol-3-Yl)-1H-1,2,3-triazol-1-yl)methyl)piperidin-1-yl)ethyl)-4-isobutylbenzenesulfonamide (10). Following General Procedure K, a solution of indole **63** (60 mg, 0.30 mmol) and azide **29** (117 mg, 0.31 mmol) in tetrahydrofuran/*tert*-butanol/water (2.4 mL) was treated with 2.0 M aqueous sodium ascorbate (522 μL, 1.04 mmol) and 7.5% aqueous copper(II) sulfate pentahydrate (432 μL, 0.26 mmol). The crude product was purified via flash column chromatography on silica gel (methanol/dichloromethane, 0:100 → 4:96) to provide compound **10** as pale yellow solid (124 mg, 0.21 mmol, 72% yield). ^{1}H NMR (500 MHz, DMSO-d_6) δ 12.07 (d, J = 6.2 Hz, 1H), 8.61 (d, J = 6.6 Hz, 1H), 7.80 (ddd, J = 10.0, 6.6, 2.6 Hz, 1H), 7.76−7.67 (m, 2H), 7.60−7.49 (m, 1H), 7.35 (t, J = 7.5 Hz, 10 3H), 7.24 (tdd, J = 9.1, 6.6, 2.7 Hz, 1H), 4.34 (d, J = 7.0 Hz, 2H), 2.83 (q, J = 6.6 Hz, 2H), 2.66 (d, J = 11.2 Hz, 2H), 2.52 (s, 3H), 2.24 (t, J = 6.6 Hz, 2H), 1.89−1.72 (m, 4H), 1.48−1.38 (m, 2H), 1.27−1.15 (m, 4H), 0.82 (t, J = 6.6 Hz, 6H). ^{13}C NMR (126 MHz, DMSO-d_6) δ 191.0 (C_{quat}), 157.5 (d, J = 234.3 Hz, C_{quat}), 146.0 (C_{quat}), 140.0 (C_{quat}), 133.0 (C_{quat}), 132.9 (C_{quat}), 129.7 (C_{quat}), 126.6 (d, J = 10.1 Hz, C_{quat}), 129.5 (CH), 126.4 (CH), 125.0 (CH), 114.8 (d, J = 27.5 Hz, CH), 114.2 (d, J = 10.6 Hz, CH), 110.8 (d, J = 5.5 Hz, C_{quat}), 106.8 (d, J = 23.1 Hz, CH), 56.8 (CH_2), 54.5 (CH_2), 52.5 (CH_2), 44.1 (CH_2), 40.2 (CH_2), 36.4 (CH), 29.0 (CH_2), 28.7 (CH_3), 29.5 (CH), 22.0 (CH_3). ^{19}F NMR (471 MHz, DMSO-d_6) δ −122.4. MS (ESI) m/z 581.3 $[M + H]^+$.

N-(2-(4-((4-(2-acetyl-5-fluoro-1H-indol-3-yl)-1H-1,2,3-triazol-1-yl)methyl)piperidin-1-yl)ethyl)-2′-(trifluoromethyl)-[1,1′-biphenyl]-4-sulfonamide (11). Following General Procedure K, a solution of indole **63** (60 mg, 0.30 mmol) and azide **105** (146 mg, 0.31 mmol) in tetrahydrofuran/*tert*-butanol/water (2.4 mL) was treated with 2.0 M aqueous sodium ascorbate (522 μL, 1.04 mmol) and 15% aqueous copper(II) sulfate pentahydrate (432 μL, 0.26 mmol). The crude product was purified via flash column chromatography on silica gel (methanol/dichloromethane, 0:100 → 4:96) to provide compound **11** as white solid (136 mg, 0.20 mmol, 67% yield). ^{1}H NMR (500 MHz, DMSO-d_6) δ 12.06 (s, 1H), 8.61 (s, 1H), 7.88 (d, J = 6.6 Hz, 2H), 20 7.84 (dd, J = 7.9, 1.3 Hz, 1H), 7.79 (dd, J = 10.1, 2.6 Hz, 1H), 7.74 (td, J = 7.6, 1.4 Hz, 1H), 7.69−7.59 (m, 2H), 7.57−7.50 (m, 3H), 7.49−7.39 (m, 1H), 7.23 (td, J = 9.1, 2.6 Hz, 1H), 4.36 (d, J = 7.1 Hz, 2H), 2.93 (t, J = 6.9 Hz, 2H), 2.72 (dd, J = 9.5, 5.0 Hz, 2H), 2.50 (s, 3H), 2.29 (t, J = 6.9 Hz, 2H), 1.96−1.77 (m, 3H), 1.53−1.38 (m, 2H), 1.38−1.18 (m, 2H). ^{13}C RMN (126 MHz, DMSO-d_6) δ 191.0 (C_{quat}), 158.5 (C_{quat}), 156.6 (C_{quat}), 141.5 (d, J = 390.3 Hz, C_{quat}), 140.3 (C_{quat}), 134.0 (C_{quat}), 139.1 (C_{quat}), 133.0 (C_{quat}), 132.9 (CH), 132.4 (CH), 131.8 (CH), 129.5 (CH), 128.6 (CH), 126.8 (d, J = 29.4 Hz, CH), 126.6 (d, J = 10.5 Hz, C_{quat}), 126.1 (C_{quat}), 125.1 (C_{quat}), 124.0 (d, J = 273.8 Hz, C_{quat}), 122.9 (C_{quat}), 114.8 (d, J = 26.9 Hz, CH), 114.2 (d, J = 9.6 Hz, CH), 110.8 (d, J = 5.5 Hz, C_{quat}), 106.9 (d, J = 24.0 Hz, CH), 56.9 (CH_2), 54.5 (CH_2), 52.5 (CH_2), 40.3 (CH_2), 36.5 (CH), 29.0 (CH_2), 28.7 (CH_3). ^{19}F NMR (471 MHz, DMSO-d_6) δ −55.36, −122.11 (td, J = 9.6, 4.5 Hz). MS (ESI) m/z 669.2 $[M + H]^+$.

N-(2-(4-((4-(2-acetyl-5-fluoro-1H-indol-3-yl)-1H-1,2,3-triazol-1-Yl)methyl)piperidin-1-yl)ethyl)-2′-fluoro-6′-(trifluoromethyl)-[1,1′-biphenyl]-4-sulfonamide (12). Following General Procedure K, a solution of indole **63** (60 mg, 0.30 mmol) and azide **106** (152 mg, 0.31 mmol) in tetrahydrofuran/*tert*-butanol/water (2.4 mL) was treated with 2.0 M aqueous of sodium ascorbate (522 μL, 1.04 mmol) and 15% aqueous copper(II) sulfate pentahydrate (432 μL, 0.26 mmol). The crude product was purified via flash column chromatography on silica gel (methanol/dichloromethane, 0:100 → 4:96) to provide compound **12** as white solid (133 mg, 0.19 mmol, 63% yield). ^{1}H NMR (500 MHz, DMSO-d_6) δ 12.05 (s, 1H), 8.60 (s, 1H), 7.93−7.88 (m, 2H), 7.78 (dd, J = 10.2, 2.6 Hz, 1H), 7.74−7.64

https://doi.org/10.1021/acs.jmedchem.5c00695
J. Med. Chem. XXXX, XXX, XXX−XXX

(m, 3H), 7.63 (s, 1H), 7.58−7.51 (m, 3H), 7.23 (td, J = 9.1, 2.6 Hz, 1H), 4.35 (d, J = 7.0 Hz, 2H), 2.94 (t, J = 6.9 Hz, 2H), 2.70 (dt, J = 10.9, 3.7 Hz, 2H), 2.48 (s, 3H), 2.26 (t, J = 6.8 Hz, 2H), 1.97−1.77 (m, 3H), 1.53−1.42 (m, 2H), 1.34−1.21 (m, 2H). ^{13}C RMN (126 MHz, DMSO-d_6) δ 191.0 (C_{quat}), 160.3 (C_{quat}), 158.3 (C_{quat}), 157.6 (d, J = 234.1 Hz, C_{quat}), 141.0 (C_{quat}), 139.9 (C_{quat}), 135.4 (C_{quat}), 133.0 (C_{quat}), 132.9 (C_{quat}), 131.0 (d, J = 8.8 Hz, CH), 130.5 (CH), 126.8 (CH), 126.6 (d, J = 10.4 Hz, C_{quat}), 126.2 (CH), 125.0 (CH), 122.2 (CH), 120.1 (d, J = 23.2 Hz, CH), 114.8 (d, J = 27.1 Hz, CH), 114.2 (d, J = 9.5 Hz, CH), 110.7 (d, J = 5.5 Hz, C_{quat}), 106.8 (d, J = 24.1 Hz, CH), 56.8 (CH_2), 54.5 (CH_2), 52.5 (CH_2), 40.3 (CH_2), 36.5 (CH), 29.0 (CH_2), 28.7 (CH_3). ^{19}F NMR (471 MHz, DMSO-d_6) δ −55.94, −111.83 − −111.89 (m), −122.11 (dd, J = 9.5, 4.5 Hz). MS (ESI) m/z 687.2 $[M + H]^+$.

N-(2-(4-((4-(2-acetyl-5-fluoro-1H-indol-3-yl)-1H-1,2,3-triazol-1-yl)methyl)piperidin-1-yl)ethyl)-2′,6′-dimethoxy-[1,1′-biphenyl]-4-sulfonamide (13). Following General Procedure K, a solution of indole **63** (60 mg, 0.30 mmol) and azide **107** (144 mg, 0.31 mmol) in tetrahydrofuran/*tert*-butanol/water (2.4 mL) was treated with 2.0 M aqueous sodium ascorbate (522 μL, 1.04 mmol) and 15% aqueous copper(II) sulfate pentahydrate (432 μL, 0.26 mmol). The crude product was purified via flash column chromatography on silica gel (methanol/dichloromethane, 0:100 → 4:96) to provide compound **13** as pale yellow solid (135 mg, 0.20 mmol, 67% yield). ^{1}H NMR (500 MHz, DMSO-d_6) δ 12.06 (s, 1H), 8.61 (s, 1H), 7.90−7.73 (m, 3H), 7.54 15 (dd, J = 9.0, 4.7 Hz, 1H), 7.50 (s, 1H), 7.48−7.38 (m, 2H), 7.32 (t, J = 8.4 Hz, 1H), 7.24 (td, J = 9.1, 2.6 Hz, 1H), 6.74 (d, J = 8.4 Hz, 2H), 4.36 (d, J = 7.0 Hz, 2H), 3.66 (s, 6H), 3.36 (s, 2H), 2.92 (t, J = 6.8 Hz, 2H), 2.81−2.70 (m, 2H), 2.32 (q, J = 5.9 Hz, 2H), 1.86 (t, J = 11.3 Hz, 3H), 1.61−1.40 (m, 2H), 1.40−1.09 (m, 3H). ^{13}C NMR (126 MHz, DMSO-d_6) δ 191.0 (C_{quat}), 157.6 (d, J = 234.4 Hz, C_{quat}), 156.9 (C_{quat}), 140.0 (C_{quat}), 138.7 (C_{quat}), 138.5 (C_{quat}), 133.0 (C_{quat}),132.9 (C_{quat}), 135.1 (CH), 129.7 (CH), 126.6 (d, J = 11.1 Hz, C_{quat}), 125.7 (CH), 125.0 (CH), 117.0 (C_{quat}), 114.8 (d, J = 27.0 Hz, CH), 114.2 (CH),114.1 (CH), 110.7 (d, J = 5.5 Hz, C_{quat}), 106.9 (d, J = 22.1 Hz, CH), 104.4 (CH), 57.0 (CH_2), 55.7 (CH_3), 54.5 (CH_2), 52.6 (CH_2), 40.4 (CH_2), 36.5 (CH), 29.1 (CH_2), 28.7 (CH_3). ^{19}F NMR (471 MHz, DMSO-d_6) δ −122.1 (td, J = 9.5, 4.6 Hz). MS (ESI) m/z 661.3 $[M + H]^+$.

N-(2-(4-((4-(2-acetyl-5-fluoro-1H-indol-3-yl)-1H-1,2,3-triazol-1-yl)methyl)piperidin-1-yl)ethyl)-2′,6′-dimethoxy-2-methyl-[1,1′-biphenyl]-4-sulfonamide (14). Following General Procedure K, a solution of indole **63** (60 mg, 0.30 mmol) and azide **108** (148 mg, 0.31 mmol) in tetrahydrofuran/*tert*-butanol/water (2.4 mL) was treated with 2.0 M aqueous sodium ascorbate (522 μL, 1.04 mmol) and 15% aqueous copper(II) sulfate pentahydrate (432 μL, 0.26 mmol). The crude product was purified via flash column chromatography on silica gel (methanol/dichloromethane, 0:100 → 4:96) to provide compound **14** as pale yellow solid (130 mg, 0.19 mmol, 63% yield). ^{1}H NMR (500 MHz, DMSO-d_6) δ 12.06 (s, 1H), 8.61 (s, 1H), 7.79 (dd, J = 10.2, 2.6 Hz, 1H), 7.67 (d, J = 2.1 Hz, 1H), 7.59 (dd, J = 7.9, 2.1 Hz, 1H), 7.54 (dd, J = 9.0, 4.6 Hz, 1H), 7.41 (s, 1H), 7.32 (d, J = 8.4 Hz, 1H), 7.27−7.17 (m, 2H), 6.73 (d, J = 8.5 Hz, 2H), 4.36 (d, J = 7.1 Hz, 2H), 3.66 (s, 6H) 2.92 (t, J = 7.0 Hz, 2H), 2.80−2.68 (m, 2H), 2.30 (t, J = 6.9 Hz, 2H), 2.02 (s, 3H), 1.95−1.80 (m, 3H), 1.54−1.43 (m, 2H), 1.27 (td, J = 11.8, 3.2 Hz, 2H), 1.27−1.14 (m, 3H). ^{13}C NMR (126 MHz, DMSO-d_6) δ 191.0 (C_{quat}), 157.6 (d, J = 234.3 Hz, C_{quat}), 156.8 (C_{quat}), 140.0 (C_{quat}) 139.1 (C_{quat}), 138.9 (C_{quat}), 138.1 (C_{quat}), 133.0 (C_{quat}), 132.9 (C_{quat}), 131.5 (CH), 129.7 (CH), 127.1 (CH), 126.6 (d, J = 10.5 Hz, C_{quat}), 125.0 (CH), 123.4 (CH), 116.4 (C_{quat}), 114.8 (d, J = 26.8 Hz, CH), 114.2 (d, J = 9.6 Hz, CH), 110.8 (d, J = 5.5 Hz, C_{quat}), 106.9 (d, J = 24.2 Hz, CH), 104.2 (CH), 97.2 (CH), 65.7 (CH_2), 57.0 (CH_2), 55.6 (CH_3), 54.6 (CH_2), 52.6 (CH_2), 40.3 (CH_2), 36.5 (CH), 33.2 (CH_2), 29.1 (CH_2), 28.7 (CH_3), 19.4 (CH_3). ^{19}F NMR (471 MHz, DMSO-d_6) δ 122.1 (td, J = 9.5, 4.9 Hz). MS (ESI) m/z 675.3 $[M + H]^+$.

N-(2-(4-((4-(2-acetyl-5-fluoro-1H-indol-3-yl)-1H-1,2,3-triazol-1-yl)methyl)piperidin-1-yl)ethyl)-2′-methoxy-2-methyl-[1,1′-biphenyl]-4-sulfonamide (15). Following General Procedure K, a solution of indole **63** (120 mg, 0.60 mmol) and azide **109** (279 mg, 0.63 mmol) in tetrahydrofuran/*tert*-butanol/water (2.4 mL) was treated with 2.0 M aqueous sodium ascorbate (600 μL, 1.20 mmol) and 15% aqueous copper(II) sulfate pentahydrate (600 μL, 0.36 mmol). The crude product was purified via flash column chromatography on silica gel (methanol/dichloromethane, 0:100 → 4:96) to provide compound **15** as yellow solid (80 mg, 0.12 mmol, 20% yield). ^{1}H NMR (500 MHz, DMSO-d_6) δ 12.06 (s, 1H), 8.61 (s, 1H), 7.79 (dd, J = 10.1, 2.6 Hz, 1H), 7.69−7.66 (m, 1H), 7.63 (dd, J = 7.9, 2.0 Hz, 1H), 7.56−7.52 (m, 1H), 7.47 (s, 1H), 7.41−7.37 (m, 1H), 7.30 (d, J = 7.9 Hz, 1H), 7.24 (td, J = 9.1, 2.6 Hz, 1H), 7.12−7.08 (m, 2H), 7.02 (td, J = 7.4, 1.0 Hz, 1H), 4.36 (d, J = 7.1 Hz, 2H), 3.70 (s, 3H), 2.96−2.87 (m, 2H), 2.79−2.71 (m, 2H), 2.50 (s, 3H), 2.32 (t, J = 6.8 Hz, 2H), 2.12 (s, 3H), 1.91−1.81 (m, 1H), 1.52−1.45 (m, 2H), 1.28−1.21 (m, 2H). ^{13}C RMN (126 MHz, DMSO-d_6) δ 191.0 (C_{quat}), 157.6 (d, J = 234.3 Hz, C_{quat}), 155.9 (C_{quat}), 142.6 (C_{quat}), 140.0 (C_{quat}), 139.3 (C_{quat}), 137.5 (C_{quat}), 133.0 (C_{quat}), 132.9 (C_{quat}), 130.6 (CH), 130.2 (CH), 129.5 (CH), 128.5 (C_{quat}), 127.2 (CH), 126.6 (d, J = 10.5 Hz, C_{quat}), 125.0 (CH), 123.7 (CH), 120.5 (CH), 114.8 (d, J = 26.9 Hz, CH), 114.2 (d, J = 9.6 Hz, CH), 111.2 (CH), 110.7 (d, J = 5.5 Hz, C_{quat}), 106.9 (d, J = 24.0 Hz, CH), 57.0 (CH_2), 55.3 (CH_3), 54.6 (CH_2), 52.6 (CH_2), 40.3 (CH_2), 36.5 (CH), 29.1 (CH_2), 28.7 (CH_3), 19.6 (CH_3). ^{19}F NMR (471 MHz, DMSO-d_6) δ −122.1 (td, J = 9.5, 4.5 Hz). MS (ESI) m/z 667.2 $[M + H]^+$.

N-(2-(4-((4-(2-acetyl-5-fluoro-1H-indol-3-yl)-1H-1,2,3-triazol-1-yl)methyl)piperidin-1-yl)ethyl)-2-methyl-2′-(methylthio)-[1,1′-biphenyl]-4-sulfonamide (16). Following General Procedure K, a solution of indole **63** (120 mg, 0.60 mmol) and azide **110** (214 mg, 0.63 mmol) in tetrahydrofuran/*tert*-butanol/water (2.4 mL) was treated with 2.0 M aqueous sodium ascorbate (600 μL, 1.20 mmol) and 15% aqueous copper(II) sulfate pentahydrate (600 μL, 0.36 mmol). The crude product was purified via flash column chromatography on silica gel (methanol/dichloromethane, 0:100 → 4:96) to provide compound **16** as yellow solid (20 mg, 0.03 mmol, 5% yield). ^{1}H NMR (500 MHz, DMSO-d_6) δ 12.07 (s, 1H), 8.61 (s, 1H), 7.79 (dd, J = 10.1, 2.6 Hz, 1H), 7.73 (d, J = 2.0 Hz, 1H), 7.66 (dd, J = 7.9, 2.0 Hz, 1H), 7.56−7.49 (m, 2H), 7.41 (td, J = 7.6, 1.5 Hz, 1H), 7.34 (dd, J = 8.2, 1.2 Hz, 1H), 7.28−7.19 (m, 3H), 7.08 (dd, J = 7.5, 1.5 Hz, 1H), 4.36 (d, J = 7.1 Hz, 2H), 3.77 (s, 1H), 2.93 (t, J = 6.8 Hz, 2H), 2.89 (s, 1H), 2.80−2.71 (m, 3H), 2.50 (s, 3H), 2.35 (s, 3H), 2.09 (s, 3H), 1.95−1.85 (m, 2H), 1.49 (d, J = 12.4 Hz, 2H), 1.29−1.22 (m, 2H). ^{13}C RMN (126 MHz, DMSO-d_6) δ 191.0 (C_{quat}), 158.4 (d, J = 23.3 Hz, C_{quat}), 156.6 (C_{quat}), 143.7 (C_{quat}), 139.9 (d, J = 4.7 Hz), 137.9 (C_{quat}), 137.2 (C_{quat}), 137.0 (C_{quat}), 133.0 (C_{quat}), 132.9 (C_{quat}), 130.3 (CH), 128.8 (CH), 128.6 (CH), 127.6 (CH), 126.6 (d, J = 10.5 Hz, C_{quat}), 125.0 (CH), 124.6 (d, J = 5.0 Hz, CH), 123.9 (CH), 117.7 (C_{quat}), 115.2 (CH), 114.8 (d, J = 26.9 Hz, CH), 114.2 (d, J = 9.6 Hz, CH), 110.7 (d, J = 5.4 Hz, C_{quat}), 106.9 (d, J = 23.9 Hz, CH), 56.8 (CH_2), 55.6 (CH_3), 54.5 (CH_2), 52.5 (CH_2), 40.2 (CH_2), 36.4 (CH), 28.9 (CH_2), 28.7 (CH_3), 19.5 (CH_3). ^{19}F NMR (471 MHz, DMSO-d_6) δ −122.1 (td, J = 9.4, 4.4 Hz). MS (ESI) m/z 661.2 $[M + H]^+$.

N-(2-(4-((4-(2-acetyl-5-fluoro-1H-indol-3-yl)-1H-1,2,3-triazol-1-yl)methyl)piperidin-1-yl)ethyl)-4-(benzo[b]thiophen-7-yl)-3-methylbenzenesulfonamide (17). Following General Procedure K, a solution of indole **63** (36 mg, 0.18 mmol) and azide **111** (90 mg, 0.19 mmol) in tetrahydrofuran/*tert*-butanol/water (2.4 mL) was treated with 2.0 M aqueous sodium ascorbate (180 μL, 0.36 mmol) and 15% aqueous copper(II) sulfate pentahydrate (180 μL, 0.11 mmol). The crude product was purified via flash column chromatography on silica gel (methanol/dichloromethane, 0:100 → 10:90) to provide compound **17** as yellow solid (22 mg, 0.03 mmol, 17% yield). ^{1}H NMR (500 MHz, DMSO-d_6) δ 12.05 (s, 1H), 8.60 (s, 1H), 7.93 (dd, J = 8.0, 1.1 Hz, 1H), 7.83 (d, J = 2.0 Hz, 1H), 7.80−7.72 (m, 3H), 7.56−7.51 (m, 4H), 7.51−7.46 (m, 1H), 7.26−7.21 (m, 2H), 4.36 (d, J = 7.1 Hz, 2H), 2.98−2.94 (m, 2H), 2.78−2.70 (m, 2H), 2.49 (s, 3H), 2.32 (t, J = 6.9 Hz, 2H), 2.16 (s, 3H), 1.92−1.83 (m, 3H), 1.52−1.45 (m, 2H), 1.30−1.20 (m, 2H). ^{13}C RMN (126 MHz, DMSO-d_6) δ 191.0 (C_{quat}), 157.6 (d, J = 234.3 Hz, C_{quat}), 143.5 (C_{quat}), 140.4 (C_{quat}), 140.0 (C_{quat}), 139.8 (C_{quat}), 138.8 (C_{quat}),

https://doi.org/10.1021/acs.jmedchem.5c00695
J. Med. Chem. XXXX, XXX, XXX−XXX

136.8 (C_{quat}), 134.4 (C_{quat}), 133.0 (C_{quat}), 132.9 (C_{quat}), 123.0 (CH), 128.2 (CH), 127.8 (CH), 126.6 (d, J = 10.5 Hz, C_{quat}), 125.0 (CH), 124.7 (CH), 124.5 (d, J = 8.1 Hz, CH), 124.2 (CH), 123.2 (CH), 114.8 (d, J = 26.9 Hz, CH), 114.2 (d, J = 9.5 Hz, CH), 110.7 (d, J = 5.5 Hz, C_{quat}), 106.9 (d, J = 24.1 Hz, CH), 56.9 (CH_2), 54.5 (CH_2), 52.6 (CH_2), 40.3 (CH_2), 36.50 (CH), 29.1 (CH_2), 28.7 (CH_3), 19.5 (CH_3). ^{19}F NMR (471 MHz, DMSO-d_6) δ 122.1 (td, J = 9.6, 4.9 Hz). MS (ESI) m/z 671.2 $[M + H]^+$.

N-(2-(4-((4-(2-acetyl-5-fluoro-1H-indol-3-yl)-1H-1,2,3-triazol-1-yl)methyl)piperidin-1-yl)ethyl)-2′-hydroxy-[1,1′-biphenyl]-4-sulfonamide (18). Following General Procedure K, a solution of indole **63** (60 mg, 0.30 mmol) and azide **112** (130 mg, 0.31 mmol) in tetrahydrofuran/*tert*-butanol/water (2.4 mL) was treated with 2.0 M aqueous sodium ascorbate (522 μL, 1.04 mmol) and 15% aqueous copper(II) sulfate pentahydrate (432 μL, 0.26 mmol). The crude product was purified via flash column chromatography on silica gel (methanol/dichloromethane, 0:100 → 4:96) to provide compound **18** as white solid (122 mg, 0.20 mmol, 66% yield). ^{1}H NMR (500 MHz, DMSO-d_6) δ 12.05 (s, 1H), 9.75 (s, 1H), 8.60 (s, 1H), 7.85−7.71 (m, 5H), 7.53 (dd, J = 9.0, 4.6 Hz, 1H), 7.50 (s, 1H), 7.30 (dd, J = 7.6, 1.7 Hz, 1H), 7.27−7.16 (m, 2H), 6.97 (dd, J = 8.1, 1.2 Hz, 1H), 6.89 (td, J = 7.4, 1.2 Hz, 1H), 4.35 (d, J = 7.0 Hz, 2H), 2.89 (t, J = 6.9 Hz, 2H), 2.74 (dd, J = 9.4, 5.5 Hz, 2H), 2.48 (s, 1H), 2.32 (t, J = 6.8 Hz, 2H), 1.86 (t, J = 11.3 Hz, 3H), 1.53−1.38 (m, 2H), 1.22 (dq, J = 11.0, 5.3 Hz, 2H), 1.14 (s, 2H). ^{13}C RMN (126 MHz, DMSO-d_6) δ 208.4 (C_{quat}), 190.9 (C_{quat}), 157.6 (d, J = 234.4 Hz, C_{quat}), 154.5 (C_{quat}), 142.5 (C_{quat}), 139.9 (C_{quat}), 138.5 (C_{quat}), 133.0 (d, J = 6.4 Hz, C_{quat}), 130.4 (CH), 129.6 (CH), 129.5 (CH), 126.6 (d, J = 10.3 Hz, C_{quat}), 126.2 (d, J = 11.7 Hz, CH), 125.0 (CH), 119.6 (CH), 116.2 (CH), 114.8 (d, J = 26.8 Hz, CH), 114.2 (d, J = 9.5 Hz, CH), 110.8 (d, J = 5.5 Hz, C_{quat}), 106.9 (d, J = 24.1 Hz, CH), 68.5 (C_{quat}), 57.0 (CH_2), 54.6 (CH_2), 52.6 (CH_2), 40.3 (CH_2), 36.5 (CH), 29.0 (CH_2), 28.7 (CH_3). ^{19}F NMR (471 MHz, DMSO-d_6) δ −122.1 (td, J = 9.5, 4.5 Hz). MS (ESI) m/z 617.2 $[M + H]^+$.

N-(2-(4-((4-(2-acetyl-5-fluoro-1H-indol-3-yl)-1H-1,2,3-triazol-1-yl)methyl)piperidin-1-yl)ethyl)-2′-fluoro-6′-hydroxy-[1,1′-biphenyl]-4-sulfonamide (19, KDX1381). Following General Procedure K, a solution of indole **63** (60 mg, 0.30 mmol) and azide **113** (136 mg, 0.31 mmol) in tetrahydrofuran/*tert*-butanol/water (2.4 mL) was treated with 2.0 M aqueous sodium ascorbate (522 μL, 1.04 mmol) and 15% aqueous copper(II) sulfate pentahydrate (432 μL, 0.26 mmol). The crude product was purified via flash column chromatography on silica gel (methanol/dichloromethane, 0:100 → 4:96) to provide compound **19** as white solid (117 mg, 0.18 mmol, 60% yield). ^{1}H NMR (500 MHz, DMSO-d_6) δ 12.06 (s, 1H), 10.11 (s, 1H), 8.60 (s, 1H), 7.92−7.75 (m, 3H), 7.66−7.46 (m, 4H), 7.27−7.16 (m, 2H), 6.82 (d, J = 8.2 Hz, 1H), 6.73 (ddd, J = 9.5, 8.2, 1.0 Hz, 1H), 4.35 (d, J = 7.1 Hz, 2H), 2.91 (t, J = 6.9 Hz, 2H), 2.74 (dt, J = 11.7, 3.4 Hz, 2H), 2.32 (t, J = 6.9 Hz, 2H), 2.01−1.78 (m, 3H), 1.58−1.41 (m, 2H), 1.40−1.13 (m, 4H), 0.90−0.79 (m, 1H). ^{13}C RMN (126 MHz, DMSO-d_6) δ 191.0 (C_{quat}), 160.9 (C_{quat}), 158.72 (d, J = 50.0 Hz, C_{quat}), 156.7 (C_{quat}), 156.0 (d, J = 6.8 Hz, C_{quat}), 140.0 (C_{quat}), 139.3 (C_{quat}), 136.0 (C_{quat}), 133.0 (d, J = 10.0 Hz, C_{quat}), 131.2 (CH), 129.8 (d, J = 11.4 Hz, CH), 126.6 (d, J = 10.4 Hz, CH), 126.1 (CH), 125.0 (CH), 115.1 (C_{quat}), 115.0 (d, J = 2.7 Hz, CH), 114.7 (CH), 114.2 (d, J = 9.5 Hz, CH), 111.9 (d, J = 3.2 Hz, C_{quat}), 110.8 (d, J = 5.4 Hz, C_{quat}), 106.9 (d, J = 24.1 Hz, CH), 106.0 (d, J = 23.2 Hz, CH), 56.9 (CH_2), 54.5 (CH_2), 52.5 (CH_2), 40.1 (CH_2), 36.4 (CH), 28.9 (CH_2), 28.7 (CH_3). ^{19}F NMR (471 MHz, DMSO-d_6) δ −116.2 − −116.3 (m), −122.05 (td, J = 9.5, 4.5 Hz). MS (ESI) m/z 635.2 $[M + H]^+$.

N-(2-(4-((4-(2-acetyl-5-fluoro-1H-indol-3-yl)-1H-1,2,3-triazol-1-yl)methyl)piperidin-1-yl)ethyl)-2′-chloro-6′-hydroxy-[1,1′-biphenyl]-4-sulfonamide (20). Following General Procedure K, a solution of indole **63** (85 mg, 0.42 mmol) and azide **114** (200 mg, 0.44 mmol) in tetrahydrofuran/*tert*-butanol/water (2.4 mL) was treated with 2.0 M aqueous sodium ascorbate (440 μL, 0.88 mmol) and 15% aqueous copper(II) sulfate pentahydrate (420 μL, 0.25 mmol). The crude product was purified via flash column chromatography on silica gel (methanol/dichloromethane, 0:100 → 10:90) to provide compound **20** as yellow solid (58 mg, 0.09 mmol, 20% yield). ^{1}H NMR (500 MHz, DMSO-d_6) δ 12.05 (s, 1H), 9.96 (s, 1H), 8.60 (s, 1H), 7.85−7.81 (m, 2H), 7.78 (dd, J = 10.0, 2.6 Hz, 1H), 7.57−7.51 (m, 2H), 7.48−7.45 (m, 2H), 7.25−7.18 (m, 2H), 6.98 (dd, J = 8.1, 1.0 Hz, 1H), 6.93 (dd, J = 8.2, 1.1 Hz, 1H), 4.35 (d, J = 7.1 Hz, 2H), 2.92 (t, J = 7.1 Hz, 2H), 2.76−2.69 (m, 2H), 2.50 (s, 3H), 2.30 (t, J = 6.9 Hz, 2H), 1.89−1.80 (m, 3H), 1.50−1.44 (m, 2H), 1.29−1.19 (m, 2H). ^{13}C RMN (126 MHz, DMSO-d_6) δ 191.0 (C_{quat}), 157.6 (d, J = 234.3 Hz, C_{quat}), 156.0 (C_{quat}), 140.0 (C_{quat}), 139.6 (d, J = 17.4 Hz, C_{quat}), 133.0 (d, J = 7.7 Hz, C_{quat}), 132.5 (C_{quat}), 131.1 (CH), 129.8 (CH), 126.6 (d, J = 10.5 Hz, C_{quat}), 126.2 (C_{quat}), 126.1 (CH), 125.0 (CH), 119.8 (CH), 114.8 (d, J = 27.0 Hz, CH), 114.5 (CH), 114.2 (d, J = 9.6 Hz, CH), 110.8 (d, J = 5.7 Hz, C_{quat}), 106.9 (d, J = 24.1 Hz, CH), 57.0 (CH_2), 54.6 (CH_2), 52.6 (CH_2), 41.1 (CH_2), 36.5 (CH), 28.9 (CH_2), 28.7 (CH_3). ^{19}F NMR (471 MHz, DMSO-d_6) δ −122.1 (td, J = 9.5, 4.5 Hz). MS (ESI) m/z 651.2 $[M + H]^+$.

N-(2-(4-((4-(2-acetyl-5-fluoro-1H-indol-3-yl)-1H-1,2,3-triazol-1-yl)methyl)piperidin-1-yl)ethyl)-2′-fluoro-6′-methoxy-[1,1′-biphenyl]-4-sulfonamide (21). Following General Procedure K, a solution of indole **63** (60 mg, 0.30 mmol) and azide **115** (140 mg, 0.31 mmol) in tetrahydrofuran/*tert*-butanol/water (2.4 mL) was treated with 2.0 M aqueous sodium ascorbate (522 μL, 1.04 mmol) and 15% aqueous copper(II) sulfate pentahydrate (432 μL, 0.26 mmol). The crude product was purified via flash column chromatography on silica gel (methanol/dichloromethane, 0:100 → 4:96) to provide compound **21** as pale yellow solid (138 mg, 0.22 mmol, 73% yield). ^{1}H NMR (500 MHz, DMSO-d_6) δ 12.06 (s, 1H), 8.60 (s, 1H), 7.85 (d, J = 8.2 Hz, 2H), 7.78 (dd, J = 10.1, 2.6 Hz, 1H), 7.54 (dd, J = 10.4, 6.2 Hz, 4H), 7.41 (td, J = 8.4, 6.8 Hz, 1H), 7.23 (td, J = 9.1,2.6 Hz, 1H), 6.98 (d, J = 8.4 Hz, 1H), 6.92 (t, J = 8.9 Hz, 1H), 4.35 (d, J = 7.0 Hz, 2H), 3.74 (s, 3H), 2.92 (t, J = 6.7 Hz, 2H), 2.73 (d, J = 10.9 Hz, 2H), 2.47 (s, 3H), 2.31 (q, J = 6.3 Hz, 2H), 1.85 (t, J = 11.1 Hz, 3H), 1.56−1.41 (m, 2H), 1.23 (qd, J = 11.5, 3.5 Hz, 2H). ^{13}C RMN (126 MHz, DMSO-d_6) δ 191.0 (C_{quat}), 158.5 (d, J = 9.3 Hz, C_{quat}), 157.4 (d, J = 6.8 Hz, C_{quat}), 156.6 (C_{quat}), 139.9 (C_{quat}), 139.7 (C_{quat}), 135.6 (C_{quat}), 133.0 (C_{quat}), 132.9 (C_{quat}), 131.2 (CH), 130.3 (d, J = 10.8 Hz, CH), 126.58 (d, J = 10.4 Hz, C_{quat}), 126.1 (CH), 125.0 (CH), 116.5 (d, J = 17.5 Hz, C_{quat}), 114.9 (CH), 114.7 (CH), 114.2 (d, J = 9.5 Hz, CH), 110.8 (d, J = 5.5 Hz, C_{quat}), 108.0 (d, J = 22.9 Hz, CH), 107.7 (d, J = 2.7 Hz, CH), 106.9 (d, J = 24.0 Hz, CH), 57.0 (CH_2), 56.3 (CH_3), 55.8 (CH_2), 54.5 (CH_2), 52.6 (CH_2), 40.3 (CH_2), 36.5 (CH), 29.0 (CH_2), 28.7 (CH_3). ^{19}F NMR (471 MHz, DMSO-d_6) δ −116.0 (t, J = 8.2 Hz), −122.1 (td, J = 9.5, 4.5 Hz). MS (ESI) m/z 649.2 $[M + H]^+$.

N-(2-(4-((4-(2-acetyl-5-fluoro-1H-indol-3-yl)-1H-1,2,3-triazol-1-yl)methyl)piperidin-1-yl)ethyl)-2′-fluoro-6′-hydroxy-2-methyl-[1,1′-biphenyl]-4-sulfonamide (22). Following General Procedure K, a solution of indole **63** (76 mg, 0.38 mmol) and azide **116** (180 mg, 0.40 mmol) in tetrahydrofuran/*tert*-butanol/water (2.4 mL) was treated with 2.0 M aqueous sodium ascorbate (400 μL, 0.80 mmol) and 15% aqueous copper(II) sulfate pentahydrate (380 μL, 0.23 mmol). The crude product was purified via flash column chromatography on silica gel (methanol/dichloromethane, 0:100 → 4:96) to provide compound **22** as yellow solid (41 mg, 0.06 mmol, 16% yield). ^{1}H NMR (500 MHz, DMSO-d_6) δ 12.06 (s, 1H), 9.97 (s, 1H), 8.60 (s, 1H), 7.78 (dd, J = 10.0, 2.6 Hz, 1H), 7.73 (d, J = 2.0 Hz, 1H), 7.64 (dd, J = 7.9, 2.0 Hz, 1H), 7.55−7.45 (m, 2H), 7.34 (d, J = 8.0 Hz, 1H), 7.26−7.20 (m, 2H), 6.80 (d, J = 8.3 Hz, 1H), 6.74−6.67 (m, 1H), 4.35 (d, J = 7.1 Hz, 2H), 2.92 (t, J = 6.9 Hz, 2H), 2.76−2.70 (m, 2H), 2.34−2.30 (m, 2H), 2.15 (s, 3H), 1.91−1.80 (m, 3H), 1.50−1.44 (m, 2H), 1.28−1.20 (m, 2H). ^{13}C RMN (126 MHz, DMSO-d_6) δ 190.8 (C_{quat}), 159.4 (d, J = 270.6 Hz, C_{quat}), 158.6 (C_{quat}), 156.5 (C_{quat}), 156.1 (d, J = 88.1 Hz, C_{quat}), 155.8 (C_{quat}), 139.7 (d, J = 11.7 Hz, C_{quat}), 138.1 (C_{quat}), 136.0 (C_{quat}), 132.8 (d, J = 7.1 Hz, C_{quat}), 131.3 (CH), 129.6 (d, J = 10.8 Hz, CH), 127.2 (CH), 126.4 (d, J = 10.4 Hz, C_{quat}), 124.9 (CH), 123.4 (CH), 114.7 (d, J = 14.8 Hz, CH), 114.6 (d, J = 6.9 Hz, CH), 114.0 (d, J = 9.6 Hz, C_{quat}), 111.4 (d, J = 2.5 Hz, CH), 110.6 (d, J = 5.6 Hz, C_{quat}), 106.7 (d, J = 24.0 Hz, CH), 105.6 (d, J = 22.4 Hz, CH), 56.9 (CH_2), 54.4 (CH_2), 52.4 (CH_2), 40.2 (CH_2), 36.3 (CH), 28.9 (CH_2), 28.6 (CH_3), 19.3

https://doi.org/10.1021/acs.jmedchem.5c00695
J. Med. Chem. XXXX, XXX, XXX−XXX

(CH_3). ^{19}F NMR (471 MHz, DMSO-d_6) δ −114.6 (t, J = 8.0 Hz), −122.1 (td, J = 9.6, 4.6 Hz). MS (ESI) m/z 649.2 $[M + H]^+$.

N-(2-(4-((4-(2-acetyl-5-fluoro-1H-indol-3-yl)-1H-1,2,3-triazol-1-yl)methyl)piperidin-1-yl)ethyl)-2-chloro-2′-fluoro-6′-hydroxy-[1,1′-biphenyl]-4-sulfonamide (23). Following General Procedure K, a solution of indole **63** (88 mg, 0.44 mmol) and azide **117** (220 mg, 0.47 mmol), 2.0 M aqueous of sodium ascorbate (440 μL, 0.88 mmol) and 15% aqueous of copper(II) sulfate pentahydrate (440 μL, 0.26 mmol), in tetrahydrofuran/*tert*-butanol/water (2.4 mL). The crude product was purified via flash column chromatography on silica gel (methanol/dichloromethane, 0:100 → 10:90) to provide compound **23** as yellow solid (39 mg, 0.06 mmol, 14% yield). ^1H NMR (500 MHz, DMSO-d_6) δ 12.06 (s, 1H), 10.14 (s, 1H), 8.61 (s, 1H), 7.94 (d, J = 1.8 Hz, 1H), 7. 81−7.67 (m, 3H), 7.59−7.52 (m, 2H), 7.30−7.22 (m, 2H), 6.82 (d, J = 8.3 Hz, 1H), 6.77−6.72 (m, 1H), 4.35 (d, J = 7.1 Hz, 2H), 2.97 (t, J = 6.7 Hz, 2H), 2.77−2.71 (m, 2H), 2.31 (t, J = 6.7 Hz, 2H), 1.89−1.81 (m, 3H), 1.51−1.44 (m, 2H), 1.28−1.21 (m 2H). ^{13}C RMN (126 MHz, DMSO-d_6) δ 191.0 (C_{quat}), 159.6 (d, J = 272.3 Hz, C_{quat}), 157.45 (d, J = 323.3 Hz, C_{quat}), 156.4 (d, J = 66.1 Hz, C_{quat}), 142.0 (C_{quat}), 139.9 (C_{quat}), 135.4 (C_{quat}), 134.4 (C_{quat}), 133.5 (CH), 130.5 (d, J = 10.8 Hz, C_{quat}), 130.5 (d, J = 10.8 Hz, CH), 126.8 (CH), 126.60 (d, J = 10.4 Hz, C_{quat}), 125.0 (CH), 124.8 (CH), 115.0 (C_{quat}), 114.85 (d, J = 26.8 Hz, CH), 114.19 (d, J = 9.6 Hz, CH), 113.0 (d, J = 18.5 Hz, C_{quat}), 111.7 (d, J = 2.7 Hz, CH), 110.8 (d, J = 5.7 Hz, C_{quat}), 106.9 (d, J = 24.0 Hz, CH), 105.6 (d, J = 22.1 Hz, CH), 57.0 (CH_2), 54.6 (CH_2), 52.6 (CH_2), 40.3 (CH_2), 36.5 (CH), 29.0 (CH_2), 28.7 (CH_3). ^{19}F NMR (471 MHz, DMSO-d_6) δ −114.2 (t, J = 8.0 Hz), −122.1 (td, J = 9.5, 4.4 Hz). MS (ESI) m/z 669.2 $[M + H]^+$.

N-(2-(4-((4-(2-acetyl-5-fluoro-1H-indol-3-yl)-1H-1,2,3-triazol-1-yl)methyl)piperidin-1-yl)ethyl)-2′-fluoro-6′-hydroxy-2-(trifluoromethyl)-[1,1′-biphenyl]-4-sulfonamide (24). Following General Procedure K, a solution of indole **63** (64 mg, 0.32 mmol) and azide **118** (170 mg, 0.34 mmol) in tetrahydrofuran/*tert*-butanol/water (2.4 mL) was treated with 2.0 M aqueous sodium ascorbate (340 μL, 0.68 mmol) and 15% aqueous copper(II) sulfate pentahydrate (320 μL, 0.19 mmol). The crude product was purified via flash column chromatography on silica gel (methanol/dichloromethane, 0:100 → 20:80) to provide compound **24** as yellow solid (33 mg, 0.05 mmol, 15% yield). ^1H NMR (500 MHz, DMSO-d_6) δ 12.06 (s, 1H), 10.07 (s, 1H), 8.60 (s, 1H), 8.18 (d, J = 1.9 Hz, 1H), 8.13 (dd, J = 8.0, 1.9 Hz, 1H), 7.89 (s, 1H), 7.78 (dd, J = 10.1, 2.6 Hz, 1H), 7.63 (d, J = 8.0 Hz, 1H), 7.56−7.52 (m, 1H), 7.30−7.22 (m, 2H), 6.79 (d, J = 8.3 Hz, 1H), 6.74−6.69 (m, 1H), 4.35 (d, J = 7.1 Hz, 2H), 2.99 (t, J = 6.7 Hz, 2H), 2.72 (d, J = 10.9 Hz, 2H), 2.29 (t, J = 6.7 Hz, 2H), 1.84 (t, J = 11.3 Hz, 3H), 1.47 (d, J = 12.2 Hz, 2H), 1.28−1.20 (m, 2H). ^{13}C RMN (126 MHz, DMSO-d_6) δ 191.0 (C_{quat}), 159.7 (d, J = 242.3 Hz, C_{quat}), 158.5 (C_{quat}), 156.6 (C_{quat}), 156.4 (d, J = 6.5 Hz, C_{quat}), 141.4 (C_{quat}), 139.9 (C_{quat}), 135.3 (C_{quat}), 134.2 (CH), 132.9 (d, J = 6.2 Hz, CH), 130.6 (d, J = 10.6 Hz, CH), 130.0 (CH), 129.5 (d, J = 30.4 Hz, C_{quat}), 126.6 (d, J = 10.4 Hz, C_{quat}), 125.0 (CH), 124.2 (C_{quat}), 123.9 (d, J = 5.5 Hz, CH), 122.0 (C_{quat}), 114.8 (d, J = 26.9 Hz, CH), 114.2 (d, J = 9.5 Hz, CH), 112.8 (d, J = 19.2 Hz, C_{quat}), 111.3 (CH), 110.7 (d, J = 5.6 Hz, C_{quat}), 106.8 (d, J = 24.3 Hz, CH), 105.2 (d, J = 21.9 Hz, CH), 57.0 (CH_2), 54.5 (CH_2), 52.5 (CH_2), 40.3 (CH_2), 36.5 (CH), 29.0 (CH_2), 28.7 (CH_3). ^{19}F NMR (471 MHz, DMSO-d_6) δ −60.3 (d, J = 4.1 Hz), −113.6 (dq, J = 8.7, 4.4 Hz), −122.1 (td, J = 9.6, 4.7 Hz). MS (ESI) m/z 703.2 $[M + H]^+$.

N-(2-(4-((4-(2-acetyl-5-fluoro-1H-indol-3-yl)-1H-1,2,3-triazol-1-yl)methyl)piperidin-1-yl)ethyl)-2-cyano-2′-fluoro-6′-hydroxy-[1,1′-biphenyl]-4-sulfonamide (25). Following General Procedure K, a solution of indole **63** (82 mg, 0.41 mmol) and azide **119** (200 mg, 0.43 mmol) in tetrahydrofuran/*tert*-butanol/water (2.4 mL) was treated with 2.0 M aqueous sodium ascorbate (410 μL, 0.82 mmol) and 15% aqueous copper(II) sulfate pentahydrate (410 μL, 0.25 mmol). The crude product was purified via flash column chromatography on silica gel (methanol/dichloromethane, 0:100 → 10:90) to provide compound **25** as yellow solid (23 mg, 0.04 mmol, 10% yield). ^1H NMR (500 MHz, DMSO-d_6) δ 12.04 (s, 1H), 8.64 (tt, J = 3.8, 1.9 Hz, 2H), 8.57 (s, 1H), 8.35−8.30 (m, 1H), 7.94 (s, 1H), 7.76 (dd, J = 10.0, 2.6 Hz, 1H), 7.68−7.63 (m, 1H), 7.53−7.50 (m, 1H), 7.37−7.31 (m, 2H), 7.25−7.20 (m, 1H), 4.31 (d, J = 7.1 Hz, 2H), 2.96−2.89 (m, 2H), 2.77−2.68 (m, 2H), 2.49 (s, 3H), 2.32 (t, J = 6.6 Hz, 2H), 1.91−1.78 (m, 2H), 1.49−1.41 (m, 2H), 1.28−1.12 (m, 4H). ^{13}C RMN (126 MHz, DMSO-d_6) δ 191.0 (C_{quat}), 159.9 (d, J = 252.9 Hz, C_{quat}), 159.1 (C_{quat}), 157.5 (d, J = 234.1 Hz, C_{quat}), 152.1 (d, J = 6.1 Hz, C_{quat}), 141.2 (C_{quat}), 140.0 (C_{quat}), 134.6 (C_{quat}), 133.0 (C_{quat}), 132.9 (C_{quat}), 132.7 (CH), 132.1 (d, J = 11.6 Hz, CH), 127.9 (CH), 127.5 (d, J = 22.2 Hz, CH), 126.6 (d, J = 10.8 Hz, C_{quat}), 125.0 (C_{quat}), 121.7 (C_{quat}), 114.9 (CH), 114.7 (CH), 114.2 (d, J = 9.6 Hz, CH), 113.9 (d, J = 3.1 Hz, CH), 112.4 (d, J = 23.1 Hz, CH), 110.7 (d, J = 5.5 Hz, C_{quat}), 106.9 (d, J = 7.1 Hz, C_{quat}), 106.7 (d, J = 22.1 Hz, CH), 57.0 (CH_2), 54.5 (CH_2), 52.5 (CH_2), 40.1 (CH_2), 36.4 (CH), 28.9 (CH_2), 28.7 (CH_3). ^{19}F NMR (471 MHz, DMSO-d_6) δ −110.7 (dd, J = 13.0, 6.1 Hz), −122.1 (td, J = 9.6, 4.5 Hz). MS (ESI) m/z 660.2 $[M + H]^+$.

N-(2-(4-((4-(2-acetyl-5-fluoro-1H-indol-3-yl)-1H-1,2,3-triazol-1-yl)methyl)piperidin-1-yl)ethyl)-2′-fluoro-6′-hydroxy-2-methoxy-[1,1′-biphenyl]-4-sulfonamide (26). Following General Procedure K, a solution of indole **63** (41 mg, 0.20 mmol) and azide **120** (100 mg, 0.21 mmol) in tetrahydrofuran/*tert*-butanol/water (2.4 mL) was treated with 2.0 M aqueous sodium ascorbate (205 μL, 0.41 mmol) and 15% aqueous copper(II) sulfate pentahydrate (205 μL, 0.13 mmol). The crude product was purified via flash column chromatography on silica gel (methanol/dichloromethane, 0:100 → 4:96) to provide compound **26** as yellow solid (15 mg, 0.02 mmol, 10% yield). ^1H NMR (500 MHz, DMSO-d_6) δ 12.06 (s, 1H), 9.82 (d, J = 1.7 Hz, 1H), 8.61 (s, 1H), 7.79 (dd, J = 10.1, 2.6 Hz, 1H), 7.59−7.51 (m, 2H), 7.45−7.40 (m, 2H), 7.38−7.34 (m, 1H), 7.27−7.16 (m, 2H), 6.76 (d, J = 8.3 Hz, 1H), 6.70−6.64 (m, 1H), 4.36 (d, J = 7.1 Hz, 2H), 3.78 (s, 3H), 2.95−2.89 (m, 2H), 2.78−2.71 (m, 2H), 2.35−2.31 (m, 2H), 1.91−1.83 (m, 3H), 1.51−1.44 (m, 2H), 1.29−1.18 (m, 2H) ^{13}C RMN (126 MHz, DMSO-d_6) δ 191.0 (C_{quat}), 158.9 (d, J = 95.4 Hz, C_{quat}), 157.3 (C_{quat}), 156.5 (d, J = 37.7 Hz, C_{quat}), 156.4 (C_{quat}) 141.3 (C_{quat}), 139.9 (C_{quat}), 133.1 (C_{quat}), 133.0 (C_{quat}), 132.5 (CH), 129.5 (d, J = 10.6 Hz, CH), 126.6 (d, J = 10.5 Hz, C_{quat}), 125.2 (C_{quat}), 125.0 (CH), 118.1 (CH), 114.8 (d, J = 27.1 Hz, CH), 114.2 (d, J = 9.8 Hz, CH), 112.2 (d, J = 19.1 Hz, C_{quat}), 111.5 (CH), 110.7 (d, J = 5.5 Hz, C_{quat}), 108.8 (CH), 106.9 (d, J = 24.0 Hz, CH), 105.5 (d, J = 22.5 Hz, CH), 57.0 (CH_2), 55.8 (CH_3), 54.6 (CH_2), 52.6 (CH_2), 40.4 (CH_2), 36.5 (CH), 29.0 (CH_2), 28.7 (CH_3). ^{19}F NMR (471 MHz, DMSO-d_6) δ −113.7 (t, J = 8.2 Hz), −122.1 (td, J = 9.6, 4.7 Hz). MS (ESI) m/z 665.2 $[M + H]^+$.

■ ASSOCIATED CONTENT

Supporting Information

The Supporting Information is available free of charge at https://pubs.acs.org/doi/10.1021/acs.jmedchem.5c00695.

Additional data, including cellular IC_{50} values, combination studies, physicochemical properties, *in vivo* results, crystallographic refinement statistics, detailed percent inhibition for the kinase selectivity profile of KDX1381, analytical characterization data and reaction scales for intermediates presented in Schemes 1−3, and NMR spectra for compounds 2−26(PDF)

Crystallographic data(CSV)

Accession Codes

The crystal structure of CK2α in complex with KDX1381 (PDB ID: 9HPH) is available through the RCSB Protein Data Bank (www.rcsb.org).

https://doi.org/10.1021/acs.jmedchem.5c00695
J. Med. Chem. XXXX, XXX, XXX−XXX

AUTHOR INFORMATION

Corresponding Authors

Alexandre Bancet − *Kairos Discovery, Lyon 69003, France*; orcid.org/0000-0003-4467-8684; Email: a.bancet@kairos-discovery.com

David Neves − *Kairos Discovery, Lyon 69003, France*; Email: d.neves@kairos-discovery.com

Authors

Léna Marlhoux − *Kairos Discovery, Lyon 69003, France; Université Claude Bernard Lyon 1, INSERM 1052, CNRS 5286, Centre Léon Bérard, Centre de Recherche en Cancérologie de Lyon, Institut Convergence Plascan, Team ≪ Cancer Cell Death ≫, Lyon 69373, France*

Alexandre Arnaud − *Kairos Discovery, Lyon 69003, France*

Céline Hervieu − *Kairos Discovery, Lyon 69003, France*

Gabriela Makulyte − *Kairos Discovery, Lyon 69003, France*

Charlotte Martinasso − *Université Claude Bernard Lyon 1, INSERM 1052, CNRS 5286, Centre Léon Bérard, Centre de Recherche en Cancérologie de Lyon, Institut Convergence Plascan, Team ≪ Small Molecules for Biological Targets ≫, Lyon 69373, France*

Angélique Mularoni − *Université Claude Bernard Lyon 1, INSERM 1052, CNRS 5286, Centre Léon Bérard, Centre de Recherche en Cancérologie de Lyon, Institut Convergence Plascan, Team ≪ Small Molecules for Biological Targets ≫, Lyon 69373, France*

Jean-Guy Delcros − *Université Claude Bernard Lyon 1, INSERM 1052, CNRS 5286, Centre Léon Bérard, Centre de Recherche en Cancérologie de Lyon, Institut Convergence Plascan, Team ≪ Small Molecules for Biological Targets ≫, Lyon 69373, France*

Isabelle Krimm − *Université Claude Bernard Lyon 1, INSERM 1052, CNRS 5286, Centre Léon Bérard, Centre de Recherche en Cancérologie de Lyon, Institut Convergence Plascan, Team ≪ Small Molecules for Biological Targets ≫, Lyon 69373, France*; orcid.org/0000-0002-5981-109X

Hector Hernandez-Vargas − *Genomics Consulting, Bron 69500, France*

Gabriel Ichim − *Université Claude Bernard Lyon 1, INSERM 1052, CNRS 5286, Centre Léon Bérard, Centre de Recherche en Cancérologie de Lyon, Institut Convergence Plascan, Team ≪ Cancer Cell Death ≫, Lyon 69373, France*

Olivier Meurette − *Université Claude Bernard Lyon 1, INSERM 1052, CNRS 5286, Centre Léon Bérard, Centre de Recherche en Cancérologie de Lyon, Institut Convergence Plascan, Team ≪ Cancer Cell Death ≫, Lyon 69373, France*

Complete contact information is available at: https://pubs.acs.org/10.1021/acs.jmedchem.5c00695

Author Contributions

#L.M. and A.A. contributed equally to this work. All authors have approved the final version of the manuscript.

Notes

The authors declare the following competing financial interest(s): L.M., A.A., C.H., G.M., D.N., and A.B. were employees or contractors of Kairos Discovery at the time this research was conducted, a company dedicated to the development of novel cancer therapeutics. A.A., I.K., D.N., and A.B. are co-founders and equity holders of Kairos Discovery. Additionally, I.K. and A.B. are listed as inventors on patent WO2022008475, filed by the University of Claude Bernard Lyon 1 and licensed to Kairos Discovery.

ACKNOWLEDGMENTS

This research was supported in part by funding from La Métropole de Lyon, Cancéropôle Lyon-Auvergne Rhône−Alpes, SATT de Lyon et Saint-Etienne Pulsalys, and the Agence Nationale de la Recherche et de la Technologie (ANRT) through a CIFRE fellowship (2023/1450). We are grateful to Dr. David Knapp and Dr. Andreas Krämer for providing the CK2α plasmid and for their invaluable guidance in CK2α crystallization. We acknowledge Pharmaron (Beijing, China) for conducting solubility assays, ADME studies, and pharmacokinetic evaluations. Eurofins Discovery Services (San Diego, US) performed kinase enzymatic and binding assays, kinome profiling, and OncoPanel screening. Drugabilis (Villejust, France) contributed to the physical characterization and formulation optimization of the compounds. We also thank the SFR Biosciences and the Cancer Research Center of Lyon for granting access to the Protein Science and animal research facilities.

ABBREVIATIONS USED

ADME	absorption, distribution, metabolism, and excretion
AUCinf	area under the plasma concentration−time curve extrapolated to infinity
ATP	adenosine triphosphate
BID	twice daily
Boc_2O	di-*tert*-butyl dicarbonate
$CHCl_3$	chloroform
CK2	Casein kinase 2
CASP3	caspase-3
CL	clearance
Cmax	maximum plasma concentration
CRC	colorectal cancer
CuI	copper(I) iodide
DCM	dichloromethane
DIAD	diisopropyl azodicarboxylate
DIPEA	diisopropylethylamine
DMAP	4-dimethylaminopyridine
DMF	dimethylformamide
DME	dimethoxyethane
DMSO	dimethyl sulfoxide
EDCI	1-ethyl-3-(3-(dimethylamino)propyl)-carbodiimide
ESI	electrospray ionization
Et_2O,	diethyl ether
EtOH	ethanol
F	bioavailability
GBM	glioblastoma multiforme
HATU	hexafluorophosphate azabenzotriazole tetramethyl uronium
HCC	hepatocellular carcinoma
HCl	hydrochloric acid
HIF	hypoxia-inducible factor
HLB	hydrophilic−lipophilic balance
HPLC	high-performance liquid chromatography
I_2	iodine
IC_{50}	half-maximal inhibitory concentration
IP	intraperitoneal
IV	intravenous

https://doi.org/10.1021/acs.jmedchem.5c00695
J. Med. Chem. XXXX, XXX, XXX−XXX

K_2CO_3	potassium carbonate
K_i	inhibition constant
K_D	dissociation constant
KI	potassium iodide
KOH	potassium hydroxide
LC-MS/MS	liquid chromatography-tandem mass spectrometry
LiOH	lithium hydroxide
MeCN	acetonitrile
MeLi	methyllithium
MeOH	methanol
$MgCl_2$	magnesium chloride
MnO_2	manganese dioxide
n-BuLi	*n*-butyllithium
Na_2CO_3	sodium carbonate
NaCl	sodium chloride
NaH	sodium hydride
NMR	nuclear magnetic resonance
PBS	phosphate-buffered saline
PI	propidium iodide
PI3K	phosphatidylinositol 3-kinase
PIK3CA	phosphatidylinositol-4,5-bisphosphate 3-kinase catalytic subunit alpha
PK	pharmacokinetics
PPh_3	triphenylphosphine
PO	per os
PMHs	primary mouse hepatocytes
Pyry-BF_4	pyridinium tetrafluoroborate
QD	once daily
RCC	renal cell carcinoma
RNa-seq	RNA sequencing
RPTCs	renal proximal tubule epithelial cells
rt	room temperature
SAR	structure−activity relationship
S_N2	bimolecular nucleophilic substitution
SOC	standard-of-care
$t_{1/2}$	terminal half-life
TBAF	tetrabutylammonium fluoride
TEA	triethylamine
TGI	tumor growth inhibition
THF	tetrahydrofuran
TKIs	tyrosine kinase inhibitors
TLC	thin layer chromatography
TMSA	trimethylsilylacetylene
TMZ	temozolomide
t-BuOH	*tert*-Butanol
TsCl	*p*-toluenesulfonyl chloride
VEGFR	vascular endothelial growth factor receptor
VHL	Von Hippel-Lindau tumor suppressor
Vss	volume of distribution at steady-state.

REFERENCES

(1) Niefind, K. Crystal Structure of Human Protein Kinase CK2: Insights into Basic Properties of the CK2 Holoenzyme. *EMBO J.* **2001**, *20* (19), 5320−5331.

(2) Orlandini, M.; Semplici, F.; Ferruzzi, R.; Meggio, F.; Pinna, L. A.; Oliviero, S. Protein Kinase CK2α′ Is Induced by Serum as a Delayed Early Gene and Cooperates with Ha-Ras in Fibroblast Transformation. *J. Biol. Chem.* **1998**, *273* (33), 21291−21297.

(3) Deshiere, A.; Duchemin-Pelletier, E.; Spreux, E.; Ciais, D.; Combes, F.; Vandenbrouck, Y.; Couté, Y.; Mikaelian, I.; Giusiano, S.; Charpin, C.; Cochet, C.; Filhol, O. Unbalanced Expression of CK2 Kinase Subunits Is Sufficient to Drive Epithelial-to-Mesenchymal Transition by Snail1 Induction. *Oncogene* **2013**, *32* (11), 1373−1383.

(4) Filhol, O.; Giacosa, S.; Wallez, Y.; Cochet, C. Protein Kinase CK2 in Breast Cancer: The CK2β Regulatory Subunit Takes Center Stage in Epithelial Plasticity. *Cell. Mol. Life Sci.* **2015**, *72* (17), 3305−3322.

(5) Borgo, C.; D'Amore, C.; Sarno, S.; Salvi, M.; Ruzzene, M. Protein Kinase CK2: A Potential Therapeutic Target for Diverse Human Diseases. *Signal Transduct. Target. Ther.* **2021**, *6* (1), 183.

(6) Trembley, J. H.; Kren, B. T.; Afzal, M.; Scaria, G. A.; Klein, M. A.; Ahmed, K. Protein Kinase CK2 − Diverse Roles in Cancer Cell Biology and Therapeutic Promise. *Mol. Cell. Biochem.* **2023**, *478* (4), 899−926.

(7) Luo, J.; Solimini, N. L.; Elledge, S. J. Principles of Cancer Therapy: Oncogene and Non-Oncogene Addiction. *Cell* **2009**, *136* (5), 823−837.

(8) Firnau, M.-B.; Brieger, A. CK2 and the Hallmarks of Cancer. *Biomedicines* **2022**, *10* (8), 1987.

(9) Ortega, C. E.; Seidner, Y.; Dominguez, I. Mining CK2 in Cancer. *PLoS One* **2014**, *9* (12), No. e115609.

(10) Chua, M. M. J.; Ortega, C. E.; Sheikh, A.; Lee, M.; Abdul-Rassoul, H.; Hartshorn, K. L.; Dominguez, I. CK2 in Cancer: Cellular and Biochemical Mechanisms and Potential Therapeutic Target. *Pharmaceuticals* **2017**, *10* (1), 18.

(11) Chua, M. M. J.; Lee, M.; Dominguez, I. Cancer-Type Dependent Expression of CK2 Transcripts. *PLoS One* **2017**, *12* (12), No. e0188854.

(12) Buontempo, F.; McCubrey, J. A.; Orsini, E.; Ruzzene, M.; Cappellini, A.; Lonetti, A.; Evangelisti, C.; Chiarini, F.; Evangelisti, C.; Barata, J. T.; Martelli, A. M. Therapeutic Targeting of CK2 in Acute and Chronic Leukemias. *Leukemia* **2018**, *32* (1), 1−10.

(13) Bruserud, Ø.; Reikvam, H. Casein Kinase 2 (CK2): A Possible Therapeutic Target in Acute Myeloid Leukemia. *Cancers* **2023**, *15* (14), 3711.

(14) Borgo, C.; D'Amore, C.; Cesaro, L.; Itami, K.; Hirota, T.; Salvi, M.; Pinna, L. A. A N-Terminally Deleted Form of the CK2α′ Catalytic Subunit Is Sufficient to Support Cell Viability. *Biochem. Biophys.L Res. Com.* **2020**, *531* (3), 409−415.

(15) Husain, K.; Williamson, T. T.; Nelson, N.; Ghansah, T. Protein Kinase 2 (CK2): A Potential Regulator of Immune Cell Development and Function in Cancer. *Immunol. Med.* **2021**, *44* (3), 159−174.

(16) Chen, L.; Zhang, S.; Li, Q.; Li, J.; Deng, H.; Zhang, S.; Meng, R. Emerging Role of Protein Kinase CK2 in Tumor Immunity. *Front. Oncol.* **2022**, *12*, 1065027.

(17) Silva-Pavez, E.; Tapia, J. C. Protein Kinase CK2 in Cancer Energetics. *Front. Oncol.* **2020**, *10*, 893.

(18) Borgo, C.; Ruzzene, M. Role of Protein Kinase CK2 in Antitumor Drug Resistance. *J. Exp. Clin. Cancer Res.* **2019**, *38* (1), 287.

(19) Sarno, S.; Reddy, H.; Meggio, F.; Ruzzene, M.; Davies, S. P.; Donella-Deana, A.; Shugar, D.; Pinna, L. A. Selectivity of 4,5,6,7-tetrabromobenzotriazole, an ATP Site-directed Inhibitor of Protein Kinase CK2 ("Casein Kinase-2"). *FEBS Lett.* **2001**, *496* (1), 44−48.

(20) Sarno, S.; de Moliner, E.; Ruzzene, M.; Pagano, M. A.; Battistutta, R.; Bain, J.; Fabbro, D.; Schoepfer, J.; Elliott, M.; Furet, P.; Meggio, F.; Zanotti, G.; Pinna, L. A. Biochemical and Three-Dimensional-Structural Study of the Specific Inhibition of Protein Kinase CK2 by [5-Oxo-5,6-Dihydroindolo-(1,2-a)Quinazolin-7-Yl]-Acetic Acid (IQA). *Biochem. J.* **2003**, *374* (Pt 3), 639−646.

(21) Pagano, M. A.; Meggio, F.; Ruzzene, M.; Andrzejewska, M.; Kazimierczuk, Z.; Pinna, L. A. 2-Dimethylamino-4,5,6,7-Tetrabromo-1H-Benzimidazole: A Novel Powerful and Selective Inhibitor of Protein Kinase CK2. *Biochem. Biophys.L Res. Com.* **2004**, *321* (4), 1040−1044.

(22) Laudet, B.; Barette, C.; Dulery, V.; Renaudet, O.; Dumy, P.; Metz, A.; Prudent, R.; Deshiere, A.; Dideberg, O.; Filhol, O.; Cochet, C. Structure-Based Design of Small Peptide Inhibitors of Protein Kinase CK2 Subunit Interaction. *Biochem. J.* **2007**, *408* (3), 363−373.

(23) Perea, S. E.; Reyes, O.; Baladron, I.; Perera, Y.; Farina, H.; Gil, J.; Rodriguez, A.; Bacardi, D.; Marcelo, J. L.; Cosme, K.; Cruz, M.; Valenzuela, C.; López-Saura, P. A.; Puchades, Y.; Serrano, J. M.;

https://doi.org/10.1021/acs.jmedchem.5c00695
J. Med. Chem. XXXX, XXX, XXX−XXX

Mendoza, O.; Castellanos, L.; Sanchez, A.; Betancourt, L.; Besada, V.; Silva, R.; López, E.; Falcón, V.; Hernández, I.; Solares, M.; Santana, A.; Díaz, A.; Ramos, T.; López, C.; Ariosa, J.; González, L. J.; Garay, H.; Gómez, D.; Gómez, R.; Alonso, D. F.; Sigman, H.; Herrera, L.; Acevedo, B. CIGB-300a Novel Proapoptotic Peptide That Impairs the CK2 Phosphorylation and Exhibits Anticancer Properties Both in Vitro and in Vivo. *Mol. Cell. Biochem.* **2008**, *316* (1−2), 163−167.

(24) Cozza, G.; Mazzorana, M.; Papinutto, E.; Bain, J.; Elliott, M.; di Maira, G.; Gianoncelli, A.; Pagano, M. A.; Sarno, S.; Ruzzene, M.; Battistutta, R.; Meggio, F.; Moro, S.; Zagotto, G.; Pinna, L. A. Quinalizarin as a Potent, Selective and Cell-Permeable Inhibitor of Protein Kinase CK2. *Biochem. J.* **2009**, *421* (3), 387−395.

(25) Cozza, G.; Gianoncelli, A.; Bonvini, P.; Zorzi, E.; Pasquale, R.; Rosolen, A.; Pinna, L. A.; Meggio, F.; Zagotto, G.; Moro, S. Urolithin as a Converging Scaffold Linking Ellagic Acid and Coumarin Analogues: Design of Potent Protein Kinase CK2 Inhibitors. *ChemMedchem* **2011**, *6* (12), 2273−2286.

(26) Lolli, G.; Cozza, G.; Mazzorana, M.; Tibaldi, E.; Cesaro, L.; Donella-Deana, A.; Meggio, F.; Venerando, A.; Franchin, C.; Sarno, S.; Battistutta, R.; Pinna, L. A. Inhibition of Protein Kinase CK2 by Flavonoids and Tyrphostins. A Structural Insight. *Biochemistry* **2012**, *51* (31), 6097−6107.

(27) Dowling, J. E.; Alimzhanov, M.; Bao, L.; Chuaqui, C.; Denz, C. R.; Jenkins, E.; Larsen, N. A.; Lyne, P. D.; Pontz, T.; Ye, Q.; Holdgate, G. A.; Snow, L.; O'Connell, N.; Ferguson, A. D. Potent and Selective CK2 Kinase Inhibitors with Effects on Wnt Pathway Signaling in Vivo. *ACS Med. Chem. Lett.* **2016**, *7* (3), 300−305.

(28) Brear, P.; North, A.; Iegre, J.; Hadje Georgiou, K.; Lubin, A.; Carro, L.; Green, W.; Sore, H. F.; Hyvönen, M.; Spring, D. R. Novel Non-ATP Competitive Small Molecules Targeting the CK2 α/β Interface. *Bioorg. Med. Chem.* **2018**, *26* (11), 3016−3020.

(29) Iegre, J.; Brear, P.; Baker, D. J.; Tan, Y. S.; Atkinson, E. L.; Sore, H. F.; O'Donovan, D. H.; Verma, C. S.; Hyvönen, M.; Spring, D. R. Efficient Development of Stable and Highly Functionalised Peptides Targeting the CK2α/CK2β Protein-Protein Interaction. *Chem. Sci.* **2019**, *10* (19), 5056−5063.

(30) Kufareva, I.; Bestgen, B.; Brear, P.; Prudent, R.; Laudet, B.; Moucadel, V.; Ettaoussi, M.; Sautel, C. F.; Krimm, I.; Engel, M.; Filhol, O.; Borgne, M. L.; Lomberget, T.; Cochet, C.; Abagyan, R. Discovery of Holoenzyme-Disrupting Chemicals as Substrate-Selective CK2 Inhibitors. *Sci. Rep.* **2019**, *9* (1), 15893.

(31) Oshima, T.; Niwa, Y.; Kuwata, K.; Srivastava, A.; Hyoda, T.; Tsuchiya, Y.; Kumagai, M.; Tsuyuguchi, M.; Tamaru, T.; Sugiyama, A.; Ono, N.; Zolboot, N.; Aikawa, Y.; Oishi, S.; Nonami, A.; Arai, F.; Hagihara, S.; Yamaguchi, J.; Tama, F.; Kunisaki, Y.; Yagita, K.; Ikeda, M.; Kinoshita, T.; Kay, S. A.; Itami, K.; Hirota, T. Cell-Based Screen Identifies a New Potent and Highly Selective CK2 Inhibitor for Modulation of Circadian Rhythms and Cancer Cell Growth. *Sci. Adv.* **2019**, *5* (1), No. eaau9060.

(32) Wells, C. I.; Drewry, D. H.; Pickett, J. E.; Tjaden, A.; Krämer, A.; Müller, S.; Gyenis, L.; Menyhart, D.; Litchfield, D. W.; Knapp, S.; Axtman, A. D. Development of a Potent and Selective Chemical Probe for the Pleiotropic Kinase CK2. *Cell Chem. Biol.* **2021**, *28* (4), 546−558.e10.

(33) Siddiqui-Jain, A.; Drygin, D.; Streiner, N.; Chua, P.; Pierre, F.; O'Brien, S. E.; Bliesath, J.; Omori, M.; Huser, N.; Ho, C.; Proffitt, C.; Schwaebe, M. K.; Ryckman, D. M.; Rice, W. G.; Anderes, K. CX-4945, an Orally Bioavailable Selective Inhibitor of Protein Kinase CK2, Inhibits Prosurvival and Angiogenic Signaling and Exhibits Antitumor Efficacy. *Cancer Res.* **2010**, *70* (24), 10288−10298.

(34) Pierre, F.; Chua, P. C.; O'Brien, S. E.; Siddiqui-Jain, A.; Bourbon, P.; Haddach, M.; Michaux, J.; Nagasawa, J.; Schwaebe, M. K.; Stefan, E.; Vialettes, A.; Whitten, J. P.; Chen, T. K.; Darjania, L.; Stansfield, R.; Anderes, K.; Bliesath, J.; Drygin, D.; Ho, C.; Omori, M.; Proffitt, C.; Streiner, N.; Trent, K.; Rice, W. G.; Ryckman, D. M. Discovery and SAR of 5-(3-Chlorophenylamino)Benzo[c][2,6]-Naphthyridine-8-Carboxylic Acid (CX-4945), the First Clinical Stage Inhibitor of Protein Kinase CK2 for the Treatment of Cancer. *J. Med. Chem* **2011**, *54* (2), 635−654.

(35) Atkinson, E. L.; Iegre, J.; Brear, P. D.; Zhabina, E. A.; Hyvönen, M.; Spring, D. R. Downfalls of Chemical Probes Acting at the Kinase ATP-Site: CK2 as a Case Study. *Molecules* **2021**, *26* (7), 1977.

(36) Lovly, C. M.; Shaw, A. T. Molecular Pathways: Resistance to Kinase Inhibitors and Implications for Therapeutic Strategies. *Clin. Cancer Res.* **2014**, *20* (9), 2249−2256.

(37) Cohen, N. A.; Kim, T. S.; DeMatteo, R. P. Principles of Kinase Inhibitor Therapy for Solid Tumors. *Ann. Surg.* **2017**, *265* (2), 311−319.

(38) Yang, Y.; Li, S.; Wang, Y.; Zhao, Y.; Li, Q. Protein Tyrosine Kinase Inhibitor Resistance in Malignant Tumors: Molecular Mechanisms and Future Perspective. *Signal Transduct. Target. Ther.* **2022**, *7* (1), 329.

(39) Zhang, J.; Yang, P. L.; Gray, N. S. Targeting Cancer with Small Molecule Kinase Inhibitors. *Nat. Rev. Cancer* **2009**, *9* (1), 28−39.

(40) Vulpetti, A.; Bosotti, R. Sequence and Structural Analysis of Kinase ATP Pocket Residues. *Il Farmaco* **2004**, *59* (10), 759−765.

(41) Kim, H.; Choi, K.; Kang, H.; Lee, S.-Y.; Chi, S.-W.; Lee, M.-S.; Song, J.; Im, D.; Choi, Y.; Cho, S. Identification of a Novel Function of CX-4945 as a Splicing Regulator. *PLoS One* **2014**, *9* (4), No. e94978.

(42) Olsten, M. E. K.; Weber, J. E.; Litchfield, D. W. CK2 Interacting Proteins: Emerging Paradigms for CK2 Regulation? *Mol. Cell. Biochem.* **2005**, *274* (1−2), 115−124.

(43) Montenarh, M.; Götz, C. The Interactome of Protein Kinase CK2. In *Protein Kinase CK2*; Wiley: 2013, 76-116.

(44) Brear, P.; De Fusco, C.; Hadje Georgiou, K.; Francis-Newton, N. J.; Stubbs, C. J.; Sore, H. F.; Venkitaraman, A. R.; Abell, C.; Spring, D. R.; Hyvönen, M. Specific Inhibition of CK2α from an Anchor Outside the Active Site. *Chem. Sci.* **2016**, *7* (11), 6839−6845.

(45) De Fusco, C.; Brear, P.; Iegre, J.; Georgiou, K. H.; Sore, H. F.; Hyvönen, M.; Spring, D. R. A Fragment-Based Approach Leading to the Discovery of a Novel Binding Site and the Selective CK2 Inhibitor CAM4066. *Bioorg. Med. Chem.* **2017**, *25* (13), 3471−3482.

(46) Lindenblatt, D.; Applegate, V.; Nickelsen, A.; Klußmann, M.; Neundorf, I.; Götz, C.; Jose, J.; Niefind, K. Molecular Plasticity of Crystalline CK2α'Leads to KN2, a Bivalent Inhibitor of Protein Kinase CK2 with Extraordinary Selectivity. *J. Med. Chem.* **2022**, *65* (2), 1302−1312.

(47) Bancet, A.; Frem, R.; Jeanneret, F.; Mularoni, A.; Bazelle, P.; Roelants, C.; Delcros, J.-G.; Guichou, J.-F.; Pillet, C.; Coste, I.; Renno, T.; Battail, C.; Cochet, C.; Lomberget, T.; Filhol, O.; Krimm, I. Cancer Selective Cell Death Induction by a Bivalent CK2 Inhibitor Targeting the ATP Site and the Allosteric αD Pocket. *iScience* **2024**, *27* (2), 108903.

(48) Brear, P.; De Fusco, C.; Atkinson, E. L.; Iegre, J.; Francis-Newton, N. J.; Venkitaraman, A. R.; Hyvönen, M.; Spring, D. R. A Fragment-Based Approach Leading to the Discovery of Inhibitors of CK2α with a Novel Mechanism of Action. *RSC Med. Chem.* **2022**, *13* (11), 1420−1426.

(49) Metz, K. S.; Deoudes, E. M.; Berginski, M. E.; Jimenez-Ruiz, I.; Aksoy, B. A.; Hammerbacher, J.; Gomez, S. M.; Phanstiel, D. H. Coral: Clear and Customizable Visualization of Human Kinome Data. *Cell Syst.* **2018**, *7* (3), 347−350.e1.

(50) Lin, K.-Y.; Tai, C.; Hsu, J.-C.; Li, C.-F.; Fang, C.-L.; Lai, H.-C.; Hseu, Y.-C.; Lin, Y.-F.; Uen, Y.-H. Overexpression of Nuclear Protein Kinase CK2 α Catalytic Subunit (CK2α) as a Poor Prognosticator in Human Colorectal Cancer. *PLoS One* **2011**, *6* (2), No. e17193.

(51) Zou, J.; Luo, H.; Zeng, Q.; Dong, Z.; Wu, D.; Liu, L. Protein Kinase CK2α Is Overexpressed in Colorectal Cancer and Modulates Cell Proliferation and Invasion via Regulating EMT-Related Genes. *J. Transl. Med.* **2011**, *9* (1), 97.

(52) Zhang, H.-X.; Jiang, S.-S.; Zhang, X.-F.; Zhou, Z.-Q.; Pan, Q.-Z.; Chen, C.-L.; Zhao, J.-J.; Tang, Y.; Xia, J.-C.; Weng, D.-S. Protein Kinase CK2α Catalytic Subunit Is Overexpressed and Serves as an Unfavorable Prognostic Marker in Primary Hepatocellular Carcinoma. *Oncotarget* **2015**, *6* (33), 34800−34817.

(53) Rabjerg, M.; Guerra, B.; Oliván-Viguera, A.; Mikkelsen, M. L. N.; Köhler, R.; Issinger, O.-G.; Marcussen, N. Nuclear Localization of

https://doi.org/10.1021/acs.jmedchem.5c00695
J. Med. Chem. XXXX, XXX, XXX−XXX

the CK2α-Subunit Correlates with Poor Prognosis in Clear Cell Renal Cell Carcinoma. *Oncotarget* **2017**, *8* (1), 1613−1627.
(54) Vilardell, J.; Alcaraz, E.; Sarró, E.; Trilla, E.; Cuadros, T.; De Torres, I.; Plana, M.; Ramón Y Cajal, S.; Pinna, L. A.; Ruzzene, M.; Morote, J.; Meseguer, A.; Itarte, E. Under-Expression of CK2β Subunit in ccRCC Represents a Complementary Biomarker of p-STAT3 Ser727 That Correlates with Patient Survival. *Oncotarget* **2018**, *9* (5), 5736−5751.
(55) Di Maira, G.; Salvi, M.; Arrigoni, G.; Marin, O.; Sarno, S.; Brustolon, F.; Pinna, L. A.; Ruzzene, M. Protein Kinase CK2 Phosphorylates and Upregulates Akt/PKB. *Cell Death Differ* **2005**, *12* (6), 668−677.
(56) Rowland, M.; Tozer, T. N. *Clinical Pharmacokinetics and Pharmacodynamics: Concepts and Applications*, 5th ed.; Wolters Kluwer: Philadelphia, 2023.
(57) Lehár, J.; Krueger, A. S.; Avery, W.; Heilbut, A. M.; Johansen, L. M.; Price, E. R.; Rickles, R. J.; Short Iii, G. F.; Staunton, J. E.; Jin, X.; Lee, M. S.; Zimmermann, G. R.; Borisy, A. A. Synergistic Drug Combinations Tend to Improve Therapeutically Relevant Selectivity. *Nat. Biotechnol.* **2009**, *27* (7), 659−666.
(58) Ianevski, A.; Giri, A. K.; Aittokallio, T. SynergyFinder 3.0: An Interactive Analysis and Consensus Interpretation of Multi-Drug Synergies across Multiple Samples. *Nucleic Acids Res.* **2022**, *50* (W1), W739−W743.
(59) Zhai, B.; Hu, F.; Jiang, X.; Xu, J.; Zhao, D.; Liu, B.; Pan, S.; Dong, X.; Tan, G.; Wei, Z.; Qiao, H.; Jiang, H.; Sun, X. Inhibition of Akt Reverses the Acquired Resistance to Sorafenib by Switching Protective Autophagy to Autophagic Cell Death in Hepatocellular Carcinoma. *Mol. Cancer The.* **2014**, *13* (6), 1589−1598.
(60) Guo, H.; German, P.; Bai, S.; Barnes, S.; Guo, W.; Qi, X.; Lou, H.; Liang, J.; Jonasch, E.; Mills, G. B.; Ding, Z. The PI3K/AKT Pathway and Renal Cell Carcinoma. *J. Genet. Genomics* **2015**, *42* (7), 343−353.
(61) Liu, R.; Wettersten, H. I.; Park, S.-H.; Weiss, R. H. Small-Molecule Inhibitors of P21 As Novel Therapeutics For Chemotherapy-Resistant Kidney Cancer. *Future Med. Chem.* **2013**, *5* (9), 991−994.
(62) Abbas, T.; Dutta, A. P21 in Cancer: Intricate Networks and Multiple Activities. *Nat. Rev. Cancer* **2009**, *9* (6), 400−414.
(63) Wilhelm, S. M.; Adnane, L.; Newell, P.; Villanueva, A.; Llovet, J. M.; Lynch, M. Preclinical Overview of Sorafenib, a Multikinase Inhibitor That Targets Both Raf and VEGF and PDGF Receptor Tyrosine Kinase Signaling. *Mol. Cancer Ther.* **2008**, *7* (10), 3129−3140.
(64) Padwa, A. 1,3-Dipolar Cycloaddition Reactions. In *Tetrahedron Organic Chemistry Series*; Elsevier: 1990, Vol. *8*; pp. 269−331.
(65) Sonogashira, K. Development of Pd−Cu Catalyzed Cross-Coupling of Terminal Acetylenes with Sp2-Carbon Halides. *J. Organomet. Chem.* **2002**, *653* (1−2), 46−49.
(66) Mitsunobu, O.; Yamada, M. Preparation of Esters of Carboxylic and Phosphoric Acid via Quaternary Phosphonium Salts. *Bull. Chem. Soc. Jpn.* **1967**, *40* (10), 2380−2382.
(67) Miyaura, N.; Suzuki, A. Palladium-Catalyzed Cross-Coupling Reactions of Organoboron Compounds. *Chem. Rev.* **1995**, *95* (7), 2457−2483.
(68) Moser, D.; Duan, Y.; Wang, F.; Ma, Y.; O'Neill, M. J.; Cornella, J. Selective Functionalization of Aminoheterocycles by a Pyrylium Salt. *Angew. Chem., Int. Ed.* **2018**, *57* (34), 11035−11039.
(69) Copeland, R. A. *Enzymes: A practical introduction to structure, mechanism, and data analysis*, 2nd ed.; Wiley-VCH: New York, 2000.
(70) Pietsch, M.; Viht, K.; Schnitzler, A.; Ekambaram, R.; Steinkrüger, M.; Enkvist, E.; Nienberg, C.; Nickelsen, A.; Lauwers, M.; Jose, J.; Uri, A.; Niefind, K. Unexpected CK2β-antagonistic functionality of bisubstrate inhibitors targeting protein kinase CK2. *Bioorg. Chem.* **2020**, *96*, 103608.
(71) Monaco, S.; Gordon, E.; Bowler, M. W.; Delagenière, S.; Guijarro, M.; Spruce, D.; Svensson, O.; McSweeney, S. M.; McCarthy, A. A.; Leonard, G.; Nanao, M. H. Automatic Processing of Macromolecular Crystallography X-Ray Diffraction Data at the ESRF. *J. Appl. Crystallogr.* **2013**, *46* (3), 804−810.
(72) Emsley, P.; Cowtan, K. Coot: Model-Building Tools for Molecular Graphics. *Acta Crystallogr., Sect. D: biol. Crystallogr.* **2004**, *60* (12), 2126−2132.
(73) Adams, P. D.; Afonine, P. V.; Bunkóczi, G.; Chen, V. B.; Davis, I. W.; Echols, N.; Headd, J. J.; Hung, L.-W.; Kapral, G. J.; Grosse-Kunstleve, R. W.; McCoy, A. J.; Moriarty, N. W.; Oeffner, R.; Read, R. J.; Richardson, D. C.; Richardson, J. S.; Terwilliger, T. C.; Zwart, P. H. PHENIX: A Comprehensive Python-Based System for Macromolecular Structure Solution. *Acta Crystallogr., Sect. D: biol. Crystallogr.* **2010**, *66* (2), 213−221.
(74) Bancet, A.; Cochet, C.; Filhol-Cochet, O.; Krimm, I.; Lomberget, T.; Borgne, M. L. *Indole Derivatives and Uses Thereof for Treating a Cancer*; WO 2,022,008,475 A5, 2022.

https://doi.org/10.1021/acs.jmedchem.5c00695
J. Med. Chem. XXXX, XXX, XXX−XXX